Development of level set methods for computing the semiclassical limit of Schrödinger equations with potentials

by

Zhongming Wang

A dissertation submitted to the graduate faculty

in partial fulfillment of the requirements for the degree of

DOCTOR OF PHILOSOPHY

Major: Applied Mathematics

Program of Study Committee:
Hailiang Liu, Major Professor
Lisheng Hou
Paul Sacks
Sunder Sethuraman
Moulay Tidriri

Iowa State University

Ames, Iowa

2008

Copyright © Zhongming Wang, 2008. All rights reserved.

UMI Number: 3307047

INFORMATION TO USERS

The quality of this reproduction is dependent upon the quality of the copy submitted. Broken or indistinct print, colored or poor quality illustrations and photographs, print bleed-through, substandard margins, and improper alignment can adversely affect reproduction.

In the unlikely event that the author did not send a complete manuscript and there are missing pages, these will be noted. Also, if unauthorized copyright material had to be removed, a note will indicate the deletion.

UMI Microform 3307047
Copyright 2008 by ProQuest LLC
All rights reserved. This microform edition is protected against unauthorized copying under Title 17, United States Code.

ProQuest LLC
789 East Eisenhower Parkway
P.O. Box 1346
Ann Arbor, MI 48106-1346

To my wife, Miaomiao

TABLE OF CONTENTS

LIST OF TABLES

LIST OF FIGURES

ABSTRACT

In this thesis, we propose one approach to compute the multi-valued density via the existing level set method in computing multi-valued velocity of WKB system in high frequency wave dynamics and a superposition property is proved and numerically validated, too. Several novel level set methods are developed and analyzed for computing multi-valued solutions to the Euler-Poisson equations and the Schrödinger equation with periodic structures.

For the WKB system arising in high frequency wave dynamics, we propose a approach for computing the multi-valued density, which is useful for reconstruction of the original wave field. We also show that physical observables evaluated in Jin et al. (2005a,c) are simply the superposition of their multi-valued correspondents. Our method applies to the wave fields in both the Schrödinger equation and the optical wave equation. For these two applications a series of numerical tests is performed to compute multi-valued quantities and validate the established superposition properties.

For one-dimensional Euler-Poisson equations, we propose a novel level set method. The method involves an implicit Eulerian formulation in an augmented space—called field space, which incorporates both velocity and electric fields into the configuration. Both velocity and electric fields are captured through common zeros of two level set functions, which are governed by a field transport equation. Simultaneously we obtain a weighted density f by solving again the field transport equation but with initial density as starting data. The averaged density is then resolved by the integration of the obtained f against the Dirac delta-function of two level set functions in the field space. Moreover, we prove that such obtained averaged density is simply a linear superposition of all multi-valued densities; and the averaged field quantities are weighted superposition of corresponding multi-valued ones. Computational results are

presented and compared with some exact solutions which demonstrate the effectiveness of the proposed method.

For computing the semiclassical limit of one-dimensional Schrödinger equations in periodic medium, we develop a Bloch band based level set method. A hybrid of the WKB approximation and homogenization leads to the Bloch eigenvalue problem and an associated Hamilton-Jacobi system for the phase, with Hamiltonian being the Bloch eigenvalues. We develop a Bloch band based level set method, which is a hybrid numerical scheme—splitting the solution process into several steps: i) initialize the level set function from the band decomposition of the initial data; ii) solve the Bloch eigenvalue problem to compute Bloch waves; iii) evolve the band level set equation to compute multi-valued velocity and density on each Bloch band; iv) evaluate the total position density over a sample set of bands using Bloch waves and band densities obtained in step ii) and iii), respectively. Numerical results with different number of bands are provided to demonstrate the good quality of the method.

CHAPTER 1. GENERAL INTRODUCTION

General Background

The Schrödinger equation is the fundamental equation of physics for describing quantum mechanical behavior. It plays a centrally important role in the theory of quantum mechanics, as the role of Newton's second law does in classical mechanics.

The Schrödinger-type equations, in one dimension, include the linear Schrödinger equation,

$$i\epsilon\partial_t\psi^\epsilon + \frac{\epsilon^2}{2}\partial_{xx}\psi^\epsilon = V(x)\psi^\epsilon, \quad x \in \mathbb{R}, \quad t \geq 0, \tag{1.1}$$

and Schrödinger-Poisson equations

$$i\epsilon\partial_t\psi^\epsilon = -\frac{\epsilon^2}{2}\partial_x^2\psi^\epsilon + KV\psi^\epsilon, \quad x \in \mathbb{R}, \quad t \geq 0, \tag{1.2}$$

$$\partial_x^2 V = c(x) - |\psi^\epsilon|^2, \tag{1.3}$$

both subject to highly oscillatory initial condition

$$\psi^\epsilon(0,x) = A(x)\exp(iS_0(x)/\epsilon).$$

Here ψ^ϵ is complex wave field, V is a potential, either given as in (1.1) or governed by the Poisson equation (1.3), i is the imaginary unit, ϵ is the rescaled Planck constant and K is a physical constant, which indicates the property of forcing in the Schrödinger-Poisson equations.

In the semiclassical regime $\epsilon \ll 1$, the wavelength of the solution ψ^ϵ is of order $\mathcal{O}(\epsilon)$ and other physical observables become highly oscillatory. Due to this fact, direct computation becomes numerically infeasible and asymptotic approximation models should be applied. The semiclassical limits are considered in the small scale $\epsilon \to 0$ and these approximation models are often nonlinear, which develop singularities in finite time in general. After singularity, instead

of shock wave solutions, multi-valued solutions are usually sought, since classical entropy or viscosity solutions developed in Crandall and Lions (1983) are inadequate when multi-valued solutions appear in these situations. Thus efficient algorithms for computing multi-valued solutions are needed. Multi-valued solutions are also sought in the context of dispersive waves by Flaschka et al. (1980); Lax and Levermore (1983a,b,c); Whitham (1974), optical waves by Cockburn et al. (2005); Engquist and Runborg (1996, 2003); Gosse (2002); Leung et al. (2004); Osher et al. (2002); Runborg (2000), seismic waves by Fomel and Sethian (2002); Symes and Qian (2003); Trier and Symes (1991), semiclassical limits of Schrödinger equations by Cheng et al. (2003); Gosse et al. (2003); Jin and Li (2003); Sparber et al. (2003), electron beam modulation in vacuum electronic devices by Hutter (1960); Li et al. (2004), etc.

Semiclassical Approximation

One effective method to resolve highly oscillatory solutions to (1.1) and (1.2)-(1.3) is to compute the limit solution when $\epsilon \to 0$, which is termed the *semiclassical approximation*. The classical approach is the WKB* method. The WKB ansatz takes the form of

$$\psi^\epsilon(t,x) = A(t,x)\exp(iS(t,x)/\epsilon), \quad A = A_0 + \epsilon A_1 + \epsilon A_2 + \cdots \tag{1.4}$$

assuming the amplitude A and the phase S are smooth. Balancing the leading terms in ϵ, one can obtain equations for both $\rho = |A_0|^2$ and S, i.e., from (1.1) and (1.2)–(1.3), one obtains

$$S_t + \frac{1}{2}S_x^2 + V(x) = 0, \tag{1.5}$$

$$\rho_t + (\rho S_x)_x = 0, \tag{1.6}$$

and

$$\rho_t + (\rho u)_x = 0, \tag{1.7}$$

$$u_t + uu_x = KE, \tag{1.8}$$

$$E_x = \rho - c(x), \tag{1.9}$$

respectively with $u = S_x$.

*after Wentzel-Kramers-Brillouin, also known as Wentzel-Kramers-Brillouin-Jeffreys

Solutions of the nonlinear systems (1.5)–(1.6) and (1.7)–(1.9) have finite time singularities in general. After singularity, multi-valued solutions need to be considered, see in Sparber et al. (2003). There are many numerical methods to compute the multi-valued solutions in the literature. One classical way to solve (1.5) is ray tracing, which solves the following system directly:

$$\frac{dx}{dt} = u, \quad \frac{du}{dt} = -V'(x). \tag{1.10}$$

This method is easy to implement and tracks the multi-valued solution, but with limited spatial resolutions in regions with diverging rays, and thus a delicate interpolation is needed. This drawback is avoided by a Eulerian method, which directly computes the solution of (1.5) on a uniform grid, see Benamou (1999). The difficulty of this Eulerian method is in handling multi-valuedness after singularity.

An alternative approach for improving physical-space-based Eulerian methods is the use of a kinetic formulation in phase space. Through a particle density distribution function $\omega(t, x, p)$, the Liouville equation is derived as follows

$$\omega_t + p\omega_x - V'(x)\omega_p = 0. \tag{1.11}$$

This alternative Eulerian approach based on a kinetic formulation has a drawback in numerical computation since it involves a large number of independent variables in phase space. To remedy this drawback, currently there are two categories of treatments.

One is the moment closure method. The use of moment closure method in application to the Schrödinger equation is by Jin and Li (2003). This method was used earlier in Brenier and Corrias (1998); Engquist and Runborg (1996) and also carried out in other works, e.g., by Runborg (2000); Gosse et al. (2003). The other approach is to compute special wave fronts. For tracking wave fronts in geometric optics, geometry based methods in phase space, such as Engquist et al. (2002); Cheng et al. (2004); Osher et al. (2002).

More recently, with a geometric point of view in place of the kinetic one in phase space, a new level set method framework has been developed for computing multi-valued phases and other physical observables in the entire physical domain, e.g., by Cheng et al. (2003) in

computation of high-frequency wave propagation with applications to the semiclassical limit of Schrödinger equations, Jin and Osher (2003) in capturing multi-valued solutions to scalar quasi-linear hyperbolic PDEs and certain Hamilton-Jacobi equations, Liu et al. (2005) in multi-valued solutions to general nonlinear first-order equations and Jin et al. (2005a,c) in computing multi-valued solutions to semiclassical limit of the Schrödinger equation and symmetric hyperbolic systems.

Among all those Eulerian methods, despite its high dimension, the level set method is preferred due to its capability and convenience in handling complex wave patterns. Our new development of level set methods in computational high frequency wave propagation is summarized in the following three sections.

Superposition of Multi-valued Solutions in High Frequency Wave Dynamics

We consider WKB systems of the form

$$\partial_t S + H(x, \nabla_x S) = 0, \quad t \in \mathbb{R}^+, \quad x \in \mathbb{R}^n, \tag{1.12}$$

$$\partial_t \rho + \nabla_x \cdot (\rho \nabla_p H(x, \nabla_x S)) = 0, \quad p = \nabla_x S \in \mathbb{R}^n, \tag{1.13}$$

subject to the initial data

$$S(0, x) = S_0(x), \quad \rho(0, x) = \rho_0(x). \tag{1.14}$$

In Cheng et al. (2003); Jin et al. (2005c); Jin and Osher (2003), a level set framework for computing multi-valued solutions of the Hamilton-Jacobi system has been developed. The key idea is to represent the $n-$dimensional bi-characteristic manifold of the Hamilton-Jacobi equation in phase space by an implicit vector level set function $\Phi(t, x, p)$, whose components solve the Liouville equation

$$\partial_t \Phi + \nabla_p H \cdot \nabla_x \Phi - \nabla_x H \cdot \nabla_p \Phi = 0, \quad \Phi(0, x, p) = p - \nabla_x S_0. \tag{1.15}$$

The multi-valued velocity $\{u_j(x, t)\}$ is determined by the zero level set, i.e.,

$$u_j(t, x) \in \{p| \quad \Phi(t, x, p) = 0\}, \quad (t, x) \in \mathbb{R}^+ \times \mathbb{R}. \tag{1.16}$$

The amplitude is hence evaluated by

$$\bar{\rho} = \int f\delta(\Phi)dp, \tag{1.17}$$

where the quantity f solves

$$\partial_t f + \nabla_p H \cdot \nabla_x f - \nabla_x H \cdot \nabla_p f = 0, \quad f(0,x,p) = \rho_0. \tag{1.18}$$

We propose a new way to evaluate the multi-valued density by

$$\rho_i = \left\{ \frac{f}{|\det(\nabla_p \Phi)|}, \quad \Phi = 0 \right\}.$$

Based on the multi-valued density, we also prove the superposition principle in density and other quantities. Let $\{\rho_j\}_{j=1}^N$ be multi-valued densities corresponding to multi-valued velocity u_j determined in (1.16). Then we showed that

$$\bar{\rho}(t,x) = \sum_{i=1}^{N} \rho_i(t,x). \tag{1.19}$$

Similar results hold for other quantities, such as momentum and energy. We then compute multi-valued quantities related to density, momentum and energy, and conduct numerical comparison with results from (1.17) and (1.19) in applications to $H(x,p) = \frac{1}{2}|p|^2 + V(x)$ and $H(x,p) = c(x)|p|$, respectively.

During numerical simulation,the second order ENO (essentially nonoscillatory) scheme by Osher and Shu (1991) and second order Runge-Kutta method are used in space and time respectively to solve (1.15) and (1.18). In the post processing step (1.17), a regularization of $\delta-$function is needed. We use the cosine kernel, i.e.,

$$\delta_\epsilon^{\cos}(\phi) = \frac{1}{2\epsilon}\left(1 + \cos\left(\frac{\pi\phi}{\epsilon}\right)\right) I_{[-\epsilon,\epsilon]}(\phi), \tag{1.20}$$

where $I_{[-\epsilon,\epsilon]}(\phi)$ is a standard indicator function. The choice of ϵ plays an important role in controlling the error. Through a series of numerical tests, we find that the optimal ϵ depends on $\min_{x_i,p_j} |\nabla_p \Phi|$, where $\{(x_i,p_j)\}$ are the grid points. Our results show that optimal ϵ should be proportional to $\min_{x_i,p_j} |\nabla_p \Phi|$, which is consistent with the conclusion in Jin et al. (2005a,c). This regularization issue has also been studied in other works including Engquist et al. (2005); Raviart (1983); Tornberg and Engquist (2003). More details of our results are in Liu and Wang (2008b).

A Field Space Based Level set Method for Computing Multi-valued Solutions to 1D Euler-Poisson Equations

We consider the 1D Euler-Poisson system (1.7)-(1.9). A generic feature of this system is the so called critical threshold phenomenon, which was observed and rigorously justified by Engelberg et al. (2001). It was shown there that for a sub-critical set of initial data, solutions of the system will develop singularity at a finite time. The main goal of our work is to develop a novel level set method for computing multi-valued solutions after singularity. Since the Euler-Poisson equations are strongly coupled, the level set method in phase space doesn't apply. Our idea is to introduce a new *field space*-based level set method, which incorporates both velocity u and electric field E.

Our main result is to use a vector level set function $\Phi = (\phi_1, \phi_2)^\top \in \mathbb{R}^2$ in field space $(x, p, q) \in \mathbb{R}^3$ with $p = u(t, x)$ and $q = E(t, x)$ to describe dynamics of the 1-D Euler-Poisson system (1.7)-(1.9). The vector level set function $\Phi = \Phi(t, x, p, q)$ is shown to satisfy the field transport equation

$$\partial_t \Phi + p\partial_x \Phi + Kq\partial_p \Phi - c(x)p\partial_q \Phi = 0. \tag{1.21}$$

The zero level set of this vector function, initiated as

$$\Phi_0(x, p, q) := (p - u_0(x), q - E_0(x))^\top, \tag{1.22}$$

forms a one-dimensional manifold in field space $(x, p, q) \in \mathbb{R}^3$; the interaction of two 2-D manifolds $\{\phi_1 = 0\} \cap \{\phi_2 = 0\}$. This gives implicitly multi-valued velocity and electric fields through

$$(u, E) \in \{(p, q) |\ \Phi(t, x, p, q) = 0\},\ \forall (t, x) \in \mathbb{R}^+ \times \mathbb{R}. \tag{1.23}$$

Note that Φ as a solution of the field transport equation is bounded in any domain where the initial velocity and electric fields are bounded.

We evaluate the density function by simultaneously solving the field transport equation for

a new quantity f near $\{(x,p,q);\ \Phi=0\}$ but with initial density as starting data, i.e.,

$$\partial_t f + p\partial_x f + Kq\partial_p f - c(x)p\partial_q f = 0, \tag{1.24}$$

$$f(0,x,p,q) = \rho_0(x). \tag{1.25}$$

The averaged density is thus resolved by the integration of f against the Dirac $\delta-$function of two level set functions in field space,

$$\bar{\rho}(t,x) = \int_{\mathsf{IR}^2_{p,q}} f(t,x,p,q)\delta(\phi_1)\delta(\phi_2)dpdq. \tag{1.26}$$

Superposition properties are established for quantities such as density, momentum and energy in Liu and Wang (2007b). Let $\{\rho_i\}_{i=1}^N$ be multi-valued densities corresponding to multi-valued fields $\{(u_i,E_i),\ i=1,\cdots,N\}$ determined by

$$(u_i,E_i) \in \{(p,q) : \phi_l(t,x,p,q) = 0, l = 1,2\},$$

then

$$\bar{\rho}(t,x) = \sum_{i=1}^N \rho_i(t,x), \tag{1.27}$$

$$\bar{u}(t,x) = \frac{\sum_{i=1}^N u_i(t,x)\rho_i(t,x)}{\bar{\rho}}, \tag{1.28}$$

$$\bar{E}(t,x) = \frac{\sum_{i=1}^N E_i(t,x)\rho_i(t,x)}{\bar{\rho}}. \tag{1.29}$$

This result shows that the linear superposition principle holds for the density of the non-linear Euler-Poisson system in the sense that direct summation of all multi-valued densities gives the physical observed density. To our knowledge, this is the first rigorous proof via the *field space* configuration.

Numerically, second order ENO and second order Runge-Kutta method are used in space and time respectively. The cosine kernel (1.20) is used in post processing step (1.26). A series of $\epsilon = mh,\ m = 1,2,\cdots$ are tested in searching for optimal ϵ, where $h = \max\{\Delta p,\ \Delta q\}$.

More details on the derivation of the level set method in capturing multi-valued (u,E) and numerical examples can be found in Liu and Wang (2007a); details on computation and verification of superposition principle in density and other quantities can be found in Liu and Wang (2007b).

A Bloch Band Based Level Set Method for Computing the Semiclassical Limit in Schrödinger Equations

We study the one dimensional Schrödinger equation

$$i\epsilon\frac{\partial\psi^\epsilon}{\partial t} = -\frac{\epsilon^2}{2}\frac{\partial}{\partial x}\left(a\left(\frac{x}{\epsilon}\right)\frac{\partial\psi^\epsilon}{\partial x}\right) + V\left(\frac{x}{\epsilon}\right)\psi^\epsilon + V_e(x)\psi^\epsilon, \tag{1.30}$$

$$\psi^\epsilon(0,x) = \exp\left(\frac{iS_0}{\epsilon}\right) f\left(x, \frac{x}{\epsilon}\right), \tag{1.31}$$

where the lattice potential $V(y)$ and $a(y) > 0$ are $2\pi-$periodic functions and $V_e(x)$ is smooth. In this case, besides the semiclassical limit, homogenization is also needed due to the periodic potential.

By both WKB approximation and homogenization, on the n^{th} Bloch band, the Schrödinger equation (1.30) is re-written as the following Hamilton-Jacobi equation

$$\begin{aligned} \partial S_n + E_n(\partial_x S_n) + V_e(x) &= 0, \\ \partial_t \rho_n + \partial_x(E_n'(\partial_x S_n)\rho_n) &= 0, \end{aligned}$$

where E_n is the n^{th} eigenvalue of the Bloch eigen-problem

$$H_k(y)z_n(k,y) = E_n(k)z_n(k,y), \quad z_n(k,y+2\pi) = z_n(k,y), \tag{1.32}$$

with

$$H(k,y) := \frac{1}{2}(-i\partial_y + k)[a(y)(-i\partial_y + k)] + V(y)$$

as the differential operator parameterized by k.

Our main result is to develop a level set method to compute the multi-valued solution of $u_n := \partial_x S_n$, ρ_n and other quantities. The level set equation needed for the multi-valued velocity u_n is

$$\phi_t + E'(k)\phi_x - V_e'(x)\phi_k = 0, \tag{1.33}$$

$$\phi(0,x,k) = k - S_x(0,x). \tag{1.34}$$

The j^{th} multi-valued density on the n^{th} band ρ_n^j is computed by

$$\rho_n^j \in \left\{ \frac{f}{|\det(\nabla_k\phi)|}\middle| \quad \phi(t,x,k) = 0 \right\}, \tag{1.35}$$

where f solves

$$f_t + E'(k) f_x - V_e'(x) f_k = 0, \;\; f(0,x,k) = \rho_n(0,x). \tag{1.36}$$

The averaged density on the n^{th} band can be calculated by

$$\bar{\rho}_n(t,x) = \sum_{j=1}^{K_n} \rho_n^j(t,x), \tag{1.37}$$

where K_n is the number of multiple densities on the n^{th} band. The averaged density over all bands is computed by

$$\bar{\rho}(x) = \sum_n \sum_{j=1}^{K_n} \rho_n^j \sum_m |\hat{z}_{n,m}(u_n^j)|^2, \tag{1.38}$$

where u_n^j is the j^{th} multi-valued solution on the n^{th} band and $\hat{z}_{n,m}(u_n^j)$ satisfies

$$z_n(u_n^j, x/\epsilon) = \sum_m \hat{z}_{n,m}(u_n^j) e^{imx/\epsilon}.$$

In this problem, besides the numerical difficulties encountered in previous two sections, we need to solve the Bloch eigenvalue problem (1.32) and prepare for band-wise initial conditions $\rho_n(0,x)$. The Fourier transform method is used to compute E_n and z_n in solving (1.32). The resulting eigen-matrix often has special structure and thus eigenvalues and eigenvectors are easily found. In determining $\rho_n(0,x)$, decomposition of initial condition is needed, i.e.,

$$\rho_n(0,x) = \left| \int_{\mathsf{IR}} f(x,y) z_n\left(\partial_x S_0(x), y\right) dy \right|^2,$$

where $f(x,y)$ is given in (1.31).

Numerical tests with varies types of initial conditions have been successfully implemented. More details are in Liu and Wang (2008a).

Thesis Organization

The thesis is organizes as follows. In Chapter 2, as in Liu and Wang (2008b) a linear superposition for averaged quantities is proved via level set formulation in phase space for both the Schrödinger equation and the optical wave equation. Numerical experiments which confirm the theoretical results are also presented. This work is done under direct supervision

of my advisor Prof. Hailiang Liu. Chapter 3 and Chapter 4 are reserved for Euler-Poisson equations. Chapter 3 studies the multi-valued velocity and electric field in *field space*, while Chapter 4 focuses on the multi-valued and averaged density with theoretical results of linear superposition. This work is done with my advisor Prof. Hailiang Liu. In Chapter 5, multi-scale computation and homogenization are considered with application to the Schrödinger equation with potentials depending on the small scale. A Bloch band based level set method is developed, analyzed and validated with a series of numerical examples. This work is also done under supervision of my advisor Prof. Hailiang Liu. In Chapter 6, a general conclusion of the thesis is provided along with a plan for future research.

CHAPTER 2. SUPERPOSITION OF MULTI-VALUED SOLUTIONS IN HIGH FREQUENCY WAVE DYNAMICS

A paper published by Journal on Scientific Computation

Hailiang Liu, Zhongming Wang

Abstract

The implementation of the WKB system represents a crucial element in the simulation of high frequency wave dynamics in many applications. In recent work a new level set method framework has been introduced, applied and validated. The level set method was shown to be efficient and accurate for capturing multi-valued velocity and evaluation of some physical observables (density, momentum, energy, etc.). However, multi-valued density has not been given, and hence the desired superposition property remains to be verified. In order to address these issues, in this work we propose two approaches for computing the multi-valued density, and show that physical observables evaluated in Jin et al. (2005c,a) are simply the superposition of their multi-valued correspondents. This rigorously justifies the proposed level set method. In addition, the multi-valued density computed here proves to be useful for reconstruction of the original wave field if desired. Our method applies to the wave fields in both the Schrödinger equation and the optical wave equation. For these two applications a series of numerical tests are performed to compute multi-valued quantities and validate the established superposition properties.

Introduction

We are interested in computation of multi-valued solutions to the following WKB system

$$\partial_t S + H(x, \nabla_x S) = 0, \quad t \in \mathbb{R}^+, \quad x \in \mathbb{R}^n, \tag{2.1}$$

$$\partial_t \rho + \nabla_x \cdot (\rho \nabla_p H(x, \nabla_x S)) = 0, \quad p = \nabla_x S \in \mathbb{R}^n, \tag{2.2}$$

subject to the initial data

$$S(0, x) = S_0(x), \tag{2.3}$$

$$\rho(0, x) = \rho_0(x). \tag{2.4}$$

Here $H(x, p)$ is called Hamiltonian, S denotes phase and ρ is position density. This nonlinear system arises in many contexts such as semiclassical approximations of the Schrödinger equation

$$i\epsilon\psi_t\psi + \frac{\epsilon^2}{2}\triangle_x\psi = V(x)\psi, \tag{2.5}$$

and high frequency approximations of wave dynamics for hyperbolic equations such as

$$\partial_{tt}\psi - c^2(x)\triangle_x\psi = 0. \tag{2.6}$$

The main computational challenge for high frequency wave propagation problems is that the wave field is highly oscillatory, making direct simulation unrealistic. The WKB approximation is a classical way to approximate the wave field through an effective phase and a position density. The WKB system (2.1), (2.2) is formally derived from applying the following ansatz

$$\psi = A(t, x) \exp\left(\frac{iS(t, x)}{\epsilon}\right) \tag{2.7}$$

to the original wave equation, see e.g. Whitham (1974). The system (2.1) and (2.2) is weakly coupled, thus the effective phase S can be solved from the Hamilton-Jacobi equation, independent of the density. However, the nonlinearity of the Hamiltonian often leads to kinks in phase at finite time, which forces unbounded density to appear. The classical viscosity solutions Crandall and Lions (1983); Kružkov (1970) are not adequate in describing the wave behavior beyond singularity, where multi-valued solutions in physical space should be considered.

Computation of multi-valued solutions is challenging, there has appeared a bulk of numerical methods to address the difficulty, ranging from Lagrangian methods, Hamilton-Jacobi equation based methods to kinetic formulation based methods. We refer to Engquist and Runborg (2003) for a seminal survey on computational high-frequency wave propagation. Recently, a new level set method framework has been developed for computing multi-valued phases and other physical observables in the entire physical domain in Cheng et al. (2003); Jin and Osher (2003); Liu et al. (2005); Jin et al. (2005c,a); main development has been summarized in the review article Jin et al. (2005b). A key idea is to represent the n-dimensional bi-characteristic manifold of the Hamilton-Jacobi equation in phase space by an implicit vector level set function $\Phi(t, x, p)$, whose components solve the same Liouville equation

$$\partial_t \Phi + \nabla_p H \cdot \nabla_x \Phi - \nabla_x H \cdot \nabla_p \Phi = 0, \quad \Phi_0 = p - \nabla_x S_0.$$

The multi-valued velocity $\{u_i(x,t)\}$ is determined by the zero level set, i.e.,

$$u_i(t,x) \in \{p, \quad \Phi(t,x,p) = 0\}, \quad (t,x) \in \mathsf{IR}^+ \times \mathsf{IR}.$$

The amplitude is hence evaluated by

$$\bar{\rho} = \int f \delta(\Phi) dp, \tag{2.8}$$

where the quantity f also solves the same Liouville equation with ρ_0 as initial data. Such a level set method is simple to implement, and in high dimensions more robust than the moment methods Brenier and Corrias (1998); Engquist and Runborg (1996); Gosse (2002); Jin and Li (2003). Also the computational cost in the phase space can be reduced by using the local level set method Min (2004); Osher et al. (2002); Peng et al. (1999). Recently, an efficient semi-Lagrangian method is introduced in Cheng (2006) for the phase space wavefront reconstruction in three space dimensions.

However, multi-valued density has not been given explicitly, and whether the desired superposition property is preserved by (2.8) remains to be verified. Multi-valued density is also required for reconstruction of the original wave field. The aim of this paper is to introduce techniques for computing multi-valued quantities related to density, momentum and energy,

and conduct numerical comparison with the averaged physical observables evaluated in Jin et al. (2005a,c).

Recall that in our recent work a field space based level set method is developed in Liu and Wang (2007a,b) for computing multi-valued velocity and electric fields governed by 1D Euler-Poisson equations

$$\partial_t \rho + \partial_x(\rho u) = 0, \quad x \in \mathbb{R},\ t > 0,$$
$$\partial_t u + u\partial_x u = KE,$$
$$\partial_x E = \rho - c(x).$$

In particular, multi-valued density is computed from

$$\rho_i \in \left\{ \frac{f}{\left|\det\left(\frac{\partial(\phi_1,\phi_2)}{\partial(p,q)}\right)\right|} \Big| \phi_1 = 0, \phi_2 = 0 \right\},$$

where ϕ_1, ϕ_2 are two level set functions satisfying the transport equation,

$$\Phi_t + p\Phi_x + Kq\Phi_p - c(x)p\Phi_q = 0, \quad \Phi = [\phi_1, \phi_2]^{\mathrm{T}}$$

and f solves the same transport equation in field space (x, p, q), subject to the given initial density ρ_0. It was shown that a superposition of these multi-valued density gives the averaged density over the zero level set manifold. Note that the obtained density from this formula will become unbounded wherever $\frac{\partial(\phi_1,\phi_2)}{\partial(p,q)}$ becomes zero, which corresponds to the density concentration near focus of particle paths. This phenomenon is numerically observed as sharp peaks in density.

Following Liu and Wang (2007b), we shall compute multi-valued density of the WKB system (2.1)-(2.2) either by

$$\rho_i \in \left\{ \frac{f}{|\det(\nabla_p \Phi)|} \Big| \Phi(t, x, p) = 0 \right\}, \tag{2.9}$$

or

$$\rho_i \in \left\{ \frac{\rho_0(\alpha)}{|\det(\frac{\partial x(t,\alpha)}{\partial \alpha})|} \Big| \quad x = x(t, \alpha) \right\}, \tag{2.10}$$

where $x(t, \alpha)$ denotes the deformation map satisfying $\frac{dx}{dt} = \nabla_p H(x, p)|_{p=\nabla_x S}$ with $x(t, 0) = \alpha$. As remarked above, these two formulas are valid both before and after the caustics.

Within the level set framework we prove that the averaged density $\bar{\rho}$ is simply a linear superposition of multi-valued density, i.e.,

$$\bar{\rho}(t,x) = \sum_{i=1}^{N} \rho_i(t,x),$$

where ρ_i is the i^{th} branch of multi-valued density ($1 \le i \le N$). Similar superposition properties are shown to also hold for other quantities such as momentum and energy. These properties are confirmed by a series of numerical examples.

We now conclude this section by outlining the rest of this paper. In Section 2 we review the level set framework introduced in Cheng et al. (2003); Jin et al. (2005c); Jin and Osher (2003), to compute multi-valued velocity, phase and averaged density of the system (2.1) and (2.2), since our results are based on the formulation derived therein. In Section 3 we discuss two techniques for computing the multi-valued density, one by the level set method, and another by the Lagrangian method. Superposition properties for multi-valued density, momentum as well as energy are established in Section 4. Numerical procedures are detailed in Section 5. Finally, in Section 6 a series of numerical examples is presented to compute multi-valued observables and validate the superposition properties. Justification of the formula (2.10) is given in the Appendix.

Review of Level Set Formulation and Computation of Averaged Density

Level Set Formulation for Velocity

The classical way to compute the multi-valued solution is to use Lagrangian method, i.e., following the characteristics of the Hamilton-Jacobi equation (2.1),

$$\frac{dx}{dt} = \nabla_p H(x,p), \quad \frac{dp}{dt} = -\nabla_x H(x,p), \tag{2.11}$$

$$x(0) = \alpha, \quad p(0) = \nabla_x S_0(\alpha). \tag{2.12}$$

Here p is the moment variable in phase space, i.e., $p = \nabla_x S$.

Following Cheng et al. (2003), let $\Phi(t,x,p)$ be a global invariant of (2.11) in the (x,p) space, then

$$\frac{d}{dt}\Phi(t,x(t),p(t)) \equiv 0,$$

which leads to the following level set equation

$$\partial_t\Phi + \nabla_p H(x,p)\cdot\nabla_x\Phi - \nabla_x H(x,p)\cdot\nabla_p\Phi = 0. \tag{2.13}$$

Thus the multi-valued velocity is determined by the zero level set of Φ. The initial condition could be chosen as

$$\Phi(0,x,p) = p - \nabla_x S_0(x). \tag{2.14}$$

Note that other choice of initial data is also admissible, as long as its zero level set uniquely determines the initial phase gradient $\nabla_x S_0$. We will see in later sections that the choice (2.14) would simplify the evaluation of density ρ.

Level Set Formulation for both Velocity and Phase

In addition to the bi-characteristic system (2.11), we have

$$\frac{dS(t,x)}{dt} = -H(x,p) + p\cdot\nabla_p H(x,p), \quad S(0,x) = S_0(\alpha). \tag{2.15}$$

Similarly let $\Phi(t,x,p,q)$ be a global invariant in the (x,p,q) space with $q = S$ along the zero level set, then

$$\frac{d}{dt}\Phi(t,x(t),p(t),q(t)) \equiv 0,$$

which becomes

$$\partial_t\Phi + \nabla_p H\cdot\nabla_x\Phi - \nabla_x H\cdot\nabla_p\Phi + (p\cdot\nabla_p H - H)\partial_q\Phi = 0. \tag{2.16}$$

The initial condition for $\Phi = (\phi_1,\phi_2,\cdots,\phi_{n+1})^T$ could be chosen as

$$\phi_i(0,x,p,q) = p_i - \partial_{x_i}S_0(x), \quad i = 1,2,\cdots,n$$
$$\phi_{n+1}(0,x,p,q) = q - S_0(x).$$

Here the necessity of doing computation in $2n+1$-dimension space is to capture the phase S as well. However, as pointed out in Cheng et al. (2003), multi-valued phase can also be recovered in phase space by

$$S(t,x) \in \left\{ \tilde{S}(t,x,p) | \quad \Phi(t,x,p) = 0 \right\},$$

where the level set function Φ is solved from (2.13), and $\tilde{S}$ solves

$$\partial_t \tilde{S} + \nabla_p H \cdot \nabla_x \tilde{S} - \nabla_x H \cdot \nabla_p \tilde{S} = p \cdot \nabla_p H - H,$$
$$\tilde{S}(0,x,p) = S_0(x).$$

Evaluation of Averaged Density

Let f be a function solving

$$f_t + \nabla_p H \cdot \nabla_x f - \nabla_x H \cdot \nabla_p f = 0, \quad f_0 = \rho_0. \tag{2.17}$$

Then the average density can be determined by

$$\bar{\rho}(t,x) = \int_{\mathbb{R}^n} f \delta(\Phi) dp. \tag{2.18}$$

Note that the momentum $\bar{J}$ and energy $\bar{E}$ can be evaluated by

$$\bar{J} = \int_{\mathbb{R}^n} H_p(x,p) f \delta(\Phi) dp, \tag{2.19}$$
$$\bar{E} = \int_{\mathbb{R}^n} H(x,p) f \delta(\Phi) dp. \tag{2.20}$$

Computation of Multi-valued Density

As is known, the position density, say $|\Psi^\epsilon|^2$ for (2.5), also becomes oscillatory as $\epsilon \to 0$. The quantity computed in (2.18) may be regarded as the weak limit of the position density. We now show how to compute the multi-valued density to the WKB system through this level set approach.

Let L be a Liouville operator given by

$$L := \partial_t + \nabla_p H \cdot \nabla_x - \nabla_x H \cdot \nabla_p,$$

and $\tilde{\rho}$ be a representation of $\rho(t,x)$ in phase space with $\tilde{\rho}(t,x,\nabla_x S) = \rho(t,x)$ and $J = \det(\nabla_p \Phi)$, then it is shown in Jin et al. (2005c) that

$$L(\tilde{\rho}|J|) \equiv 0. \tag{2.21}$$

The equation (2.17) can be rewritten as

$$L(f) = 0, \quad f_0 = \rho_0. \tag{2.22}$$

This shows that f and $\tilde{\rho}|J|$ satisfies the same Liouville equation with the same initial condition($|J_0| = 1$). Therefore, after we solve (2.13) for Φ and (2.17) for f, uniqueness leads to

$$f = \tilde{\rho}|J|. \tag{2.23}$$

Hence, we can determine multi-valued density by

$$\rho_i \in \left\{ \frac{f}{|\det(\nabla_p \Phi)|} \Big| \quad \Phi(t,x,p) = 0 \right\}. \tag{2.24}$$

Note that the formula (2.24) remains valid wherever $|\det(\nabla_p \Phi)| \neq 0$.

We now summarize the procedure for computation of the multi-valued density in general setting using the following pseudo-algorithm:

1. Solve the level set equation (2.13) for Φ and equation (2.17) for f.
2. Compute $|\det(\nabla_p \Phi)|$. It is simple to evaluate the determinant for $n = 1, 2, 3$.
3. Evaluate the quantity $\frac{f}{|\det(\nabla_p \Phi)|}$ on zero level set of Φ.

The above approach works in general cases, but it is sometimes possible to adopt an easier approach in computing the multi-valued density.

Recalling the ODE system (2.11), if we can solve x and p in terms of t and α explicitly, we could use Lagrangian approach to evaluate multi-valued density. By defining

$$\Gamma(t,\alpha) = \nabla_\alpha x, \tag{2.25}$$

we can find density by the following parameterized solution

$$\rho(t, x(t,\alpha)) = \frac{\rho_0(\alpha)}{|\det(\Gamma)|}. \tag{2.26}$$

The justification of this formula is given in the Appendix of this paper.

Superposition

Theorem 2.0.1 (**Superposition Principle for $\bar{\rho}$**). Let $\{\rho_i\}_{i=1}^N$ be multi-valued densities corresponding to multi-valued velocity u_i determined by

$$u_i \in \{p| \quad \Phi(t,x,p) = 0\},$$

and

$$\bar{\rho} = \int f\delta(\Phi)dp,$$

where f solves (2.17) and Φ solves (2.13) with initial condition (2.14).

Then

$$\bar{\rho}(t,x) = \sum_{i=1}^{N} \rho_i(t,x). \tag{2.27}$$

Proof. First note that here u_i denotes i^{th} branch of multi-valued u instead of i^{th} component of vector u. In order to evaluate the integral for $\bar{\rho}$, we assume that all $(u_i's)$ lie in a bounded domain. Use a partition of unity, $\sigma_i \in C_0^\infty$ nonvanishes near u_i, with $\sigma_i(u_i) = 1$ and $\sum \sigma_i = 1$, we have

$$\int_{\mathbb{R}^n} f\delta(\Phi)dp = \sum_{i=1}^{N} \int_{\mathbb{R}^n} f\sigma_i\delta(\Phi)dp.$$

It suffices to evaluate $\int f\sigma_i\delta(\Phi)dp$.

Recall that

$$\delta(\Phi(t,x,p)) = \frac{\delta(p-u_i)}{|\nabla_p\Phi(t,x,u_i)|},$$

wherever $|\nabla_p\Phi(t,x,u_i)|$ is nonzero.

At $p = u_i$, (2.23) gives

$$f(t,x,u_i) = \tilde{\rho}(t,x,u_i)|J|. \tag{2.28}$$

Thus near each $support(\sigma_i)$, we have

$$\begin{aligned}\int_{\mathbb{R}^n} \sigma_i f\delta(\Phi)dp &= \int_{support(\sigma_i)} \tilde{\rho}|J|\frac{\delta(p-u_i)}{|J|}dp,\\ &= \tilde{\rho}(t,x,u_i) = \rho_i(t,x).\end{aligned} \tag{2.29}$$

This, combined with the partition of unity, gives the asserted (2.27). □

This theorem shows that the linear superposition principle holds for the density of the general WKB system (2.1) and (2.2) in the sense that direct summation of all multi-valued densities gives the physical observed density.

Superposition for other quantities is summarized below.

Theorem 2.0.2 (**Superposition Principle for General Function** $g(x,p)$**)**. Let $\{\rho_i\}_{i=1}^N$ be multi-valued densities corresponding to multi-valued fields u_i determined by

$$u_i \in \{p|\Phi(t,x,p)=0\},$$

and $g(x,p)$ be any smooth function of x and p. Let

$$G=\int fg\delta(\Phi)dp,$$

where f solves (2.17) and Φ solves (2.13) with initial condition (2.14). Then

$$G \;=\; \sum_{i=1}^{N} g(x,u_i)\rho_i(t,x). \tag{2.30}$$

Proof. Following a similar argument to that in the proof of Theorem 2.0.1, we have

$$\begin{aligned} G(t,x) &= \sum_{i=1}^{N}\int_{\mathbb{R}^n}\sigma_i fg\delta(\Phi)dp,\\ &= \sum_{i=1}^{N}\int_{support(\sigma_i)} fg\frac{\delta(p-p_i)}{|J|}dp. \end{aligned}$$

Using (2.28) again, we obtain

$$\begin{aligned} G(t,x) &= \sum_{i=1}^{N}\int_{support(\sigma_i)}\tilde{\rho}|J|g\frac{\delta(p-u_i)}{|J|}dp,\\ &= \sum_{i=1}^{N}\tilde{\rho}(t,x,p_i)g(t,x,p_i),\\ &= \sum_{i=1}^{N}\rho_i(t,x)g(x,u_i). \end{aligned} \tag{2.31}$$

□

Numerical Implementation

In this section, we present our numerical procedures to compute the multi-valued velocity and other quantities. We also verify the superposition property stated in Theorem 2.0.1 and Theorem 2.0.2.

Step 1. Discretization and Initialization

We will use uniform mesh size $(\Delta x, \Delta p)$ in x and p. The computation domain is determined by using bi-characteristics if possible. The guideline is that the domain should cover the range of velocity in p direction and contain at least one period of initial velocity in x for periodic initial data. In practice we choose periodic boundary conditions in the simulation.

Step 2. Solve the level set equation (2.13) for Φ and equation (2.17) for f.

In 1D case, the transport equation (2.13) and (2.17) is semi-discretized as

$$\frac{d\Phi^{ij}(t)}{dt} = -H_P^{ij}(t)\Phi_x^{ij}(t) + H_x^{ij}(t)\Phi_p^{ij}(t) := \mathcal{P}(\Phi^{ij}(t)),$$

where $H^{ij}(t)$ and $\Phi^{ij}(t)$ are numerical approximations of H and Φ at node (x_i, p_j), respectively. Usually, H_p and H_x are given explicitly and Φ_x, Φ_p can be approximated by r^{th} order ENO construction Harten (1987, 1989); Osher and Shu (1991); Shu (1999); Shu and Osher (1989). In our simulation, second order ENO approximation is applied.

Then, for time discretization we use second order Runge-Kutta method,

$$\begin{aligned} k^{ij} &= \Phi^{ij}(t) + \Delta t \mathcal{P}(\Phi^{ij}(t)), \\ \Phi^{ij}(t+\Delta t) &= \frac{1}{2}\Phi^{ij}(t) + \frac{1}{2}\left(k^{ij} + \Delta t \mathcal{P}(k^{ij})\right). \end{aligned} \tag{2.32}$$

This method is also known as Heun's method, which has been implemented in Shu and Osher (1989). However, we refer it as second order Runge-Kutta method, which can be easily extended to higher order schemes in the category of SSP Runge-Kutta method, see Gottlieb et al. (2001).

Step 3. Visualize the multi-valued velocity by plotting the zero level set of Φ in $x - p$ space.

In 1D case, for the velocity, we plot out only grid points satisfying

$$\{(x_i, p_j) \in \Omega | \quad |\Phi(t, x_i, p_j)| < \epsilon'\},$$

where ϵ' is chosen in such a way that a unique grid point can be identified along the zero level set. Since it is computationally impossible to find the points where Φ is exactly zero, the zero level set of Φ is realized within a small interval of zero, i.e., any points, with function value close enough to zero, will be considered in the zero level set. We point out that a larger ϵ' may be necessary for the case when level set functions are rough.

Step 4. Evaluate the integral (2.18)

$$\bar{\rho}^{int}(t,x) = \int_{\mathsf{IR}} f\delta(\Phi)dp.$$

Since this integration involves the Dirac $\delta-$function in its integrand, as usual we first regularize the Dirac $\delta-$function by a smooth bounded function δ_ϵ in such a way that $\delta_\epsilon \rightharpoonup \delta$ as $\epsilon \to 0^+$. The error introduced in this regularization step depends on the choice of the approximation, whose accuracy is indicated by a so called moment condition Beyer and LeVeque (1992) of the regularization. δ_ϵ is said to satisfy r^{th} order of moment condition if $\int_{\mathsf{IR}} \delta_\epsilon(x)dx = 1$ and $\int_{\mathsf{IR}} \delta_\epsilon(x)x^k dx = 0$ for $1 \le k \le r$. Under the condition that δ_ϵ is sufficiently resolved by the grid, it is known that the higher the order of moment condition, the smaller the regularization error. Otherwise, the concept of discrete moments should be introduced, see e.g. Engquist et al. (2005). The choice of regularization δ_ϵ could be any smooth function with the above properties. However, considering the concentration of the $\delta-$function, it suffices to choose δ_ϵ to have a compact support:

$$\delta_\epsilon(x) = \begin{cases} \frac{1}{\epsilon}\Psi(\frac{x}{\epsilon}), & |x| \le \epsilon, \\ 0, & |x| > \epsilon. \end{cases}$$

One of the well accepted choices of this type of δ_ϵ is the cosine kernel, $\Psi(\eta) = \frac{1}{2}(1+\cos(\pi\eta))$, i.e.,

$$\delta_\epsilon^{\cos}(x) = \frac{1}{2\epsilon}\left(1 + cos\left(\frac{\pi x}{\epsilon}\right)\right) I_{[-\epsilon,\epsilon]}, \tag{2.33}$$

which has first order moment condition. Here $I_{[-\epsilon,\epsilon]}$ is the standard indicator function.

Replacing $\delta(\Phi)$ by $\delta_\epsilon(\Phi)$, we thus have the first approximation of $\bar{\rho}$,

$$\bar{\rho}_\epsilon^{int}(t,x) = \int_{\mathsf{IR}} f(t,x,p,)\delta_\epsilon(\Phi)dp, \tag{2.34}$$

to which standard quadrature rules can be applied. In our simulation, the rectangle rule is chosen and the numerical density is further evaluated by

$$\bar{\rho}_{\epsilon h}^{int}(t,x) = \sum_{\{|\Phi(t,x,p_j)|\le\epsilon\}} f(t,x,p_j)\delta_\epsilon^{\cos}(\Phi)\Delta p. \tag{2.35}$$

In this two-step procedure, total error is bounded by the sum of regularization error $|\bar{\rho}^{int} - \bar{\rho}_\epsilon^{int}|$ and quadrature error $|\bar{\rho}_\epsilon^{int} - \bar{\rho}_{\epsilon h}^{int}|$. For example, if the cosine kernel and the rectangle rule are used, $|\bar{\rho}^{int} - \bar{\rho}_\epsilon^{int}|$ is of order ϵ and $|\bar{\rho}_\epsilon^{int} - \bar{\rho}_{\epsilon h}^{int}|$ is of order h/ϵ, where $h = \Delta p$. Then the optimal ϵ would be order of $\sqrt{h}$, which leads to order of $\sqrt{h}$ in total error. In the simulation, ϵ is tested with a range of quantities proportional to h, i.e., $\epsilon = mh, \quad m = 1, 2, \cdots$. See Engquist et al. (2005); Liu and Wang (2007b); Raviart (1983); Teufel (2003) for details on the error analysis of approximating δ-functions. Keeping a constant ratio between h and ϵ may lead to inconvergence, as pointed out in Engquist et al. (2005).

Step 5. Computation of multi-valued density $\{\rho_i\}$.

We compute the multi-valued density by (2.24) and the detailed algorithm is discussed in §2 for the WKB system (2.11)-(2.12) with general Hamiltonian. However, in cases where $\Gamma = \nabla_\alpha x(t,\alpha)$ can be explicitly expressed in terms of α and t, we choose to use formula (2.26), i.e.,

$$\rho(t, x(t,\alpha)) = \frac{\rho_0(\alpha)}{|\det(\Gamma)|}.$$

This formula gives a parameterized solution in terms of α and thus can be used to plot the contour of ρ in $x-\rho$ space. In simulation, we first discretize α into nodes $\{\alpha_k| \quad k = 1, 2, \cdots\}$ and compute $(x(t,\alpha_k), \rho(t, x(t,\alpha_k)))$. Then linear interpolation is used locally for any points wherever function values are needed. In this manner, $\rho(t,x)$ can be evaluated at any point x_i. Note that, in our simulation we will utilize this formula (2.26) to compute exact multi-valued solution whenever Γ is available.

Step 6. Verify the superposition by comparing $\bar{\rho}_{\epsilon h}^{int}$ and $\bar{\rho} := \sum_i^N \rho_i$ using both figures and tables of L^1 errors. In one dimension with uniform mesh size in x, the L^1 error for $\bar{\rho}$ is defined by

$$Error_{\bar{\rho}} = \sum_i \left| \bar{\rho}_{\epsilon h}^{int}(t, x_i) - \bar{\rho}(t, x_i) \right| \Delta x,$$

where $\bar{\rho}_{\epsilon h}^{int}(t, x_i)$ and $\bar{\rho}(t, x_i)$ are defined by (2.27) and (2.35). Similar definitions apply to other quantities of interest.

Numerical Examples

The Schrödinger Equation

The semiclassical approximation of the Schrödinger equation (2.5) leads to the WKB system with the following Hamiltonian

$$H(x, p) = \frac{1}{2}|p|^2 + V(x).$$

We are interested in the evaluation of density $\bar{\rho}$, momentum $\bar{J}$ and energy $\bar{E}$, which will be determined as follows:

$$\bar{\rho} = \int f\delta(\Phi)dp,$$

$$\bar{J} = \int |p| f\delta(\Phi)dp,$$

$$\bar{E} = \int (\frac{1}{2}|p|^2 + V) f\delta(\Phi)dp.$$

We make numerical comparison of these averaged quantities with those evaluated from the superposition formula, for which we prepare the multi-valued density by using (2.24). Instead when the ODE system (2.11) can be solved explicitly we shall simply use (2.26) for obtaining the multi-valued density.

(1) Example 1: 1D and $V = 0$

$$u_0 = -\sin(\pi x),$$

$$\rho_0 = \exp(-(x - 0.5)^2).$$

This example was used in Gosse et al. (2003). Throughout the numerical simulation, unless otherwise specified, second order ENO and second order SSP Runge-Kutta methods are used.

The CFL number is taken to be 0.95 to ensure the time efficiency. In numerical figures displayed hereafter, circles denote the numerical results computed from (2.35). Solid lines represent the results evaluated from the corresponding superposition formula (2.27). In this example, computation domain is $[-1,1]\times[-1.5,1.5]$ with step sizes $(0.02,0.02)$ and time at about 0.1, 0.3 and 0.6. Here, periodic and constant boundary conditions are used in computing Φ and f, respectively.

From Fig.2.1, Fig.2.2 and Fig.2.3, we can clearly see the capacity of our method. Before the system develops multi-valuedness, two results are very similar and after singularity, peaks in all three quantities are well captured, i.e., the circle goes up when there is a peak in the solid line.

Table 2.1 shows the L^1 error for the averaged density $\bar{\rho}$, momentum $\bar{J}$ and energy $\bar{E}$, which correspond to the quantities defined in Theorem 2.0.2 with $g=1$, $g=p$ and $g=|p|^2/2$ respectively. Moreover, we also notice that there is an optimal ϵ as we pick different m in $\epsilon=mh$. At time 0.101333 the errors in $\bar{\rho}$, $\bar{J}$ and $\bar{E}$ are of order 10^{-2}, 10^{-4} and 10^{-4}, respectively, with step sizes $\Delta x=0.02$ and $\Delta p=0.02$ with an optimal ϵ. After singularity we still get very good resolution as seen in Fig.2.2 and Fig.2.3.

We also notice the effect of integration support ϵ on the error. Before multi-valued solution appears, the larger the size of the support ϵ tends to give better accuracy, due to the smoothness of the solution. We can see this from the errors for the average density, momentum and energy at time 0.101333 in Table 2.1. In the case under consideration $\epsilon=mh$ when $m=4$ or 5 gives better results in our integration approximation. However, after the formation of multi-valuedness, we have to pick smaller ϵ.

We refine mesh size to be $[0.01,0.01]$, and similar observation is made in Table 2.2. For even smaller mesh size such as $[0.005,0.005]$, we compare the error in terms of the optimal ϵ before and singularity in Table 2.3 and 2.4, respectively. It is clear that after singularity, smaller integration support with $\epsilon\geq 1.5h$ gives better results. Similar phenomenon is also observed in the following examples.

Finally, we make a special remark on the distribution of circles in the multi-valued veloc-

ity. In the up-left sub-figures in Fig.2.2 and Fig.2.3, where we observe uneven distributions of circles. This is largely caused by the projection of Φ onto its zero level set. Since the zero level set of Φ doesn't always go through our computational grid points, we can only pick out those which are very close to grid points. This wiggles in multi-valued velocity can be improved by choosing finer grids.

t	$\epsilon = 2h$	$\epsilon = 3h$	$\epsilon = 4h$	$\epsilon = 5h$	$\epsilon = 6h$
0.101333	0.0167394677	0.0135057820	0.0126285789	0.0123750004	0.0122404699
0.304000	0.1293897319	0.1670558597	0.2117553210	0.2512718005	0.2806063519
0.608000	0.2105845480	0.1407095069	0.1774095427	0.2056773509	0.2268914252

t	$\epsilon = 2h$	$\epsilon = 3h$	$\epsilon = 4h$	$\epsilon = 5h$	$\epsilon = 6h$
0.101333	0.0034993097	0.0010479213	0.0005364168	0.0004407054	0.0005107636
0.304000	0.0131135016	0.0098454853	0.0143602091	0.0225903714	0.0328003001
0.608000	0.1406452841	0.1122488771	0.1434971805	0.1673175011	0.1849303384

t	$\epsilon = 2h$	$\epsilon = 3h$	$\epsilon = 4h$	$\epsilon = 5h$	$\epsilon = 6h$
0.101333	0.0014676255	0.0005905758	0.0006434041	0.0008985308	0.0012774845
0.304000	0.0092880972	0.0102827107	0.0141035968	0.0162260022	0.0177831562
0.608000	0.0570531980	0.0486087232	0.0624852617	0.0724525964	0.0798224902

Table 2.1 Example 1, table of L^1 error for each density, momentum and energy at different time and support size $\epsilon = mh, \quad m = 2, 3, 4, 5, 6$ with mesh size $[0.02, 0.02]$.

(2) Example 2: 1D and $V = 0$

$$u_0 = -\sin(\pi x)|\sin(\pi x)|,$$

$$\rho_0 = \exp(-(x - 0.5)^2),$$

which was used in Gosse et al. (2003).

We use second order ENO and second SSP Runge-Kutta method, results at times about 0.1, 0.4 and 0.8 with step size $[0.02, 0.02]$ are plotted in Fig.2.4, Fig.2.5 and Fig.2.6. In this example, the multi-valued density is computed by (2.26).

t	$\epsilon = 2h$	$\epsilon = 3h$	$\epsilon = 4h$	$\epsilon = 5h$	$\epsilon = 6h$
0.101333	0.0051376816	0.0017909586	0.0007273995	0.0004612454	0.0002879974
0.304000	0.0401613828	0.0540509632	0.0742904492	0.0939465245	0.1097445398
0.601667	0.1790942828	0.1392930622	0.1715167965	0.2018234660	0.2187257480
t	$\epsilon = 2h$	$\epsilon = 3h$	$\epsilon = 4h$	$\epsilon = 5h$	$\epsilon = 6h$
0.101333	0.0037886964	0.0010317342	0.0004580228	0.0002600766	0.0001834229
0.304000	0.0087517411	0.0050335903	0.0062053525	0.0100639636	0.0146909349
0.601667	0.1195325754	0.1245457938	0.1682407453	0.1991976845	0.2142569738

t	$\epsilon = 2h$	$\epsilon = 3h$	$\epsilon = 4h$	$\epsilon = 5h$	$\epsilon = 6h$
0.101333	0.0015507135	0.0004300757	0.0002650783	0.0002767778	0.0003522299
0.304000	0.0044669558	0.0037550843	0.0044664726	0.0054104155	0.0060948187
0.601667	0.0473188337	0.0605047765	0.0904420081	0.1071774789	0.1139000534

Table 2.2 Example 1, table of L^1 error for each density, momentum and energy at different time and support size $\epsilon = mh, \quad m = 2, 3, 4, 5, 6$ with mesh size $[0.01, 0.01]$.

In Fig.2.4, Fig.2.5 and Fig.2.6, results from the level set method and those from superposition match quite well. Especially, before singularity, the results from level set method are very accurate, as shown in Table 2.5. At time 0.101333 the errors in $\bar{\rho}$, $\bar{J}$ and $\bar{E}$ are of order 10^{-2}, 10^{-4} and 10^{-4}, respectively with step sizes $\Delta x = 0.02$ and $\Delta p = 0.02$. After singularity we still get very good resolution as in Fig.2.5 and Fig.2.6. Here we still use periodic and constant boundary conditions in solving for Φ and f, respectively. It is observed that before singularity, ϵ should be larger and after singularity smaller ϵ is preferred.

Wave Equation

In this section, we test the following Hamiltonian

$$H(x,p) = c(x)|p|, \quad H_p = c(x)\frac{p}{|p|}.$$

This Hamiltonian comes from the WKB expansion of wave equation (2.6).

The following quantities are evaluated and compared.

$$\bar{\rho} = \int f\delta(\Phi)dp,$$

t	$\epsilon = 2h$	$\epsilon = 3h$	$\epsilon = 4h$	$\epsilon = 5h$	$\epsilon = 6h$
0.101333	0.0054255900	0.0019348151	0.0007616662	0.0004350618	0.0002721383
0.300833	0.0186806191	0.0147565168	0.0193886939	0.0388620747	0.0582130475
t	$\epsilon = 2h$	$\epsilon = 3h$	$\epsilon = 4h$	$\epsilon = 5h$	$\epsilon = 6h$
0.101333	0.0040379382	0.0011509129	0.0005013195	0.0002428330	0.0001554436
0.300833	0.0144889280	0.0096615926	0.0123598190	0.0361839326	0.0600986628

t	$\epsilon = 2h$	$\epsilon = 3h$	$\epsilon = 4h$	$\epsilon = 5h$	$\epsilon = 6h$
0.101333	0.0016727121	0.0004593942	0.0002253712	0.0001354775	0.0001186966
0.300833	0.0079236149	0.0057813211	0.0075974680	0.0246010823	0.0414202958

Table 2.3 Example 1, table of L^1 error for each density, momentum and energy at different time before singularity and support size $\epsilon = mh, \quad m = 2, 3, 4, 5, 6$ with mesh size $[0.005, 0.005]$.

Quantity	$\epsilon = h$	$\epsilon = 1.5h$	$\epsilon = 2h$	$\epsilon = 2.5h$	$\epsilon = 3h$
$\bar{\rho}$	0.3043520483	0.1102531630	4.2457918328	75.4350338239	137.7567242360
$\bar{J}$	0.1683337070	0.0529774237	6.3482644876	113.1095259437	206.5710968736
$\bar{E}$	0.0584617304	0.0167521244	4.7568178601	84.8200884047	154.9095826285

Table 2.4 Example 1, table of L^1 error for each density, momentum and energy after singularity at time 0.402167 and support size $\epsilon = mh, \quad m = 1, 1.5, 2, 2.5, 3$ with mesh size $[0.005, 0.005]$.

$$\bar{J} = \int c(x) \frac{p}{|p|} f \delta(\Phi) dp,$$

$$\bar{E} = \int c(x) |p| f \delta(\Phi) dp.$$

We call the last two quantities momentum and energy. We now test them by the following examples from Jin et al. (2005a).

(3) Example 3: 1D and constant speed $c(x) = 1$.

$$S_0 = -\frac{x^2 - 0.25}{4}, \tag{2.36}$$

$$A_0 = I_{[-0.7,-0.3]\cup[0.3,0.7]}(x), \tag{2.37}$$

where $\rho_0 = A_0^2/c^2$. Here I_Ω is the characteristic function of Ω.

t	$\epsilon = 2h$	$\epsilon = 3h$	$\epsilon = 4h$	$\epsilon = 5h$	$\epsilon = 6h$
0.101333	0.0201441257	0.0173173587	0.0163551543	0.0162149049	0.0160895224
0.405333	0.1353771931	0.2096008463	0.2570685836	0.2899839171	0.3458325428
0.810667	0.3638322043	0.3349340467	0.3721443546	0.4093349941	0.4441836011

t	$\epsilon = 2h$	$\epsilon = 3h$	$\epsilon = 4h$	$\epsilon = 5h$	$\epsilon = 6h$
0.101333	0.0024015908	0.0008418077	0.0004557995	0.0005120796	0.0006508837
0.405333	0.0824243578	0.1045426391	0.1040800957	0.1170525606	0.1358341234
0.810667	0.2234771392	0.2049319728	0.2283069834	0.2550550387	0.2760111370

t	$\epsilon = 2h$	$\epsilon = 3h$	$\epsilon = 4h$	$\epsilon = 5h$	$\epsilon = 6h$
0.101333	0.0010576917	0.0005229522	0.0006651123	0.0009172565	0.0012734635
0.405333	0.0318257465	0.0377931322	0.0354224554	0.0465411020	0.0560490059
0.810667	0.0973139057	0.0965972571	0.1084100663	0.1206675156	0.1305867870

Table 2.5 Example 2, table of L^1 error for each density momentum and energy at different time and support size $\epsilon = mh, \quad m = 2, 3, 4, 5, 6$ with step size $[0.02, 0, 02]$.

In this case, we solve the level set equation (2.13) with $H = c|p|$. Since $\nabla_p H = c\frac{p}{|p|}$ is undefined at $p = 0$, as in Jin et al. (2005a) we choose to exclude this singular set in our computation domain. In simulation, we exclude the set

$$\Omega_{exclude} = \{(x, p)\big||p| < \max_i \Delta p_i, \quad i = 1, 2, \cdots, n\},$$

where Δp_i is the step size in p_i direction. The multi-valued density is computed by (2.26). In this example, the initial velocity is $u_0 = -x/2$, which is decreasing. We know that the solution will become multi-valued immediately since the wave with negative speed is on the right and moves towards left, while the wave with positive speed is on the left and moves toward right.

In the simulation, the mesh size is picked as $[0.02, 0.02]$, and the multi-valued density is computed by (2.26). Constant extension for boundary conditions is used. From Fig.2.7, Fig.2.8 and Fig.2.9, we see that those average quantities match nicely with those evaluated from the superposition. The Table 2.6 gives the numerical L^1 error of density, momentum and energy at different time and support ϵ. This test shows that the error doesn't depend on the support size ϵ. Thus we refine our meshes to be $[0.01, 0.01]$ and display the L^1 errors in Table 2.7. We can easily see that the error doesn't change much with respect to ϵ. In the next example, same

observation is also made.

t	$\epsilon = 2h$	$\epsilon = 3h$	$\epsilon = 4h$	$\epsilon = 5h$	$\epsilon = 6h$
0.351500	0.1243459867	0.1243459894	0.1243460235	0.1243461163	0.1243450280
0.408500	0.1269397689	0.1269397703	0.1269398218	0.1269404161	0.1269415934
1.007000	0.1667407901	0.1667406964	0.1667402289	0.1667377286	0.1667242841

t	$\epsilon = 2h$	$\epsilon = 3h$	$\epsilon = 4h$	$\epsilon = 5h$	$\epsilon = 6h$
0.351500	0.1122599833	0.1122599806	0.1122599464	0.1122595708	0.1122560508
0.408500	0.1260541833	0.1260541819	0.1260541304	0.1260535361	0.1260514986
1.007000	0.1667388478	0.1667387542	0.1667382866	0.1667357863	0.1667223418

t	$\epsilon = 2h$	$\epsilon = 3h$	$\epsilon = 4h$	$\epsilon = 5h$	$\epsilon = 6h$
0.351500	0.0319705467	0.0319439985	0.0319378147	0.0319350105	0.0319335234
0.408500	0.0321329464	0.0321274079	0.0321255184	0.0321246575	0.0321242228
1.007000	0.0428831029	0.0428384220	0.0428303218	0.0428281333	0.0428269787

Table 2.6 Example 3, table of L^1 error for each density momentum and energy at different time and support size $\epsilon = mh, \quad m = 2, 3, 4, 5, 6$ with step size $[0.02, 0.02]$.

(4) Example 4: 1D and variable speed $c(x)$

$$S_0 = -\frac{x^2}{4}, \tag{2.38}$$

$$A_0 = I_{[-0.45,-0.25]\cup[0.25,0.45]}(x), \tag{2.39}$$

with $c(x) = 3 + 1.5\tanh(x)$ and $\rho_0 = A_0^2/c^2$.

This example is a re-scaled one found in Jin et al. (2005a). Constant boundary condition is used. Numerical results are given in Fig.2.10, Fig.2.11 and Fig.2.12. Here, instead of (2.26), the multi-valued density is computed by (2.24), i.e.

$$\rho_i \in \left\{ \frac{f}{|\det(\nabla_p \Phi)|} \middle| \quad \Phi(t, x, p) = 0 \right\},$$

in which the Jacobian $\nabla_p \Phi$ is approximated by using central differences.

From figures Fig.2.10, Fig.2.11 and Fig.2.12, we can clearly see the wave crossing phenomena. Moreover, the error Table 2.8 shows the L^1 error of the results from integration and

t	$\epsilon = 2h$	$\epsilon = 3h$	$\epsilon = 4h$	$\epsilon = 5h$	$\epsilon = 6h$
0.351500	0.0730752707	0.0730752707	0.0730752707	0.0730752707	0.0730752707
0.403750	0.0688340482	0.0688340482	0.0688340482	0.0688340482	0.0688340482
1.002250	0.0851973109	0.0851973109	0.0851973109	0.0851973109	0.0851973109
t	$\epsilon = 2h$	$\epsilon = 3h$	$\epsilon = 4h$	$\epsilon = 5h$	$\epsilon = 6h$
0.351500	0.0181718495	0.0181535625	0.0181474769	0.0181448518	0.0181435050
0.403750	0.0171266513	0.0171167153	0.0171139650	0.0171129193	0.0171125731
1.002250	0.0217289289	0.0216981950	0.0216887067	0.0216847314	0.0216827964

t	$\epsilon = 2h$	$\epsilon = 3h$	$\epsilon = 4h$	$\epsilon = 5h$	$\epsilon = 6h$
0.351500	0.0027198709	0.0027231238	0.0027322929	0.0027457254	0.0027629154
0.403750	0.0024778875	0.0024666502	0.0024692810	0.0024739515	0.0024868737
1.002250	0.0031984964	0.0031922123	0.0031985274	0.0032105926	0.0032280559

Table 2.7 Example 3, table of L^1 error for each density momentum and energy at different time and support size $\epsilon = mh, \quad m = 2, 3, 4, 5, 6$ with step size $[0.01, 0.01]$.

superposition. We notice that in this case the error does not depend on the support size ϵ too much.

Remark 1. In Example 4, numerical error is also introduced by the approximation of $|\det(\nabla_p \Phi)|$. The error is large where $|\det(\nabla_p \Phi)|$ is small. Numerical tests are performed on this issue in two dimensional space, and large errors are observed. Thus a more accurate, stable approximation of $|\det(\nabla_p \Phi)|$ is desired in order to use (2.24).

Remark 2. From above examples, we notice that the integration support ϵ in (2.33) plays an important role in the error control. Moreover, optimal ϵ varies before or after creation of the multi-valuedness. For some cases with $H = \frac{|p|^2}{2} + V$, the singularity appears in finite time, so optimal ϵ is larger before singularity and smaller after singularity formation. For some cases with $H = c|p|$, the multi-valued solution appears immediately, the choice of ϵ does not affect the error much, which can be observed in Table 2.6 and 2.8. This phenomenon doesn't change during mesh refinement as seen in Table 2.2 and 2.7. The reason for those observations could be that, if multi-valued u's, say u_i and u_{i+1}, are close, then ϵ is better to be small to avoid the overlap of the support in the numerical integration.

t	$\epsilon = 2h$	$\epsilon = 3h$	$\epsilon = 4h$	$\epsilon = 5h$	$\epsilon = 6h$
0.050510	0.0004124339	0.0002574400	0.0002064428	0.0001860470	0.0001836040
0.151460	0.0066038938	0.0065472959	0.0065354958	0.0065220750	0.0065486092
0.252433	0.0005593891	0.0002781005	0.0002250622	0.0002342965	0.0003174496

t	$\epsilon = 2h$	$\epsilon = 3h$	$\epsilon = 4h$	$\epsilon = 5h$	$\epsilon = 6h$
0.050510	0.1314190720	0.1314198912	0.1314201536	0.1314201914	0.1314201904
0.151460	0.1070391216	0.1070397427	0.1070394493	0.1070387782	0.1070392338
0.252433	0.1516576004	0.1516669850	0.1516688414	0.1516792368	0.1516929572

t	$\epsilon = 2h$	$\epsilon = 3h$	$\epsilon = 4h$	$\epsilon = 5h$	$\epsilon = 6h$
0.050510	0.0237754984	0.0237694404	0.0237608625	0.0237498011	0.0237362724
0.151460	0.0292403331	0.0292340795	0.0292253946	0.0292141528	0.0292005134
0.252433	0.0249560424	0.0249503050	0.0249415895	0.0249318013	0.0249203468

Table 2.8 Example 4, table of L^1 error for each density momentum and energy at different time and support size $\epsilon = mh, \quad m = 2, 3, 4, 5, 6$

Appendix

Here we justify the formula (2.26)

$$\rho(t, x(t, \alpha)) = \frac{\rho_0(\alpha)}{|\det(\Gamma)|}, \tag{A.1}$$

where $x = x(t, \alpha)$ is the characteristics satisfying $\frac{dx}{dt} = \nabla_p H|_{p=\nabla_x S}$, and $\Gamma = \frac{\partial x(t,\alpha)}{\partial \alpha}$. Let $J = \det\left(\frac{\partial x}{\partial \alpha}\right)$, then

$$\frac{\partial J}{\partial t} = \frac{\partial}{\partial t} \det\left(\frac{\partial x_i}{\partial \alpha_j}(t, \alpha)\right) = \sum_{i,j} A_i^j \frac{\partial}{\partial t} \frac{\partial x_i}{\partial \alpha_j}(t, \alpha),$$

where A_i^j is the minor of the element $\frac{\partial x_i}{\partial \alpha_j}$ of the matrix $\frac{\partial x}{\partial \alpha}$.

The minor satisfies

$$\sum_j \frac{\partial x_k}{\partial \alpha_j} A_i^j = \delta_i^k J, \quad \delta_i^k = \begin{cases} 1 & k = i, \\ 0 & k \neq i. \end{cases}$$

Thus the use of the equation $\frac{dx}{dt} = \nabla_p H$ gives

$$\begin{aligned} \frac{\partial J}{\partial t} &= \sum_{i,j} A_i^j \frac{\partial}{\partial \alpha_j} \frac{\partial}{\partial t} x_i = \sum_{i,j} A_i^j \frac{\partial}{\partial \alpha_j} (\partial_{p_i} H) \\ &= \sum_{i,j,k} A_i^j \frac{\partial x_k}{\partial \alpha_j} \left(\frac{\partial}{\partial x_k} (\partial_{p_i} H)\right) = \sum_i \frac{\partial}{\partial x_i} (\partial_{p_i} H) J \\ &= \nabla_x \cdot (\nabla_p H) J. \end{aligned}$$

For any domain Ω, the change of variables $\alpha \to x(t,\alpha)$ leads to

$$\int_{x(t,\Omega)} \rho(t,x)dx = \int_{\Omega} \rho(t,x(t,\alpha))Jd\alpha,$$

This, by differentiation in t, gives

$$\begin{aligned}
\frac{d}{dt}\int_{x(t,\Omega)} \rho(t,x)dx &= \int_{\Omega} (\rho_t + \frac{dx}{dt}\cdot\nabla_x\rho)J + \rho\frac{\partial J}{\partial t}d\alpha \\
&= \int_{\Omega} (\rho_t + H_p\cdot\nabla_x\rho)J + \rho\nabla_x\cdot\nabla_p H J d\alpha \\
&= \int_{\Omega} [\rho_t + \nabla_x\cdot(\rho\nabla_p H)]Jd\alpha \\
&= \int_{x(t,\Omega)} (\rho_t + \nabla_x\cdot(\rho\nabla_p H))dx \\
&= 0.
\end{aligned}$$

Therefore, we obtain

$$\int_{x(t,\Omega)} \rho(t,x)dx = \int_{\Omega} \rho_0(\alpha)d\alpha.$$

Since this holds for any Ω, we must have

$$\rho(t,x(t,\alpha))J = \rho_0(\alpha),$$

which gives (A.1), except for the absolute sign on J, which is needed to ensure positivity of the density after singularity.

Acknowledgments

The authors thank the anonymous referees who provided valuable comments resulting in improvements in this paper. This research was supported by the National Science Foundation under Grant DMS05-05975.

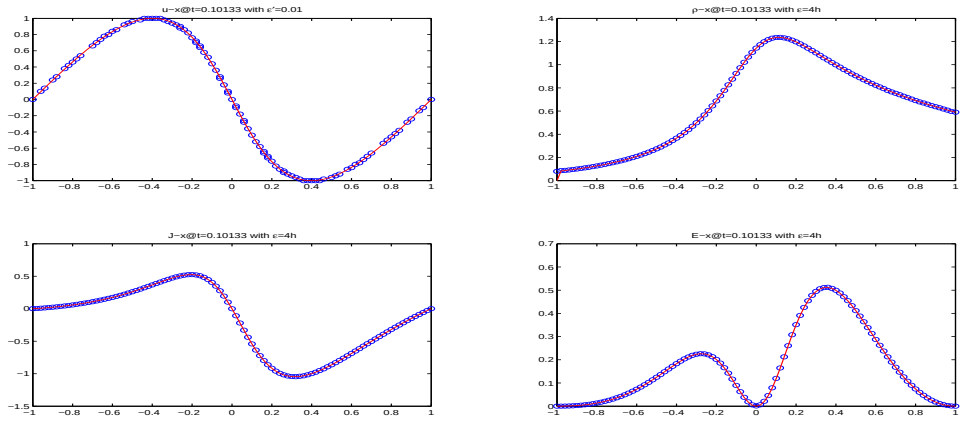

Figure 2.1 Example 1, at $t = 0.101333$. Sub-figures, from up left, are velocity, density, momentum and energy with $\epsilon' = 0.01$ and $\epsilon = 4h$. Circles and solid lines represent the results from (2.35) and (2.27) with density from (2.26), respectively.

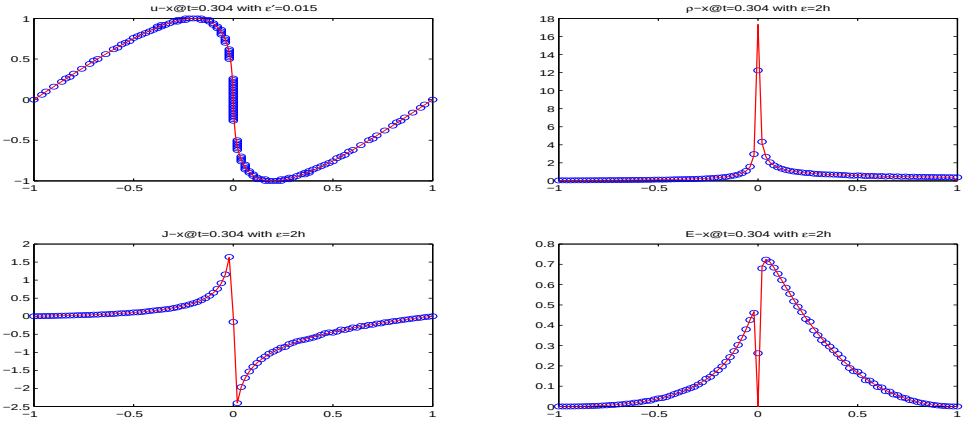

Figure 2.2 Example 1, at $t = 0.304000$. Sub-figures, from up left, are velocity, density, momentum and energy with $\epsilon' = 0.015$ and $\epsilon = 2h$. Circles and solid lines represent the results from (2.35) and (2.27) with density from (2.26), respectively.

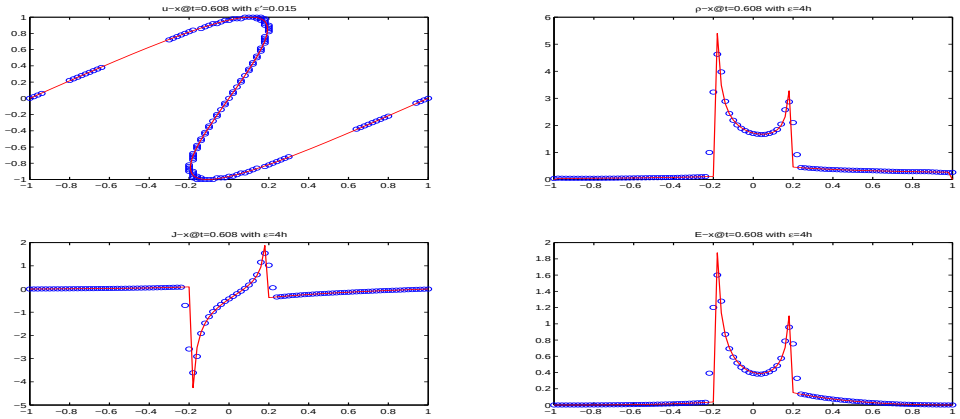

Figure 2.3 Example 1, at $t = 0.608000$. Sub-figures, from up left, are velocity, density, momentum and energy with $\epsilon' = 0.015$ and $\epsilon = 4h$. Circles and solid lines represent the results from (2.35) and (2.27) with density from (2.26), respectively.

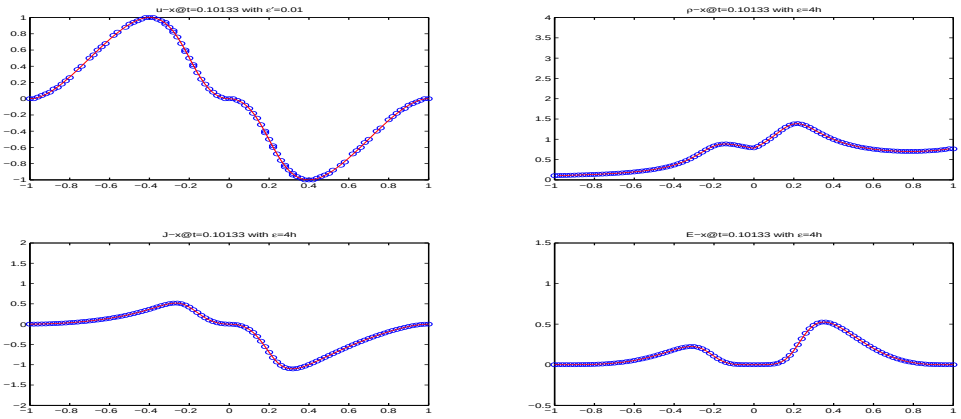

Figure 2.4 Example 2, at $t = 0.101333$. Sub-figures, from up left, are velocity, density, momentum and energy with $\epsilon' = 0.01$ and $\epsilon = 4h$. Circles and solid lines represent the results from (2.35) and (2.27) with density from (2.26), respectively.

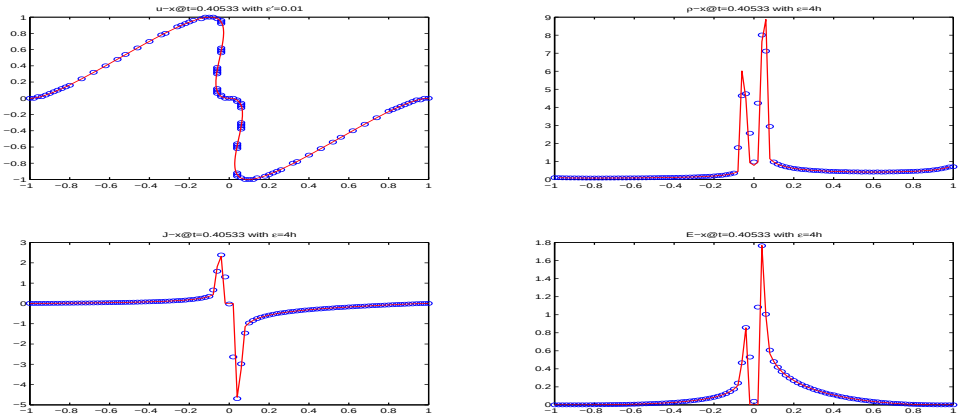

Figure 2.5 Example 2, at $t = 0.405333$. Sub-figures, from up left, are velocity, density, momentum and energy with $\epsilon' = 0.01$ and $\epsilon = 4h$. Circles and solid lines represent the results from (2.35) and (2.27) with density from (2.26), respectively.

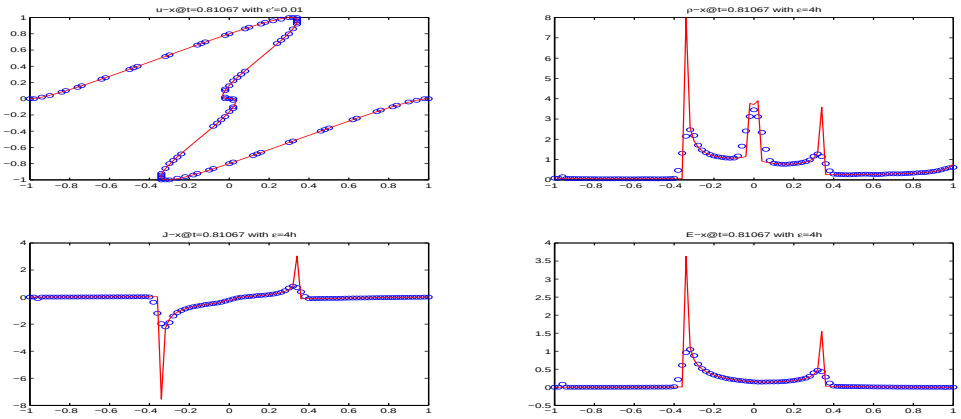

Figure 2.6 Example 2, at $t = 0.810667$. Sub-figures, from up left, are velocity, density, momentum and energy with $\epsilon' = 0.01$ and $\epsilon = 4h$. Circles and solid lines represent the results from (2.35) and (2.27) with density from (2.26), respectively.

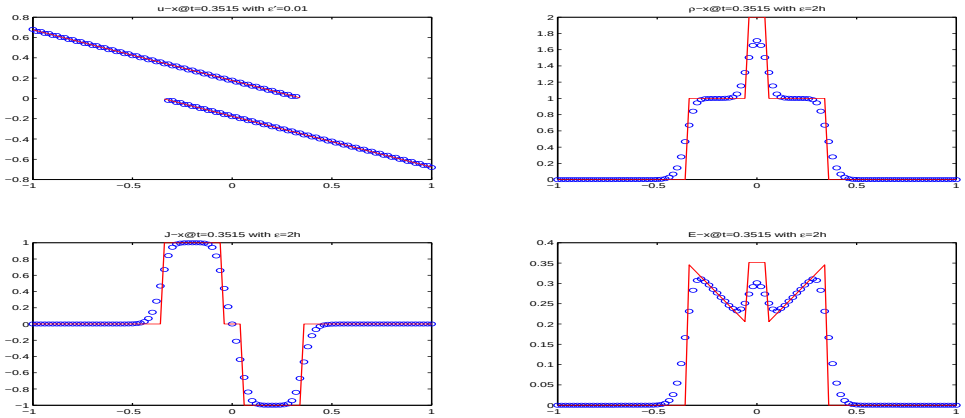

Figure 2.7 Example 3, at $t = 0.3515$. Sub-figures, from up left, are velocity, $g = 1$, $g = \nabla_p H$ and $g = H$ with $\epsilon' = 0.01$ and $\epsilon = 2h$. Circles and solid lines represent the results from (2.35) and (2.27) with density from (2.26), respectively.

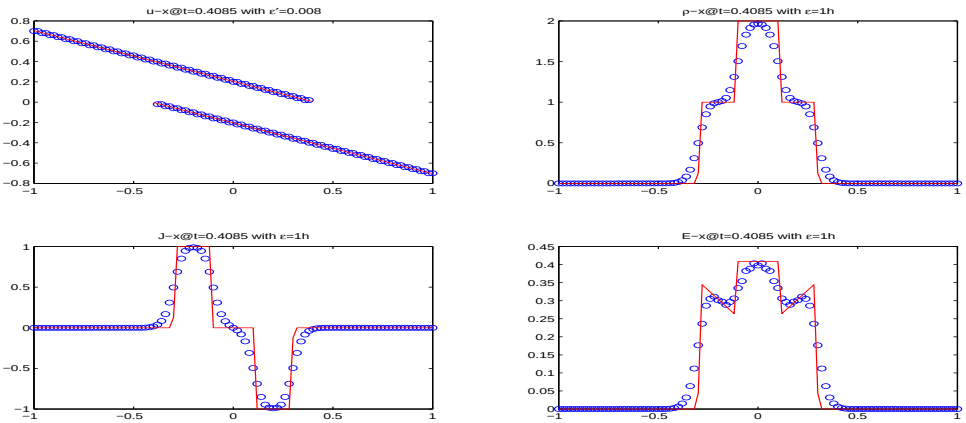

Figure 2.8 Example 3, at $t = 0.408500$. Sub-figures, from up left, are velocity, $g = 1$, $g = \nabla_p H$ and $g = H$ with $\epsilon' = 0.008$ and $\epsilon = h$. Circles and solid lines represent the results from (2.35) and (2.27) with density from (2.26), respectively.

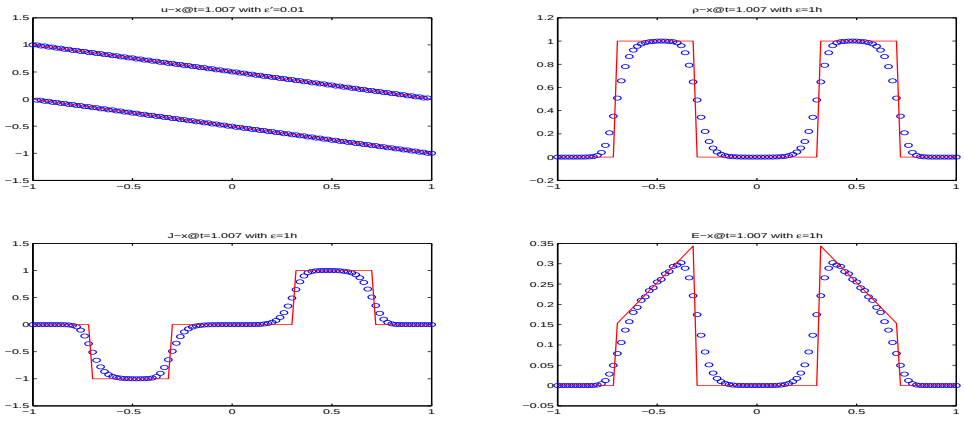

Figure 2.9 Example 3, at $t = 1.00700$. Sub-figures, from up left, are velocity, $g = 1$, $g = \nabla_p H$ and $g = H$ with $\epsilon' = 0.01$ and $\epsilon = h$. Circles and solid lines represent the results from (2.35) and (2.27) with density from (2.26), respectively.

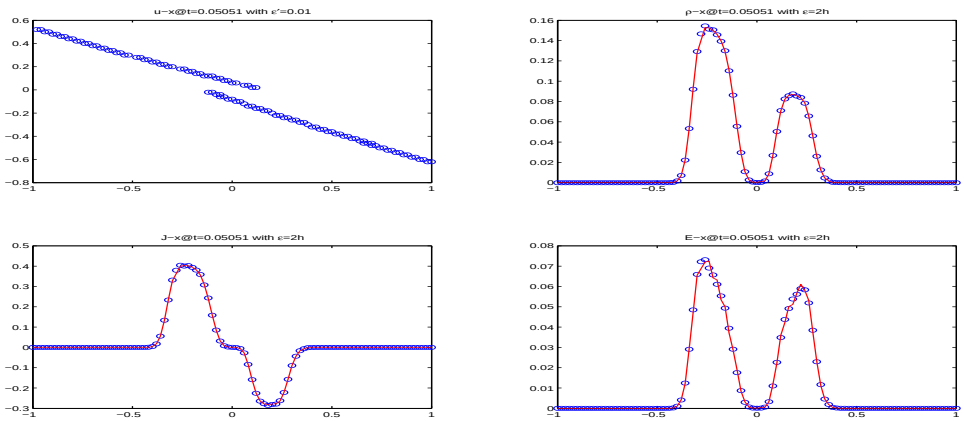

Figure 2.10 Example 4, at $t = 0.05051$. Sub-figures, from up left, are velocity, $g = 1$, $g = \nabla_p H$ and $g = H$ with $\epsilon' = 0.01$ and $\epsilon = 2h$. Circles and solid lines represent the results from (2.35) and (2.27) with density from (2.24), respectively.

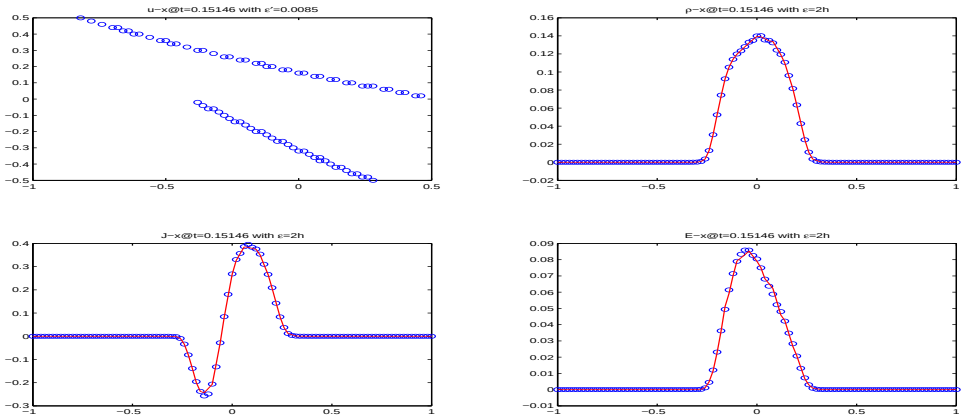

Figure 2.11 Example 4, at $t = 0.15146$. Sub-figures, from up left, are velocity, $g = 1$, $g = \nabla_p H$ and $g = H$ with $\epsilon' = 0.0085$ and $\epsilon = 2h$. Circles and solid lines represent the results from (2.35) and (2.27) with density from (2.24), respectively.

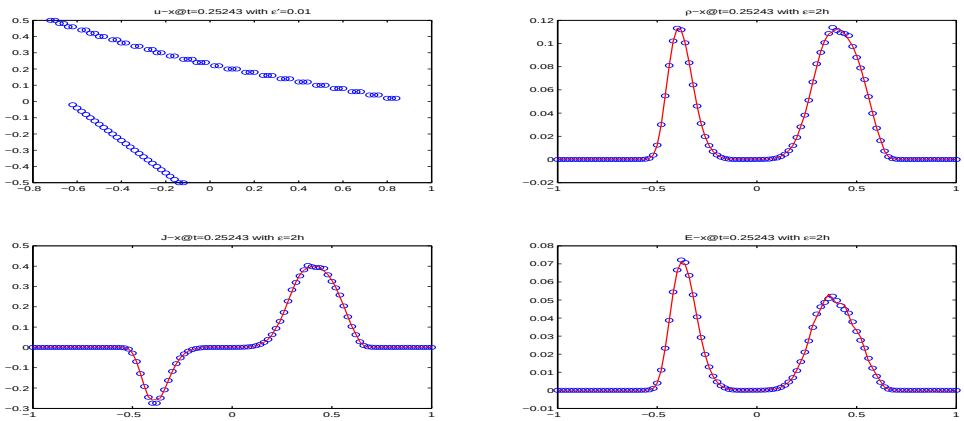

Figure 2.12 Example 4, at $t = 0.25243$. Sub-figures, from up left, are velocity, $g = 1$, $g = \nabla_p H$ and $g = H$ with $\epsilon' = 0.01$ and $\epsilon = 2h$. Circles and solid lines represent the results from (2.35) and (2.27) with density from (2.24), respectively.

CHAPTER 3. COMPUTING MULTI-VALUED VELOCITY AND ELECTRIC FIELDS FOR 1D EULER-POISSON EQUATIONS

A paper published in Applied Numerical Mathematics

Hailiang Liu, Zhongming Wang

Abstract

We develop a level set method for the computation of multi-valued velocity and electric fields of one-dimensional Euler-Poisson equations. The system of these equations arises in the semiclassical approximation of Schrödinger-Poisson equations and semiconductor modeling. This method uses an implicit Eulerian formulation in an extended space–called field space, which incorporates both velocity and electric fields into the configuration space. Multi-valued velocity and electric fields are captured through common zeros of two level set functions, which solve a linear homogeneous transport equation in the field space. Numerical examples are presented to validate the proposed level set method.

Introduction

This work together with a companion paper Liu and Wang (2007b) is devoted to the design of an efficient numerical method for computing multi-valued solutions to one-dimensional Euler-Poisson Equations of the form

$$\rho_t + (\rho u)_x = 0, \tag{A.1}$$

$$u_t + uu_x = KE - \alpha u, \tag{A.2}$$

$$E_x = \rho - c(x). \tag{A.3}$$

These are equations of conservation of mass, Newton's second law, and the Poisson equation, respectively. Here K is a physical constant, which gives the property of forcing, i.e., repulsive when $K > 0$ and attractive when $K < 0$. And $\rho(x,t)$ is the local density, $u(x,t)$ is the velocity field, $E(x,t)$ is usually the electric charge, $c(x)$ is the background charge profile, and α denotes the damping coefficient.

The Euler-Poisson system arises in many applications such as fluid dynamics, plasma dynamics, semiconductor modeling, and the semiclassical approximation of Schrödinger-Poisson equations. A remarkable feature of this system is the so called critical threshold phenomenon, which was observed and rigorously justified by Engelberg, Liu and Tadmor in Engelberg et al. (2001). It was shown there for a sub-critical set of initial data, solutions of the system will develop singularity at a finite time. In some applications such as in fluid dynamics, a shock will develop after the singularity formation. But in many other applications such as the semiclassical approximation of Schrödinger-Poisson equations and the wave breaking in Klystrons, one must allow multi-valued solutions in order to capture physically relevant phenomena. Direct shock-capturing methods can not be applied directly. We should mention that for one dimensional case the passage from the Schrödinger-Poisson Equation to the Euler-Poisson Equation was proved in Liu and Tadmor (2002) for a set of sub-critical initial data, and the passage from the Schrödinger-Poisson equation to the Vlasov-Poisson equation was proved in Zhang et al. (2002) for more general initial data.

Recently there has been a growing interest in developing efficient numerical methods for computing multi-valued solutions in the context of geometric optics Brenier and Corrias (1998); Benamou et al. (2002); Engquist and Runborg (1996); Engquist et al. (2002); Fatemi et al. (1995); Fomel and Sethian (2002); Gosse (2002); Leung et al. (2004); Osher et al. (2002); Qian et al. (2003); Qian and Leung (2004); Runborg (2000), the semiclassical approximation of Schrödinger equations Cheng et al. (2003); Gosse et al. (2003); Jin and Li (2003); Jin et al. (2005c); Gosse (2004); Gosse and Markowich (2004), and Euler-Poisson equations with applications to wave breaking in klystrons Li et al. (2004), among others. The multi-valued solutions in physical space impose tremendous numerical challenges.

For numerical implementation, there are currently two categories of methods available for computing multi-valued solutions, the Eulerian and Lagrangian method (also called ray tracing). The former one based on nonlinear PDEs in physical space, such as Hamilton-Jacobi equations, computes numerical solutions on a fixed gird, and is generally preferred over the second one, which yields additional difficulties in resolving wave front solutions in regions with inadequate rays. A relatively new PDE based Eulerian method is to use kinetic formulation in phase space such as the Liouville equation Brenier and Corrias (1998); Engquist and Runborg (1996); Engquist et al. (2002); Gosse (2002); Gosse et al. (2003); Gosse and Markowich (2004); Jin and Li (2003); Li et al. (2004); Runborg (2000). In order to reduce the computational cost, one often uses the moment method to compute moments directly or computes some special solutions such as multi-phased wave fronts.

More recently, the level set method has been developed to capture multi-valued solutions for first-order PDEs Cheng et al. (2003); Jin and Osher (2003); Liu et al. (2005) in the entire domain and in particular for the general WKB system

$$\partial_x S + H(x, \nabla_x S) = 0, \tag{A.4}$$

$$\partial_t \rho + \nabla_x \cdot (\rho \nabla_k H(x, \nabla_x S)) = 0, \tag{A.5}$$

with applications in the semiclassical approximation of the linear Schrödinger equations ($H = \frac{1}{2}|k|^2 + V(x)$) Cheng et al. (2003); Jin et al. (2005c), geometrical optics limit of the wave equation ($H = c(x)|k|$), see e.g. Jin et al. (2005a). Note that the WKB system (A.4)-(A.5) is weakly nonlinear, and the phase S can be solved independent of the density ρ. In the Euler-Poisson system the moment equation couples with the Poisson equation, hence the level set methods mentioned above do not apply. The main goal of this paper is to introduce a novel level set method to attack the difficulty caused by the nontrivial coupling with the Poisson equation.

We still follow the methodology of the phase space based level set method Cheng et al. (2003); Jin and Osher (2003); Liu et al. (2005) since the power of the level set method lies in that it automatically handles topological changes Osher and Fedkiw (2003); Sethian (1999) such as multi-phases. This method has become a very powerful numerical tool since it was

introduced in Osher and Sethian (1988). As remarked above the phase space based method does not apply to Euler-Poisson equations because it fails to resolve the nontrivial coupling with the Poisson equation. The novelty of our approach is to select an extended space, $(x, y, z) \in R^3$ with $y = u$ and $z = E$, which we call the **field space**. In this field space the dynamics of full Euler-Poisson equation can be recast into a closed ODE system along the particle path Engelberg et al. (2001). Then the level set equation is just a linear homogeneous transport equation with speed determined by the vector field of this ODE system. Multi-valued velocity and electric fields are thus resolved as common zeros of two level set functions initiated as $(y - u_0(x))$ and $(z - E_0(x))$ respectively. In a companion paper Liu and Wang (2007b) we will consider the problem of computing the density ρ showing how to combine the level set formulations developed here with a post-processing step for the evaluation of density and other physical observables.

This paper is organized as follows. §3 is devoted to the derivation of level set equations in field space for general Euler-Poisson equations, using both the particle path formulation and the PDE based formulation. The determination of the initial electric field $E_0(x)$ in different cases is also discussed. In §3 we discuss numerical procedures for computing multi-valued velocity and electrical fields via the level set formulation. Both L^1 and L^∞ stability are proved for the first-order upwind scheme applied to the level set equation. In §3 we present some numerical examples to validate the proposed level set method.

Level Set Formulation

Formulation Using Global Invariants

We start with the general one-dimensional Euler-Poisson system

$$\rho_t + (\rho u)_x = 0, \tag{A.6}$$

$$u_t + u u_x = KE - \alpha u, \tag{A.7}$$

$$E_x = \rho - c(x), \tag{A.8}$$

as described in §3 , subject to the following initial condition

$$\rho(x,0)=\rho_0(x), \quad u(x,0)=u_0(x). \tag{A.9}$$

In this model, $c(x)\geq 0$ denotes the fixed positively charged background, i.e., the doping profile in semiconductor modeling Markowich et al. (1990). For applications in plasma dynamics, the background charge is weak and ignorable, $c(x)=0$. The initial electric field needs to be determined differently for the two cases.

As shown in Engelberg et al. (2001), for Euler-Poisson equations, only a subset of initial configurations leads to global smooth solutions. For subcritical initial data the classical solution fails and the wave breakdown will occur in finite time. Beyond the breakdown time multi-valued solutions become physically relevant.

In order to capture multi-valued solutions, we propose a new method based on level set formulations in an extended space. The extended space we are taking is $(x,y,z)\in R^3$ with $y=u$ and $z=E$, called the field space since it incorporates both velocity and electrical fields. Instead of looking for explicit solutions in the field space, we are seeking implicit solutions identified as a common zero of two implicit functions in the field space, in which multi-valued velocity and electrical field are implicitly represented.

We proceed to derive the level set formulation first by employing the particle path method. Let $x=x(t)$ be a particle path determined by $\frac{dx}{dt}=u(x(t),t)$, where $u(x,t)$ is the associated velocity field, we then have

$$\frac{du}{dt} \;=\; KE-\alpha u, \quad \frac{d}{dt}\triangleq \partial_t+u\partial_x$$

along this particle path. In order to have a closed system we need also derive a dynamic equation for the electric field E. Note that $E_x(x,t)=\rho(x,t)-c(x)$ implies that $\rho_t=E_{xt}$. Therefore, by $\rho_t+(\rho u)_x=0$, we have

$$(E_t+\rho u)_x=0.$$

Integration gives

$$E_t+\rho u=C(t), \quad \forall x\in R$$

for any function $C(t)$ of t. We are interested in the physical situation that both velocity and electric fields are zero at far field. Thus we simply take $C(t)$ as zero and obtain

$$E_t = -\rho u.$$

Then using $\frac{dE}{dt} = E_t + E_x u$, we arrive at

$$\begin{aligned} \frac{dE}{dt} &= -\rho u + E_x u \\ &= -\rho u + (\rho - c(x))u \\ &= -c(x)u. \end{aligned}$$

Further we combine $\frac{dx}{dt}, \frac{du}{dt}, \frac{dE}{dt}$ together to get the following closed system

$$\frac{dx}{dt} = u, \tag{A.10}$$

$$\frac{du}{dt} = KE - \alpha u, \tag{A.11}$$

$$\frac{dE}{dt} = -c(x)u. \tag{A.12}$$

From the above autonomous ODE system, we see that the variables, $x = x(t)$, $u = u(x(t), t)$ and $E(t) = E(x(t), t)$ solve a closed ODE system. According to the ODE theory, there exists a 1-1 correspondence between the ODE solution and its trajectory in the field space (x, u, E). A global invariant is just a level set of certain implicit functions

$$\phi(t, x, u, E) = Const.$$

To recover u and E from implicit global invariants, we need two functions $\Phi = (\phi_1, \phi_2)^\top$. More precisely, where $\frac{\partial(\phi_1, \phi_2)}{\partial(u, E)}$ is nonsingular, $u(x, t)$ and $E(x, t)$ can be determined by the zero level set of Φ, i.e.,

$$\Phi(t, x(t), u(t), E(t)) \equiv 0, \quad \forall t \in R^+. \tag{A.13}$$

Differentiation of (A.13) with respect to t leads to

$$\frac{d\Phi}{dt} = \Phi_t + \frac{dx}{dt}\Phi_x + \frac{du}{dt}\Phi_y + \frac{dE}{dt}\Phi_z = 0, \quad \forall t > 0. \tag{A.14}$$

Using the above ODE system and replacing u and E by y, z respectively, we have the following

$$\Phi_t + y\Phi_x + (Kz - \alpha y)\Phi_y - c(x)y\Phi_z = 0 \quad on \quad \Phi = 0. \tag{A.15}$$

This is a transport equation derived on $\Phi = 0$ in (x, y, z) space. Following the main idea of the level set method Osher and Fedkiw (2003); Osher and Sethian (1988); Sethian (1999), we shall solve the transport equation in the vicinity of $\Phi = 0$ or a larger computational domain, and then project back to $\Phi = 0$ when the solution is needed. Note that $\Phi = 0$ is a codimension-two curve in R^3, and interaction of zero level sets of two level set functions needs to be performed. Consult Burchard et al. (2001) for more details on handling codimension-two objects.

Alternative Derivation

We now give an alternative derivation of the level set equation. Let $\Phi(t, x, y, z) \in R^2$ be a vector function and its Jacobian matrix $\det\left(\frac{\partial\Phi(t,x,y,z)}{\partial(y,z)}\right) \neq 0$, the implicit function theorem suggests that $\Phi(t, x, y, z) = 0$ may determine two functions $y = y(x, t)$ and $z = z(x, t)$, at least locally where the Jacobian matrix is nonsingular. Let $y = u(x, t)$ and $z = E(x, t)$ be a solution of the Euler-Poisson system, we thus obtain

$$\Phi(t, x, u(x, t), E(x, t)) \equiv 0, \quad (x, t) \in R \times R^+. \tag{A.16}$$

Differentiation of (A.16) with respect to t and x respectively gives

$$\begin{aligned} \Phi_t + \Phi_y u_t + \Phi_z E_t &= 0, \\ \Phi_x + \Phi_y u_x + \Phi_z E_x &= 0. \end{aligned}$$

Multiplying u to the second equation and adding to the first one results in the following

$$\Phi_t + u\Phi_x + (u_t + uu_x)\Phi_y + (E_t + uE_x)\Phi_z = 0.$$

Applying $u = y$, $u_t + uu_x = KE - \alpha u$, and $E_t + E_x u = -c(x)u$ to the above equation, we get

$$\Phi_t + y\Phi_x + (Kz - \alpha y)\Phi_y - c(x)y\Phi_z = 0, \tag{A.17}$$

which is exactly what we derived in (A.15). Note that these two different approaches of deriving level set equations verify each other.

Initialization

Given the level set equation derived for general one-dimensional Euler-Poisson equations, we discuss different cases to be considered and how initial data are chosen in each case.

The level set formulation can be rewritten into a compact form

$$\Phi_t + \overrightarrow{V}(X) \cdot \nabla_X \Phi = 0, \quad t \in R^+ \tag{A.18}$$

with $X = (x, y, z) \in R^3$, and the transport speed is expressed as

$$\overrightarrow{V}(X) \quad = \quad (y, Kz - \alpha y, -c(x)y)^\top.$$

In many cases of semiclassical mechanics, no damping is considered, i.e., $\alpha = 0$. The transport speed becomes

$$\overrightarrow{V}(X) = (y, Kz, -c(x)y).$$

For the case with zero background $c(x) = 0$, we have

$$\overrightarrow{V}(X) = (y, Kz, 0).$$

In all cases the level set equation takes the same form (A.18), in order to solve it we need to prepare initial data

$$\Phi|_{t=0} \quad = \quad \Phi_0(X).$$

Note that for the level set method the choice of initial data is not unique. But their zero level sets should uniquely embed the given initial data for u and E. Here we take

$$\phi_1(0, x, y, z) \quad = \quad y - u_0(x), \tag{A.19}$$

$$\phi_2(0, x, y, z) \quad = \quad z - E_0(x) \tag{A.20}$$

for smooth initial fields $u_0(x)$ and $E_0(x)$. Otherwise we need to use certain smoother reconstructions of the initial fields. We now discuss how to determine $E_0(x)$ from the given initial density $\rho_0(x)$ and the choice of $c(x)$.

(1)Non-zero background charge $c(x) \not\equiv 0$.

To be consistent with the Poisson equation, we assume that $E(x,0)$ satisfies $E_x(x,0) = \rho_0(x) - c(x)$. After integration of both sides in terms of x from $-\infty$ to x, we obtain

$$E(x,0) = \int_{-\infty}^{x} (\rho(\xi,0) - c(\xi))\, d\xi + C, \tag{A.21}$$

which is denoted as $E_0(x)$ for convenience. Using the conservation form, we have

$$\int_R (\rho(\xi,0) - c(\xi))\, d\xi = \int_R (\rho(\xi,t) - c(\xi))\, d\xi.$$

Without loss of generality, we set

$$\int_R (\rho(\xi,0) - c(\xi))\, d\xi = 0.$$

To be physically relevant, we should require $E_0(\pm\infty) = 0$. Thus we shall have $C = 0$ in (A.21), i.e.,

$$E(x,0) = \int_{-\infty}^{x} (\rho(\xi,0) - c(\xi))\, d\xi. \tag{A.22}$$

(2)Zero background charge $c(x) \equiv 0$.

In this case, the physical situation becomes quite different. As derived in Engelberg et al. (2001), the initial data for $E(x,t)$ in this case is determined by

$$E(x,0) = \frac{1}{2}\left(\int_{-\infty}^{x} \rho(\xi,0)d\xi - \int_{x}^{\infty} \rho(\xi,0)d\xi\right),$$

which satisfies $E(+\infty,0) = -E(-\infty,0)$, that is $E^2(+\infty,0) = E^2(-\infty,0)$. The later comes from the conservation of momentum, see Engelberg et al. (2001).

Discretization

The level set equation for cases described in previous sections all take the form

$$\Phi_t + \overrightarrow{V}(X) \cdot \nabla_X \Phi = 0, \quad t \in R^+, \quad X \in R^3 \tag{A.23}$$

subject to the initial condition

$$\Phi|_{t=0} \quad = \quad \Phi_0(X) \in R^2,$$

where $X = (x, y, z)$, denoting the field space, in which y indicates the velocity and z indicates the electric field, $\Phi_0(X) = (y - u_0(x), z - E_0(x))^\top$, and $\overrightarrow{V} = (V_1, V_2, V_3)$, depending only on X. (A.23) is a transport equation, so we may use an upwind method to solve it.

First Order Upwind Scheme

We partition the field space $(x, y, z) \in R^3$ into computation cells, centered at $\{(x_i, y_j, z_k)\}$ for $i, j, k \in \mathbb{Z}$. And, we use forward difference for time discretization. The choice of forward or backward difference of Φ_x,Φ_y and Φ_z depends on their coefficient functions. During the computation, uniform mesh is used. We use standard notation that

$$\Phi_x^+ = \frac{\Phi^n_{(i+1,j,k)} - \Phi^n_{(i,j,k)}}{\Delta x},$$
$$\Phi_x^- = \frac{\Phi^n_{(i,j,k)} - \Phi^n_{(i-1,j,k)}}{\Delta x},$$

and similar notations for Φ_y^+,Φ_y^-,Φ_z^+,Φ_z^-,Φ_t^+,Φ_t^-. Then we may obtain the following first order upwind scheme,

$$\frac{\Phi^{n+1}_{(i,j,k)} - \Phi^n_{(i,j,k)}}{\Delta t} + V_1(i,j,k)\Phi_x^\pm + V_2(i,j,k)\Phi_y^\pm + V_3(i,j,k)\Phi_z^\pm = 0, \tag{A.24}$$

where $\Phi^n_{(i,j,k)} \approx \Phi(t_n, x_i, y_j, z_k)$, and $V_m(i,j,k) = V_m(x_i, y_j, z_k)$, m=1,2,3. If $V_m(i,j,k) > 0$, we use Φ^-; otherwise, Φ^+ is applied. The CFL condition for this scheme is

$$\Delta t \max\left(\frac{|\, V_1 \,|}{\Delta x} + \frac{|\, V_2 \,|}{\Delta y} + \frac{|\, V_3 \,|}{\Delta z}\right) \leq 1. \tag{A.25}$$

In implementation, it is necessary to require that V_1,V_2,V_3 be bounded in computation domain in order to have finite Δt. Moreover, this is only a first order accuracy method, which may require finer grid to achieve high resolution. For stability concern, implicit or semi-implicit methods may also improve the results. Another fact is about re-initialization of the level set function. It is well known that general level set method requires re-initialization during the computation, consult Osher and Fedkiw (2003) for more details.

One important property for transport equations is the maximum principle. We now show that this property is well preserved in the first order upwind scheme.

Theorem 3.0.3. [Discrete Maximum Principle] Assume that $V_i(x,y,z)(i=1,2,3)$ are bounded functions in the computational domain. Let Φ^n be a numerical solution produced by the first order upwind scheme (A.24) subject to the initial data Φ^0, then

$$||\Phi^n||_\infty \leq ||\Phi^0||_\infty. \tag{A.26}$$

Proof. Denote

$$V_m^+ = \max(V_m(i,j,k),0) = \frac{|V_m(i,j,k)| + V_m(i,j,k)}{2},$$
$$V_m^- = \max(-V_m(i,j,k),0) = \frac{|V_m(i,j,k)| - V_m(i,j,k)}{2}$$

for all i,j,k in computation domain with m=1,2,3.

Then the upwind scheme can be rewritten as

$$\Phi_t^+ + V_1^+\Phi_x^- - V_1^-\Phi_x^+ + V_2^+\Phi_y^- - V_2^-\Phi_y^+ + V_3^+\Phi_z^- - V_3^-\Phi_z^+ = 0.$$

Further expanding all upwind partial derivatives, we obtain the following

$$\begin{aligned}\Phi^{n+1}_{(i,j,k)} = &\left(1-(V_1^+ + V_1^-)\frac{\Delta t}{\Delta x} - (V_2^+ + V_2^-)\frac{\Delta t}{\Delta y} - (V_3^+ + V_3^-)\frac{\Delta t}{\Delta z}\right)\Phi^n_{(i,j,k)} \\ &+V_1^+\frac{\Delta t}{\Delta x}\Phi^n_{(i-1,j,k)} + V_1^-\frac{\Delta t}{\Delta x}\Phi^n_{(i+1,j,k)} + V_2^+\frac{\Delta t}{\Delta y}\Phi^n_{(i,j-1,k)} \\ &+V_2^-\frac{\Delta t}{\Delta y}\Phi^n_{(i,j+1,k)} + V_3^+\frac{\Delta t}{\Delta z}\Phi^n_{(i,j,k-1)} + V_3^-\frac{\Delta t}{\Delta z}\Phi^n_{(i,j,k+1)}.\end{aligned} \tag{A.27}$$

Note that $V_m^+ + V_m^- = |V_m|$ for m=1,2,3. By the CFL condition (A.25), the coefficient of $\Phi^n_{(i,j,k)}$ is nonnegative, and coefficients of $\Phi^n_{(i\pm1,j,k)}, \Phi^n_{(i,j\pm1,k}, \Phi^n_{(i,j,k\pm1)}$, are all nonnegative too. Due to the positivity of all coefficients, when we take absolute value both sides and relax on the right-hand-side, we apply absolute sign only on $\Phi^n_{(i,j,k)}$,$\Phi^n_{(i\pm1,j,k)}$, $\Phi^n_{(i,j\pm1,k)}$, $\Phi^n_{(i,j,k\pm1)}$, which are all bounded by $|\Phi^n|$. Then, we obtain the following equation

$$\begin{aligned}||\Phi^{n+1}||_\infty &\leq (1-|V_1|\frac{\Delta t}{\Delta x} - |V_2|\frac{\Delta t}{\Delta y} - |V_3|\frac{\Delta t}{\Delta z})||\Phi^n||_\infty \\ &\quad +|V_1|\frac{\Delta t}{\Delta x}||\Phi^n||_\infty + |V_2|\frac{\Delta t}{\Delta y}||\Phi^n||_\infty + |V_3|\frac{\Delta t}{\Delta z}||\Phi^n||_\infty \\ &= ||\Phi^n||_\infty.\end{aligned}$$

Therefore, we obtain the stability estimate (A.26) as asserted. □

Remark 3. This conclusion holds for all bounded V_m with $m = 1, 2, 3$. Hence it is applicable to the level set equation for Euler-Poisson equations derived in previous sections.

We now turn to the L^1 stability. Define the numerical L^1 norm by

$$||\Phi^n||_1 = \sum_{i,j,k} |\Phi^n_{(i,j,k)}|\Delta x \Delta y \Delta z.$$

The L^1-stability can be stated in

Theorem 3.0.4. Assume that $V_i(x, y, z)(i = 1, 2, 3)$ are bounded and Lipschitz continuous in its i-th argument in the computational domain. Let Φ^n be a numerical solution produced by the first order upwind scheme (A.24) subject to the initial data Φ^0, then for finite time T, there exists a constant M, such that

$$||\Phi^n||_1 \leq e^{MT}||\Phi^0||_1. \tag{A.28}$$

Proof. Summation of equation (A.27) over all i, j, k, shifting the index of terms, $\Phi^n_{(i\pm1,j,k)}$,$\Phi^n_{(i,j\pm1,k)}$, and $\Phi^n_{(i,j,k\pm1)}$ leads to

$$\begin{aligned}\sum_{i,j,k} |\Phi^{n+1}_{(i,j,k)}| \leq \sum_{i,j,k} \Big(1 - (V_1^+ - V_1^+(i+1,j,k) + V_1^- - V_1^-(i-1,j,k)\Big) \frac{\Delta t}{\Delta x} \\ -(V_2^+ - V_2^+(i,j+1,k) + V_2^- - V_2^-(i,j-1,k))\frac{\Delta t}{\Delta y} \\ -(V_3^+ - V_3^+(i,j,k+1) + V_3^- - V_3^-(i,j,k-1))\frac{\Delta t}{\Delta z})|\Phi^n_{(i,j,k)}|.\end{aligned}$$

By assumption, there exist Lipschitz constants α_1,α_2, and α_3 such that

$$|V_1^\pm - V_1^\pm(i \pm 1, j, k)| \leq \alpha_1 \Delta x,$$

$$|V_2^\pm - V_2^\pm(i, j \pm 1, k)| \leq \alpha_2 \Delta y,$$

$$|V_3^\pm - V_3^\pm(i, j, k \pm 1)| \leq \alpha_3 \Delta z,$$

then

$$\sum_{i,j,k} |\Phi^{n+1}_{(i,j,k)}| \leq \sum_{i,j,k} (1 + 2(\alpha_1 + \alpha_2 + \alpha_3)\Delta t)|\Phi^n_{(i,j,k)}|.$$

Multiplying $\Delta x\Delta y\Delta z$ both sides, we obtain

$$\sum_{i,j,k}|\Phi^{n+1}_{(i,j,k)}|\Delta x\Delta y\Delta z \leq \sum_{i,j,k}(1+2(\alpha_1+\alpha_2+\alpha_3)\Delta t)|\Phi^{n}_{(i,j,k)}|\Delta x\Delta y\Delta z,$$

$$||\Phi^n||_1 \leq (1+M\Delta t)^n||\Phi^0||_1, \tag{A.29}$$

with $M = 2(\alpha_1+\alpha_2+\alpha_3)$. Moreover, in finite time T, $n = T/\Delta t$. We can simplify equation (A.29) further

$$||\Phi^n||_1 \leq e^{MT}||\Phi^0||_1, \tag{A.30}$$

as n tends to ∞. The proof is complete. □

Remark 4. This conclusion holds for all bounded and Lipschitz continuous V_m with $m = 1, 2, 3$. Hence it is applicable to level set equations for the Euler-Poisson system derived in previous sections.

Numerical Procedures

Now we highlight our algorithms for numerical simulations.

Step 1 Initialization and Discretization

First we give the initial data Φ at each grid point according to (A.19) and (A.20) with E_0 specified in §3. Then we discretize the computation domain $[a, b] \times [c, d] \times [e, f] \in R^3$ into uniform grid with fixed Δx, Δy, Δz.

Step 2 Solving Transport Equation (A.18)

During computation, the first order upwind scheme (A.24) is used. Meanwhile, both L^∞ and L^1 norms are computed. However, in reality second or higher order accurate method is generally preferred.

For second or higher order accuracy method, TVD Runge-Kutta methods may be employed for discretizing time, while Lax-Wendroff or ENO Harten (1987, 1989); Shu (1999)(WENO Jiang and Wu (1999); Montarnal and Shu (1999); Shu (1999))-type methods may be applied to variable {x,y,z}.

Step 3 Retrieving the Solution in Field Space

After we obtained Φ at desired time T, we may retrieve the solution through common zeros of two level set functions, ϕ_1 and ϕ_2. The projection of common zeros onto $x-u$ and $x-E$ spaces gives the visualizations of multi-valued $u(x,T)$ and $E(x,T)$.

Computational Experiments

In this section, we validate our level set methods with several numerical examples and compute both L^∞ and L^1 norms to demonstrate the stability. In the following experiments, the first order upwind scheme is employed.

Numerical test 1

We test the damping free model (A.6)-(A.8) with $\alpha = 0$, $c(x) = 0$, $K = 0.01$, and subject to the condition,

$$\begin{aligned} u(x,0) &= sin(x)|sin(x)|, \\ \rho(x,0) &= e^{-(x-\pi)^2/2\pi}. \end{aligned}$$

This data is used in Gosse and Markowich (2004), where the semiclassical approximation of the Schrödinger-Poisson equation is studied.

As stated in §3, for the case $c(x) = 0$, the initial value for $E(x,0)$ shall be given as

$$E(x,0) = \frac{1}{2}\left(\int_{-\infty}^{x} \rho(s,0)ds - \int_{x}^{\infty} \rho(s,0)ds\right).$$

The necessary and sufficient condition for existence of global smooth solution to the Euler-Poisson system (A.6)-(A.8) is $\partial_x u(x,0) > -\sqrt{2K\rho(x,0)}$, $\forall x \in R$, which is given in Engelberg et al. (2001). This condition is clearly violated, say for example at $x = \frac{3\pi}{4}$. Thus, the classical solution fails in finite time and develops into a multi-valued solution. Here we compute multi-valued $u(x,t)$ and $E(x,t)$ using the first order scheme (A.24) with $\Phi_0 = (y - u(x,0), z - E(x,0))^\top$. The numerical results are shown in Fig.3.1 for multi-valued u and E at time $t = 2.5$.

To check the L^∞ and L^1 stability for the scheme (A.24), we have calculated the L^∞ and L^1 norm for both ϕ_1 and ϕ_2 at $t = 0$ and $t = 2.5$ in Table 3.1. It is not hard to see in the table that the L^∞ and L^1 of ϕ_1 and ϕ_2 are both decreasing as time evolves. Thus the results of numerical experiments are consistent with the stability properties that we proved in Theorem 3.0.3 and 3.0.4 in Section 3.

Mesh	Φ	L^∞ at t=0	L^∞ at t=2.5	L^1 at t=0	L^1 at t=2.5
41×41×41	ϕ_1	2.00	1.83	39.26	37.29
	ϕ_2	4.15	4.14	87.77	79.87
61×61×61	ϕ_1	2.00	1.88	38.25	36.67
	ϕ_2	4.15	4.14	85.14	78.79
81×81×81	ϕ_1	2.00	1.91	37.75	36.41
	ϕ_2	4.15	4.14	83.85	78.39
101×101×101	ϕ_1	2.00	1.92	37.45	36.29
	ϕ_2	4.15	4.14	83.08	78.22

Table 3.1 The initial and end-time L^∞ and L^1 norms of Φ of semiclassical approximation of Schrödinger-Poisson equation

Numerical test 2

Here, we test the model (A.6)-(A.8) with $\alpha = 0$, $c(x) = 1$ and $K = 0.01$. The boundary condition is given as

$$u(0,t) = 1 + 0.2sin(5\pi t), \tag{A.31}$$

$$E(0,t) = 0. \tag{A.32}$$

This data was used in Li et al. (2004) in applications to electron beam propagation in Klystrons.

Before computation, we analyze this boundary value problem to see whether global smooth solution exists. Along the particle path $t = t(x)$, we define $\frac{dt}{dx} = \frac{1}{u}$ where $\frac{d}{dx} \triangleq \partial_x + \frac{1}{u}\partial_t$. From (A.10)-(A.12), we have

$$\frac{du}{dx} = K\frac{E}{u}, \tag{A.33}$$

$$\frac{dE}{dx} = -1. \tag{A.34}$$

By using (A.31), (A.32), we derive the following solution along characteristics,

$$u^2(x,t) = u^2(0,t) - Kx^2, \tag{A.35}$$

$$E(x,t) = -x. \tag{A.36}$$

Clearly there will be no smooth solution beyond

$$x > \sqrt{u^2(0,t)/K}. \tag{A.37}$$

Thus this boundary value problem shall develop a multi-valued solution in finite space marching.

Note that though this is a boundary value problem, a variation of the level set formulation above can still be applied. If we restrict our computation domain $(t, y, z) = (0, T) \times (a, b) \times (c, d)$ with $a > 0$, we can divide the level set equation (A.15) both sides by y to reach

$$\Phi_x + \frac{1}{y}\Phi_t + \frac{Kz}{y}\Phi_y - \Phi_z = 0.$$

Hence, we may apply our level set formulation regarding space variable x as a marching parameter with computation domain for variables (t, y, z).

Now we discuss how to determine the computation domain by using characteristic curves. By (A.35) and (A.36), we have the relation that

$$u^2 + KE^2 = u^2(0,t). \tag{A.38}$$

Along with the initial condition (A.31), (A.32), we can roughly determine the range of u and E as $(0.7, 1.3) \times (-2, 2)$.

Fig.3.2 presents the overturn beyond the critical location at $x = 1$ as predicted in (A.37). On the other hand, we know from section 3, our scheme has both L^∞ and L^1 stability, which we can observe numerically in Table 3.2.

Numerical test 3

Now, we test the model (A.6)-(A.8) with $\alpha = 0$, $K = 0.01$, and subject to condition,

$$u(x,0) = 0.3sin(x),$$

$$\rho(x,0) = 0.3e^{-(x-\pi)^2/\pi}.$$

Mesh	Φ	L^∞ at x=0	L^∞ at x=1	L^1 at x=0	L^1 at x=1
41×41×41	ϕ_1	0.50	0.44	0.19	0.16
	ϕ_2	2.00	1.33	1.06	0.79
61×61×61	ϕ_1	0.50	0.45	0.19	0.16
	ϕ_2	2.00	1.42	1.03	0.81
81×81×81	ϕ_1	0.50	0.46	0.18	0.17
	ϕ_2	2.00	1.48	1.01	0.83
101×101×201	ϕ_1	0.50	0.46	0.18	0.16
	ϕ_2	2.00	1.65	0.99	0.88

Table 3.2 The initial and end-time L^∞ and L^1 norms of Φ for modulated electron beam in a klystron

The initial data is used in Gosse and Markowich (2004), where the author studied the semi-classical approximation of the Schrödinger-Poisson equation of self-consistent electron cloud within Mathieu's potential.

Since $c(x) = 0$, the initial value for $E(x, 0)$ is determined by

$$E(x,0) = \frac{1}{2}\left(\int_{-\infty}^{x} \rho(s,0)ds - \int_{x}^{\infty} \rho(s,0)ds\right).$$

As predicted in Engelberg et al. (2001), this kind of system supports critical threshold phenomena, and subcritical initial data will develop singularity in finite time. And in this example, the classical solution does fail in finite time and hence multi-valued solutions should be computed to achieve the physically relevant solution. In Fig.3.3, we observe that the velocity develops overturns at around $x = 2.2$ and $x = 3.8$. Once again, we have included the L^∞ and L^1 norm in Table 3.3 to show the L^∞ and L^1 stability numerically.

Numerical test 4

Now, we test the model (A.6)-(A.8) with $\alpha = 0.01$, $K = 0.01$, and

$$c(x) = \begin{cases} 0.5, & x \in [-1, 1] \\ 0, & otherwise. \end{cases}$$

$Mesh$	Φ	L^∞ at t=0	L^∞ at t=5	L^1 at t=0	L^1 at t=5
61×41×41	ϕ_1	0.70	0.68	1.39	1.34
	ϕ_2	0.97	0.96	2.03	1.90
81×61×61	ϕ_1	0.70	0.69	1.36	1.31
	ϕ_2	0.97	0.96	1.98	1.87
101×81×81	ϕ_1	0.70	0.69	1.34	1.30
	ϕ_2	0.97	0.96	1.95	1.86
121×101×101	ϕ_1	0.70	0.69	1.33	1.30
	ϕ_2	0.97	0.96	1.94	1.85

Table 3.3 The initial and end-time L^∞ and L^1 norms of Φ of semiclassical approximation of Schrödinger-Poisson equation

The initial condition is

$$\begin{aligned} u(x,0) &= cos(x+0.15), \\ \rho(x,0) &= \frac{1}{2\sqrt{\pi}}\left(e^{-(x+\pi/2)^2}+e^{-(x-\pi/2)^2}\right). \end{aligned}$$

Since $c(x) \neq 0$, the initial value for $E(x,0)$ of Euler-Poisson equations with background shall be given as

$$E(x,0) = \int_{-\infty}^{x} (\rho(s,0)ds - c(s))\, ds.$$

From the Fig.3.4, we observe that the solution develops overturn before $t = 1.4$, which shows that our method captures the multi-valued solution. The sharp corner of E at time $t = 1.4$ is caused by sharp corner of initial value of E. And in Table 3.4, we show the L^∞ and L^1 stability numerically.

Conclusion

We introduce a new level set method for computing multi-valued velocity and electric fields for 1D Euler-Poisson equations. The proposed method is built upon a new level set formulation in an extended space—field space. The multi-valued fields are computed by evolving the same linear transport equation with smooth initial data $(y - u_0(x), z - E_0(x))$. The projection of common zeros of two computed level set functions enables us to obtain the sharp result

$Mesh$	Φ	L^∞ at t=0	L^∞ at t=2	L^1 at t=0	L^1 at t=2
81×51×51	ϕ_1	2.50	2.37	36.94	35.42
	ϕ_2	1.39	1.39	21.11	18.92
101×51×51	ϕ_1	2.50	2.38	36.84	35.37
	ϕ_2	1.39	1.39	21.06	18.96
101×8 1×61	ϕ_1	2.50	2.38	36.27	34.93
	ϕ_2	1.39	1.39	20.78	18.83
301×151×101	ϕ_1	2.50	2.44	35.42	34.53
	ϕ_2	1.39	1.39	20.27	18.87

Table 3.4 The initial and end-time L^∞ and L^1 norms of Φ of semiclassical approximation of Schrödinger-Poisson equation

efficiently. Moreover, both the L^∞ and L^1 stability for first-order upwind schemes of the level set equation are established. Compared to moment methods based on the Vlasov-Poisson equation introduced in Li et al. (2004), our approach automatically computes multi-valued fields that occur in the system, and the method in Li et al. (2004) gives, instead, averaged density and other moments. The computation of density and other physical quantities based on the level set method introduced here is under our current study and will appear in Liu and Wang (2007b).

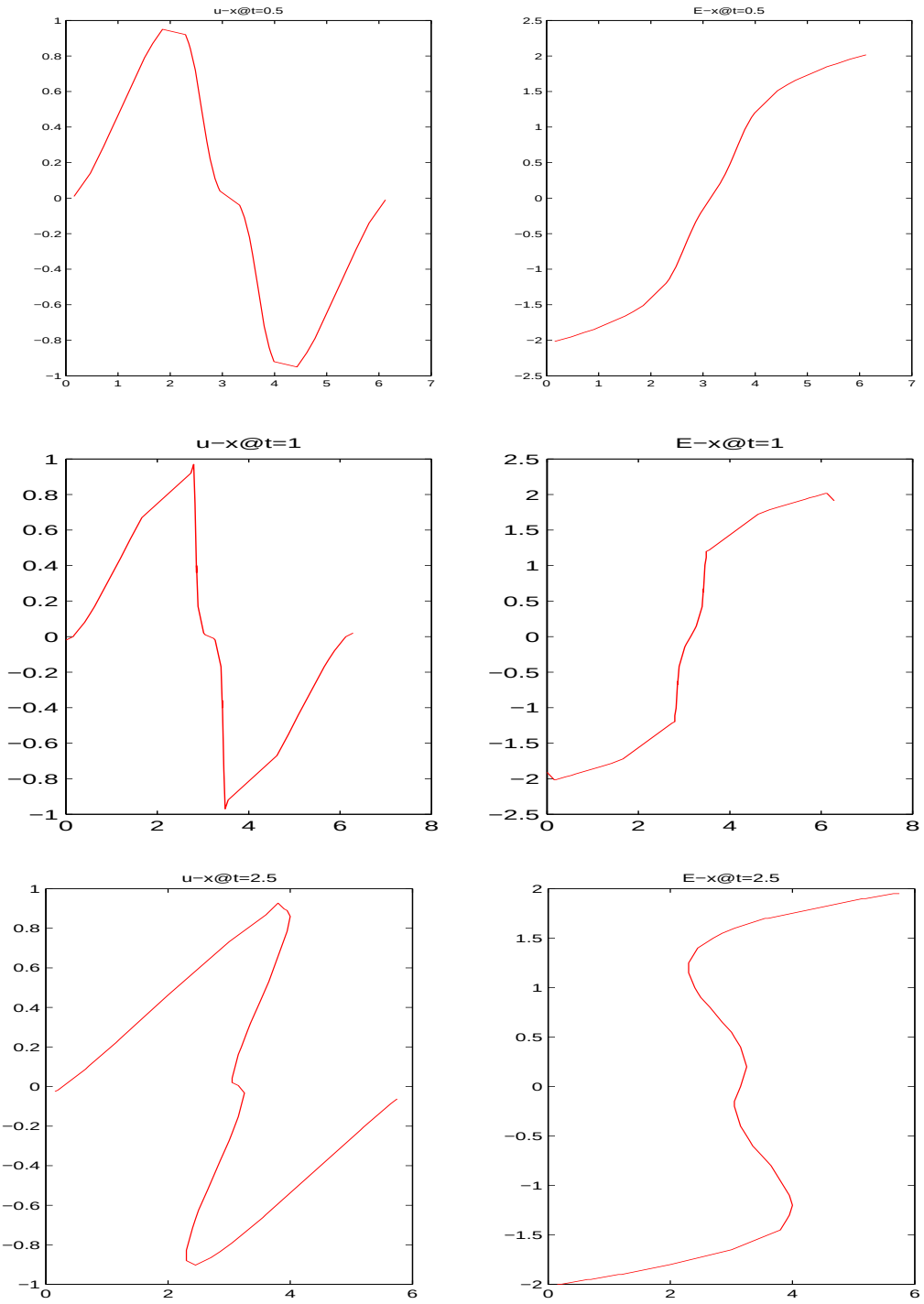

Figure 3.1 u(x,t) and E(x,t) for Euler-Poissons equations from the semiclassical approximation of Schrödinger-Poisson equation at time $t = 0.5$, 1, 2.5 from top to bottom respectively.

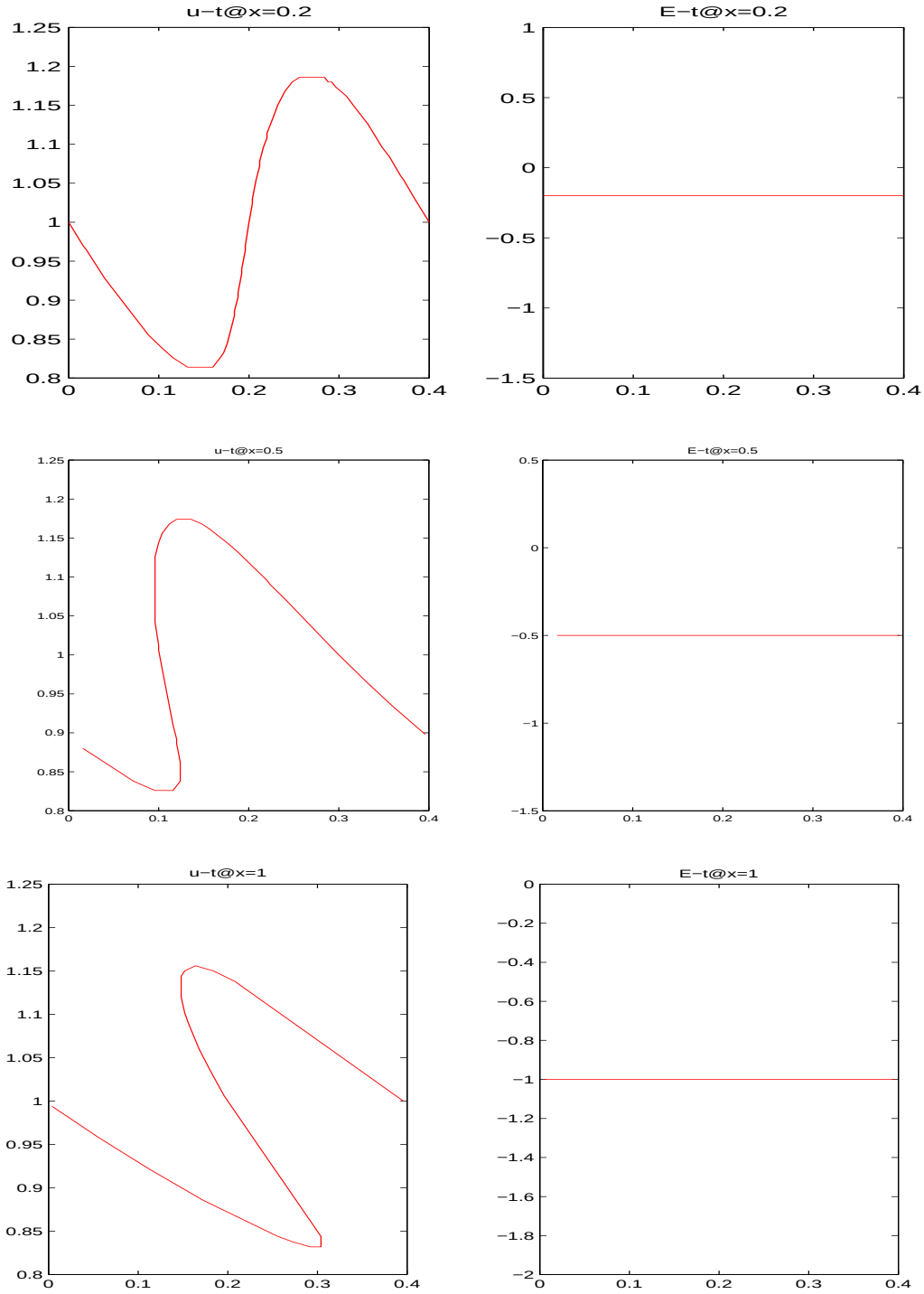

Figure 3.2 u(x,t) and E(x,t) for Euler-Poisson equations of model for modulated electron beam in a klystron at position $x = 0.2, 0.5, 1$ from top to bottom respectively

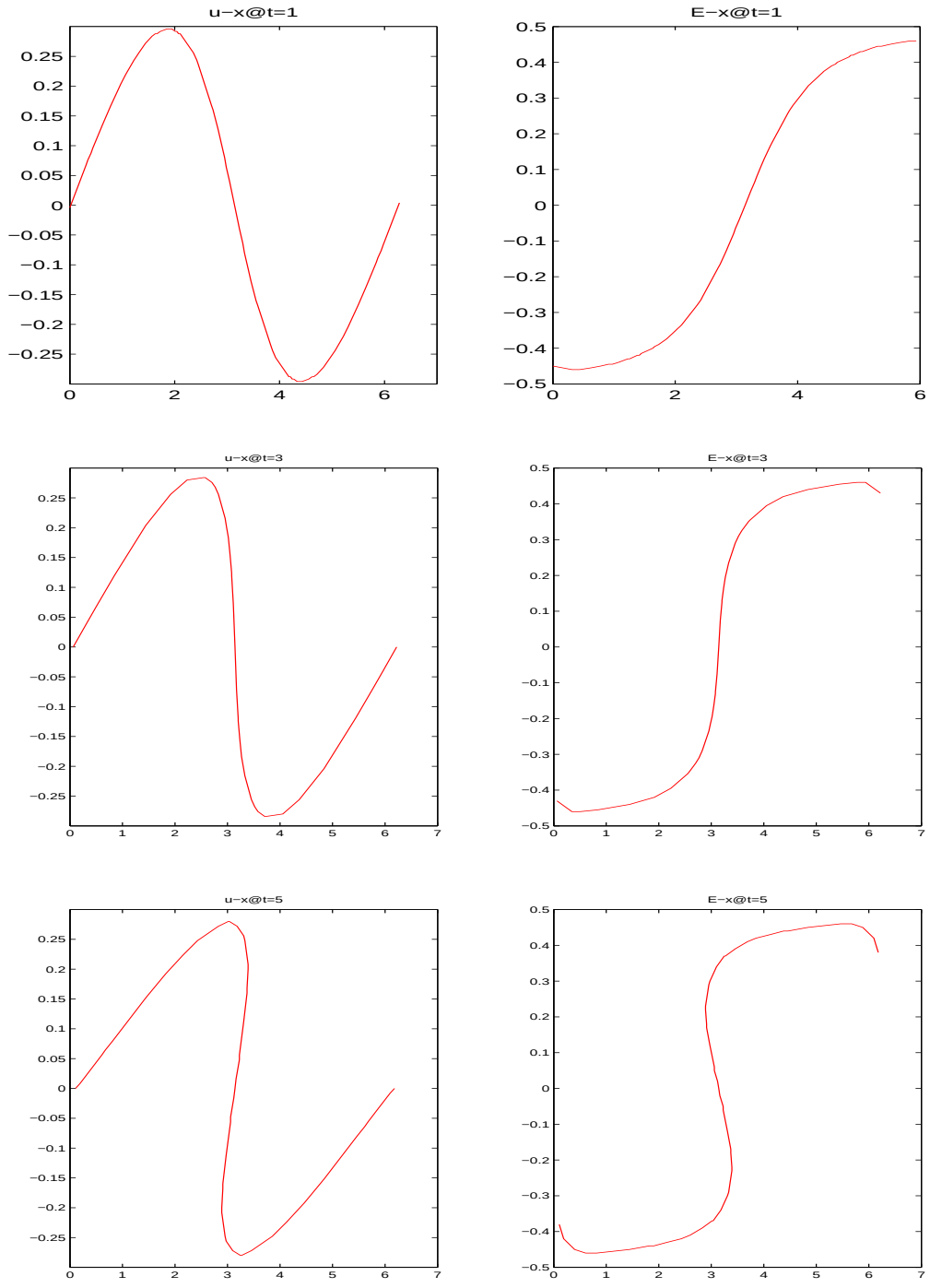

Figure 3.3 u(x,t) and E(x,t) for Euler-Poisson equations from the semiclassical approximation of Schrödinger-Poisson equation at time $t = 1, 3, 5$ from top to bottom respectively.

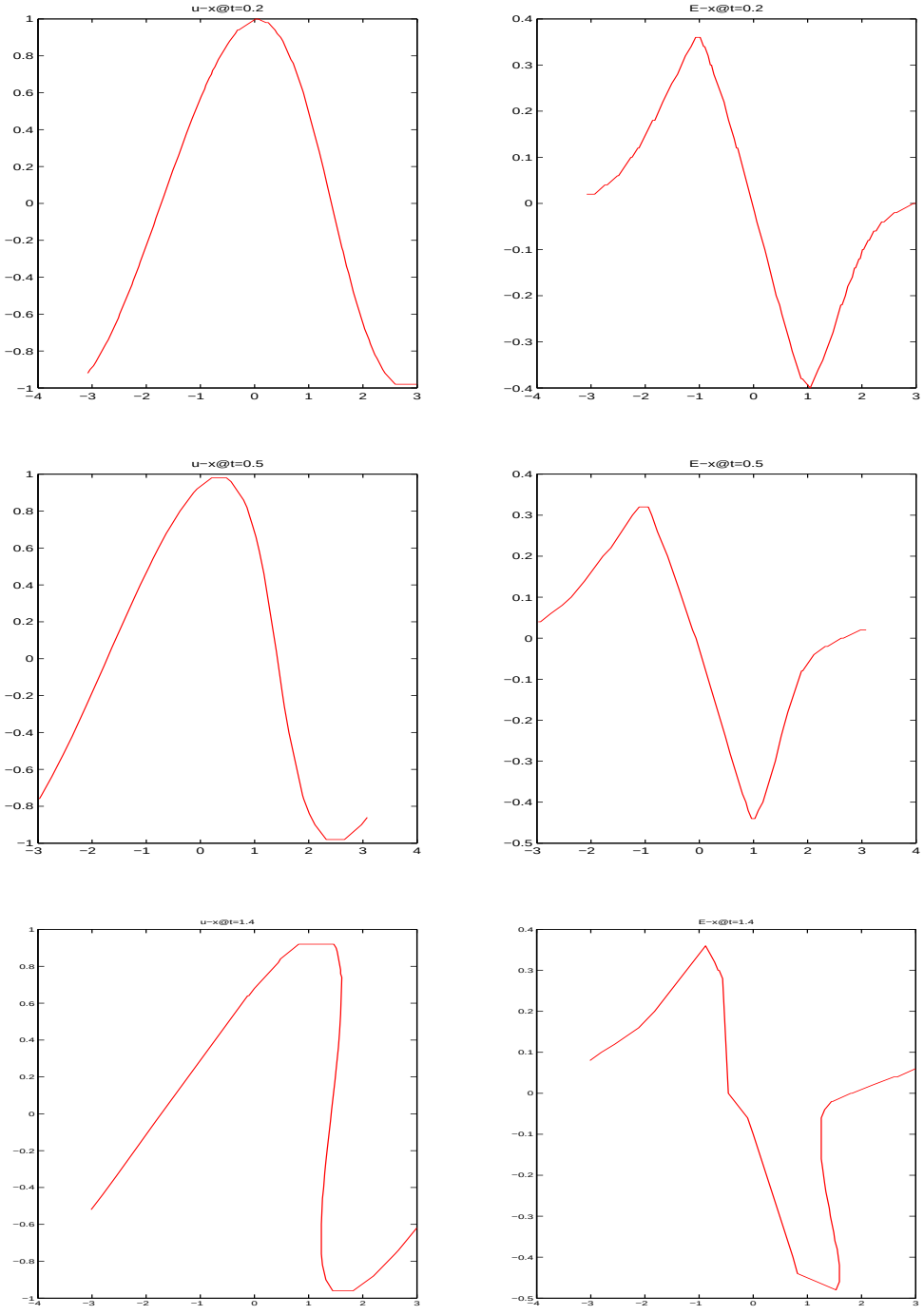

Figure 3.4 u(x,t) and E(x,t) for Euler-Poisson equations from the semiclassical approximation of Schrödinger-Poisson equation at time $t = 0.2$, 0.5, 1.4 from top to bottom respectively.

CHAPTER 4. A FIELD SPACE-BASED LEVEL SET METHOD FOR COMPUTING MULTI-VALUED SOLUTIONS TO 1D EULER-POISSON EQUATIONS

A paper published in Journal of Computational Physics

Hailiang Liu,Zhongming Wang

Abstract

We present a field space based level set method for computing multi-valued solutions to one-dimensional Euler-Poisson equations. The system of these equations has many applications, and in particular arises in semiclassical approximations of the Schrödinger-Poisson equation. The proposed approach involves an implicit Eulerian formulation in an augmented space — called field space, which incorporates both velocity and electric fields into the configuration. Both velocity and electric fields are captured through common zeros of two level set functions, which are governed by a field transport equation. Simultaneously we obtain a weighted density f by solving again the field transport equation but with initial density as starting data. The averaged density is then resolved by the integration of the obtained f against the Dirac delta-function of two level set functions in the field space. Moreover, we prove that such obtained averaged density is simply a linear superposition of all multi-valued densities; and the averaged field quantities are weighted superposition of corresponding multi-valued ones. Computational results are presented and compared with some exact solutions which demonstrate the effectiveness of the proposed method.

Introduction

The aim of this paper is to introduce a new field space based level set method for computing multi-valued solutions to the Euler-Poisson system

$$\partial_t \rho + \partial_x(\rho u) = 0, \quad x \in \mathbb{R},\ t > 0, \tag{4.1}$$

$$\partial_t u + u\partial_x u = KE, \tag{4.2}$$

$$\partial_x E = \rho - c(x). \tag{4.3}$$

These are equations of conservation of mass, Newton's second law, and the Poisson equation, respectively. Here K is a physical constant, which indicates the property of forcing, i.e., repulsive when $K > 0$ and attractive when $K < 0$. And $\rho = \rho(t, x)$ is the local density, $u = u(t, x)$ is the mean velocity field, $E = E(t, x)$ is the electric field, and $c(x)$ is the background charge profile.

The Euler-Poisson system arises in many physical problems such as fluid dynamics, plasma dynamics, gaseous stars, quantum gravity and semiconductors, etc. As is known, the simple one-dimensional unforced inviscid Burgers' solution always forms a shock discontinuity, except for the non-generic case of increasing initial profile, $u_0' \geq 0$. In contrast, it was shown in Engelberg et al. (2001) that the corresponding Euler-Poisson system has global smooth solutions as long as its initial configuration is above a critical threshold, allowing a finite, negative velocity gradient. It was also shown for a sub-critical set of initial data, solutions of the Euler-Poisson system will develop singularity at a finite time. For Euler-Poisson equations, beyond singularity generalized solutions need to be chosen and interpreted to reflect the physical relevance. In some applications such as in fluid dynamics, a shock will develop after the singularity formation. But in other applications such as the semiclassical approximation of the Schrödinger-Poisson equation and the wave breaking in Klystrons Li et al. (2004), one must allow multi-valued solutions in order to capture physically relevant phenomena. The usual shock-capturing methods for computing entropy solutions do not give desired results.

The main goal in this work is to develop a novel level set method for computing multi-valued solutions to 1D Euler-Poisson equations. Previously in Liu and Wang (2007a) we have

identified a configuration space to unfold the multi-valuedness in both velocity and electric fields. This extended configuration space from the usual phase space is hence termed as the field space. In this work we further derive a procedure to evaluate multi-valued density and field quantities.

Our approach can be summarized as follows: we use a vector level set function $\Phi = (\phi_1, \phi_2)^\top \in \mathbb{R}^2$ in field space $(x, p, q) \in \mathbb{R}^3$ with $p = u(t, x)$ and $q = E(t, x)$ to describe dynamics of the 1-D Euler-Poisson system (4.1)-(4.3). The vector level set function $\Phi = \Phi(t, x, p, q)$ is shown to satisfy the field transport equation

$$\partial_t \Phi + p\partial_x \Phi + Kq\partial_p \Phi - c(x)p\partial_q \Phi = 0.$$

The zero level set of this vector function, initiated as

$$\Phi_0(x, p, q) := (p - u_0(x), q - E_0(x))^\top,$$

forms a one-dimensional manifold in field space $(x, p, q) \in \mathbb{R}^3$: the interaction of two 2-D manifolds $\{\phi_1 = 0\} \cap \{\phi_2 = 0\}$. This gives implicitly multi-valued velocity and electric fields through

$$(u, E) \in \{(p, q) | \quad \Phi(t, x, p, q) = 0\}.$$

Note that Φ as a solution of the field transport equation is bounded in any domain where the initial velocity and electric fields are bounded.

We evaluate the density function by simultaneously solving the field transport equation for a new quantity f near $\{(x, p, q);\ \Phi = 0\}$ but with initial density as starting data, i.e.,

$$\partial_t f + p\partial_x f + Kq\partial_p f - c(x)p\partial_q f = 0,$$
$$f(0, x, p, q) = \rho_0(x).$$

The averaged density is thus resolved by the integration of f against the Dirac delta-function of two level set functions in field space,

$$\bar{\rho}(t, x) = \int_{\mathbb{R}^2_{p,q}} f(t, x, p, q)\delta(\phi_1)\delta(\phi_2)dpdq.$$

We prove that such obtained averaged density is simply a linear superposition of all multi-valued densities, i.e.,

$$\bar{\rho}(t,x) = \sum_{i=1}^{N} \rho_i(t,x). \tag{4.4}$$

Moreover, the averaged velocity and electric fields can be further evaluated by

$$\overline{u} = \frac{\int_{\mathbb{R}^2} pf\delta(\phi_1)\delta(\phi_2)dpdq}{\bar{\rho}}, \tag{4.5}$$

$$\overline{E} = \frac{\int_{\mathbb{R}^2} qf\delta(\phi_1)\delta(\phi_2)dpdq}{\bar{\rho}}. \tag{4.6}$$

Regarding these two averaged quantities we have

$$\overline{u} = \frac{\sum_{i=1}^{N} u_i(t,x)\rho_i(t,x)}{\bar{\rho}}, \tag{4.7}$$

$$\overline{E} = \frac{\sum_{i=1}^{N} E_i(t,x)\rho_i(t,x)}{\bar{\rho}}, \tag{4.8}$$

where (u_i, E_i) are multi-valued fields determined from our level set method.

We note that the Euler-Poisson system can be regarded as a semiclassical approximation of the nonlinear Schrödinger-Poisson equation

$$i\epsilon\partial_t\psi^\epsilon = -\frac{\epsilon^2}{2}\partial_x^2\psi^\epsilon + KV^\epsilon\psi^\epsilon, \quad x \in \mathbb{R}, \quad t \geq 0, \tag{4.9}$$

$$\partial_x^2 V^\epsilon = c(x) - |\psi^\epsilon|^2, \tag{4.10}$$

where $\psi^\epsilon(\cdot,t)$ is a complex-valued wave function depending on the scaled Planck constant ϵ, with K being a scaled physical constant. This equation has been studied in different contexts, and in particular, as the fundamental equation in semiconductor applications, with $c > 0$ standing for the doping profile and $K \sim \lambda^{-2}$, λ being the Debye number, consult Gasser et al. (2001) and references therein.

The electric field is determined by $E = -V_x$. Seeking the WKB-type solution of the form

$$\psi = \sqrt{\rho(t,x)}\exp(iS(t,x)/\epsilon),$$

we recover, to the leading order when $\epsilon \ll 1$, the Euler-Poisson system (4.1)-(4.3) for $(\rho, u = S_x)$. We should mention that for one dimensional case the passage from the Schrödinger-Poisson equation to the Euler-Poisson equation was proved in Liu and Tadmor (2002) for a

set of sub-critical initial data, and the passage from the Schrödinger-Poisson equation to the Vlasov-Poisson equation was proved in Zhang et al. (2002) for more general initial data, see also Lions and Paul (1993); Markowich and Mauser (1993) for earlier works.

For the Euler-Poisson system (4.1)-(4.3) alone, the authors in Engelberg et al. (2001) showed that for $K > 0$ and $c(x) = 0$, the EP system (4.1)-(4.3) admits a global smooth solution if and only if

$$u_0'(\alpha) > -\sqrt{2K\rho_0(\alpha)}, \quad \forall \alpha \in \mathsf{IR}.$$

Moreover,

$$\rho(x(\alpha,t)) = \frac{\rho_0(x)}{\Gamma(\alpha,t)}, \quad \Gamma(\alpha,t) := 1 + u_0'(\alpha)(t) + \frac{K}{2}\rho_0(\alpha)t^2. \tag{4.11}$$

If the initial slope of u_0 is too negative, then the solution will breakdown at a finite time t_c,

$$t_c = \min_\alpha\{t, \quad \Gamma(\alpha,t) = 0\},$$

beyond which multi-valued solutions should be sought. For the case of $K > 0$ and $c(x) = const > 0$, the critical regularity condition becomes

$$|u_0'(\alpha)| < \sqrt{K(2\rho_0(\alpha) - c)}, \quad \forall \alpha \in \mathsf{IR}.$$

Interestingly, if electric force becomes repulsive $K < 0$, the critical regularity condition reads

$$u_0'(\alpha) \geq \left(1 - \frac{\rho_0(\alpha)}{c}\right)\sqrt{-cK}, \quad \forall \alpha \in \mathsf{IR}.$$

We note that parameterized solutions along particle trajectory remains valid if multi-valued solutions are considered. The solution formulas and the blowup time estimates obtained in Engelberg et al. (2001) provide us a valuable guide when we check the accuracy and validity of our methods using various testing examples.

We also note that previously in Li et al. (2004) the authors evaluated averaged density of an Euler-Poisson system in Klystrons with a quite different approach, using Vlasov-Poisson equations in phase space to interpret the multi-valued solutions. We comment on this in §4. We refer to Gosse and Markowich (2004); Gosse and Mauser (2006a) for multi-phase semiclassical approximation of an electron in a 1D crystalline lattice using the K-branch solution approach Brenier and Corrias (1998).

From a broader perspective, numerical capturing of multi-valued solutions is important in many applications. Examples are the computation of dispersive waves Flaschka et al. (1980); Lax and Levermore (1983a,b,c); Whitham (1974), optical waves Cockburn et al. (2005); Engquist and Runborg (1996, 2003); Gosse (2002); Leung et al. (2004); Osher et al. (2002); Runborg (2000), seismic waves Fomel and Sethian (2002); Symes and Qian (2003); Trier and Symes (1991), semiclassical limits of Schrödinger equations Cheng et al. (2003); Gosse et al. (2003); Jin and Li (2003); Sparber et al. (2003), electron beam modulation in vacuum electronic devices Hutter (1960); Li et al. (2004), etc. In these applications when the wave field is highly oscillatory, direct numerical simulation of the wave dynamics can be prohibitively costly, and approximate models for wave propagation must be used. The resulting approximate models are often nonlinear, and classical entropy-type solutions are not adequate in describing the wave behavior beyond the singularity, where multi-valued solutions in physical space should be sought. Techniques that have been suggested in literature include ODE based Lagrangian methods, nonlinear Hamilton-Jacobi equation-based Eulerian methods.

A recent approach for improving physical space-based Eulerian methods is the use of a kinetic formulation in the phase space, consult Brenier and Corrias (1998); Engquist and Runborg (1996) for its early use in the context of multi-phase computation for optical waves. There is, however, a serious drawback with direct numerical approximations of the kinetic equation which is the need for a large set of independent variables in the phase space. To remedy this problem, two ways are suggested in the literature. One is the moment method, which is based on reducing the number of independent variables by introducing equations for moments, see e.g., Brenier and Corrias (1998); Engquist and Runborg (1996); Gosse et al. (2003); Jin and Li (2003); Runborg (2000). The other is based on computations of special wave front solutions. For tracking wave fronts in geometric optics, geometry based methods in phase space such as the segment projection method Engquist et al. (2002) and the level set method Cheng et al. (2004); Osher et al. (2002) have been recently introduced. Consult the seminal survey article Engquist and Runborg (2003) for recent development of computational high frequency wave propagation.

More recently, with a geometric point view in place of the kinetic one in phase space, a new level set method framework has been developed for computing multi-valued phases and other physical observables in the entire physical domain in Cheng et al. (2003); Jin and Osher (2003); Liu et al. (2005); Jin et al. (2005c,a). The effective equations which have been studied include general nonlinear first-order equations Liu et al. (2005) and weakly coupled WKB systems of the form

$$\partial_t S + H(x, \nabla_x S) = 0, \quad \partial_t \rho + \nabla_x \cdot (\rho \nabla_k H(x, \nabla_x S)) = 0,$$

with applications in the semiclassical approximation of Schrödinger equations ($H = \frac{1}{2}|k|^2 + V(x)$)Cheng et al. (2003); Jin et al. (2005c), geometrical optics limit of the wave equation ($H = c(x)|k|$) Jin et al. (2005a); Qian et al. (2003). We note that for first order quasi-linear hyperbolic equations, the level set formulation based on graph evolution was known much earlier, see e.g.,Courant and Hilbert (1962). We also refer to Cheng (2006); Cockburn et al. (2005); Leung et al. (2004); Qian et al. (2003) for various developments of the phase space based level set method applied to the geometric optics. The use of level set formulation for computing discontinuous solutions to Hamilton-Jacobi equations is proposed in Tsai et al. (2003). We refer to the recent review article Jin et al. (2005b) for the level set method and multi-valued solutions in computational high frequency wave propagation.

However, in the Euler-Poisson system (4.1)-(4.3) the second equation for velocity u couples with the Poisson equation (4.3), hence phase space-based level set methods introduced previously do not apply. The main novelty of our approach in this work is the use of field space in which the Lagrangian manifold is identified by $\Phi = 0$ and the dynamics of the Euler-Poisson system can be recast into a closed characteristic system along the particle trajectory in field space. Then the level set equation is just a transport equation with speed determined by the vector field of the characteristic system. Multi-valued velocity and electric fields are thus resolved as common zeros of two level set functions initiated as $(p - u_0(x))$ and $(q - E_0(x))$, respectively. A postprocessing step described above enables us to evaluate the density and other physical observables.

The rest of this paper is organized as follows. In §2 we describe the field space method

and level set formulations introduced in Liu and Wang (2007a), which are crucial ingredients for evaluating the density. §3 is devoted to a derivation of the field transport equation for a new quantity f as well as the justification of the integration procedure for computing the density. In §4 linear superposition principle for multi-valued ρ is proved; Averaged field quantities are also shown to be a weighted superposition of corresponding multi-valued ones. In §5 we discuss generalizations and possible connections with kinetic equations as well as the Schrödinger-Poisson equation. In §5 we present detailed numerical procedures for implementing the proposed method. Finally in §6 we describe the numerical strategy explored in this paper and present some numerical results to verify the capacity of our method.

Level Set Equation in Field Space

We recall the level set formulation derived in Liu and Wang (2007a) for computing multi-valued velocity and electric fields for 1D Euler-Poisson equations (4.1)-(4.3), subject to the following initial conditions

$$\rho(0,x) = \rho_0(x), \quad u(0,x) = u_0(x). \tag{4.12}$$

In this model, $c(x) \geq 0$ denotes the fixed positively charged background, i.e. the doping profile in semiconductor modeling Markowich et al. (1990). The initial electric field can be determined from the density, but in different way for cases, $c \neq 0$ and $c \equiv 0$, respectively.

As shown in Engelberg et al. (2001), for Euler-Poisson equations, only a subset of initial configurations leads to global smooth solutions. For subcritical initial data the classical solution will fail at finite time when particle trajectory collides. As pointed out in §1 beyond the singularity we are going to adopt and compute multi-valued solutions.

In order to capture multi-valued fields, we advocate a new method based on level set formulations in an augmented space. The augmented space we are taking is $(x,p,q) \in \mathbb{R}^3$ with $p = u$ and $q = E$, called the *field space* since it incorporates both velocity and electric fields. Instead of looking for explicit solutions in field space, we are seeking implicit solutions identified as a common zero of two implicit functions, in which multi-valued velocity and electric fields are implicitly represented.

We now sketch one derivation of the level set formulation by employing the given Euler-Poisson system. It is known that the electric field E satisfies a forced transport equation, see Guo (1998); Liu and Wang (2007a),

$$E_t + uE_x = -c(x)u. \tag{4.13}$$

Let $\Phi(t,x,p,q) \in \mathsf{IR}^2$ be a vector function and its Jacobian matrix $\det\left(\frac{\partial\Phi(t,x,p,q)}{\partial(p,q)}\right) \neq 0$, the implicit function theorem suggests that $\Phi(t,x,p,q) = 0$ may determine two functions $p = p(x,t)$ and $q = q(x,t)$, at least locally where the Jacobian matrix is nonsingular. Let $p = u(x,t)$ and $q = E(x,t)$ be a solution of the Euler-Poisson system, we thus obtain

$$\Phi(t,x,u(t,x),E(t,x)) \equiv 0, \quad (x,t) \in \mathsf{IR} \times \mathsf{IR}^+. \tag{4.14}$$

Differentiation of (4.14) with respect to t and x respectively gives

$$\begin{aligned} \Phi_t + \Phi_p u_t + \Phi_q E_t &= 0, \\ \Phi_x + \Phi_p u_x + \Phi_q E_x &= 0. \end{aligned}$$

Multiplying u to the second equation and adding to the first one results in the following

$$\Phi_t + u\Phi_x + (u_t + uu_x)\Phi_p + (E_t + uE_x)\Phi_q = 0.$$

Applying $u = p$, $u_t + uu_x = KE$, and $E_t + E_x u = -c(x)u$ to the above equation, we obtain

$$\Phi_t + p\Phi_x + Kq\Phi_p - c(x)p\Phi_q = 0. \tag{4.15}$$

Note that this transport equation can also be written as in conservative form

$$\Phi_t + (p\Phi)_x + (Kq\Phi)_p - (c(x)p\Phi)_q = 0,$$

since the divergence of the velocity field in (x,p,q) space is null.

The initial conditions of (4.15) can be chosen as

$$\phi_1(0,x,p,q) = p - u_0(x), \tag{4.16}$$

$$\phi_2(0,x,p,q) = q - E_0(x). \tag{4.17}$$

Note that the choice of initial condition is not unique. However the zero sets of selected level set functions should uniquely embed the given initial data u_0 and E_0.

As argued in Engelberg et al. (2001) based on the physical principle, $E_0(x)$ needs to be determined from $\rho_0(x)$ according to whether the background charge is present. For $c \neq 0$, the electric field is given by

$$E(0,x) = \int_{-\infty}^{x} (\rho(\xi,0) - c(\xi))\, d\xi, \tag{4.18}$$

and for $c \equiv 0$:

$$E(0,x) = \frac{1}{2}\left(\int_{-\infty}^{x} \rho(\xi,0)d\xi - \int_{x}^{\infty} \rho(\xi,0)d\xi\right). \tag{4.19}$$

Evaluation of Density

Equipped with the obtained level set formulation for both velocity and electric fields in field space $(x,p,q) \in \mathsf{IR}^3$, we now introduce an approach for capturing the multi-valued density ρ. Note that the density ρ formally solves the mass equation in the physical space $(t,x) \in \mathsf{IR}^+ \times \mathsf{IR}$,

$$\partial_t \rho + u\partial_x \rho = -\rho u_x.$$

When the velocity field is multi-valued, the density is forced to become multi-valued too. Note that along the particle trajectory $x = x(t,\alpha)$, governed by $\frac{d}{dt}x = u(t,x)$ with $x(0) = \alpha \in \mathsf{IR}$, we have

$$\rho(t, x(t,\alpha)) = \frac{\rho_0(\alpha)}{\Gamma(t,\alpha)},$$

where $\Gamma(t,\alpha) = \partial_\alpha x(t,\alpha)$ indicates the deformation of particle trajectories. The density would become unbounded at the instant t_c, $\Gamma(t_c,\alpha) = 0$, when the velocity field starts to become multi-valued. This difficulty makes a direct computation of ρ unrealistic.

The strategy is to first derive an evolution equation for a density representative in field space (x,p,q), and then project it onto the 1D Lagrangian manifold expressed implicitly by $\{(x,p,q)|\quad \Phi = 0\}$, involving both velocity and electric fields.

Let $\tilde{\rho}(t,x,p,q)$ be a representative of $\rho(t,x)$ in field space, i.e.,

$$\rho(t,x) \equiv \tilde{\rho}(t,x,u(t,x),E(t,x)).$$

We thus have

$$\begin{aligned}
&\partial_t\rho + u\partial_x\rho \\
&= \partial_t\tilde{\rho} + u_t\partial_p\tilde{\rho} + E_t\partial_q\tilde{\rho} + u(\partial_x\tilde{\rho} + u_x\partial_p\tilde{\rho} + E_x\partial_q\tilde{\rho}) \\
&= [\partial_t + u\partial_x + (u_t + uu_x)\partial_p + (E_t + uE_x)\partial_q]\tilde{\rho}.
\end{aligned}$$

Using the equation (4.2) and (4.13) we have

$$\partial_t\rho + u\partial_x\rho = \partial_t\tilde{\rho} + u\partial_x\tilde{\rho} + KE\partial_p\tilde{\rho} - c(x)u\partial_q\tilde{\rho}.$$

Hence the density equation in the field space follows:

$$L\tilde{\rho} = -\tilde{\rho}\partial_x u, \tag{4.20}$$

where the field transport operator is defined as

$$L := \partial_t + p\partial_x + Kq\partial_p - c(x)p\partial_q.$$

The above observation, also true for other quantities, is summarized in the following

Lemma 4.0.1. *Let $\tilde{w}(t,x,p,q)$ be a representative of $w(t,x)$ in field space such that*

$$w(t,x) = \tilde{w}(t,x,u(t,x),E(t,x)).$$

Then

$$\partial_t w + u\partial_x w = L\tilde{w}(t,x,p,q).$$

From (4.20), we still need to evaluate u_x in field space in terms of the level set function Φ. To this end we differentiate the level set equation, $L\Phi = 0$, with respect to p and q respectively and obtain

$$\begin{aligned}
L(\partial_p\Phi) + (\partial_x - c(x)\partial_q)\Phi = 0, \\
L(\partial_q\Phi) + K\partial_p\Phi = 0.
\end{aligned}$$

Set

$$J = det(\Phi_p\Phi_q) = \Phi_p \cdot \Phi_q^{\perp}, \quad \Phi^{\perp} := (\phi_2, -\phi_1)^{\top},$$

we have

$$L(J) = -det(\Phi_x \Phi_q). \tag{4.21}$$

In fact

$$\begin{aligned} L(J) &= L(\Phi_p) \cdot \Phi_q^{\perp} + \partial_p \Phi \cdot (L(\Phi_q))^{\perp} \\ &= (c\partial_q - \partial_x)\Phi \cdot \partial_q \Phi^{\perp} - K \partial_p \Phi \cdot (\partial_p \Phi)^{\perp} \\ &= -\partial_x \Phi \cdot \partial_q \Phi^{\perp} \\ &= -det(\Phi_x \Phi_q). \end{aligned}$$

In order to express u_x in (4.20) in terms of Φ, we further differentiate the relation

$$\Phi(t, x, u(t, x), E(t, x)) = 0$$

with respect to x to obtain

$$\partial_x \Phi + u_x \partial_p \Phi + E_x \partial_q \Phi = 0,$$

from which we obtain

$$u_x = -\frac{det(\Phi_x \Phi_q)}{\det(\Phi_p \Phi_q)}.$$

This when inserted into (4.20) gives

$$L(\tilde{\rho}) = \tilde{\rho} \frac{det(\Phi_x \Phi_q)}{J}. \tag{4.22}$$

Note that at the singular point, J is zero and (4.22) is not defined, where integral equation should be considered. Following Jin et al. (2005c,a) for density evaluation from phase space, we evaluate the multi-valued density in physical space by projecting its value from field space (x, p, q) onto the manifold $\Phi = 0$, i.e., for any x we compute

$$\bar{\rho}(t, x) = \int_{\mathbb{R}_{p,q}} \tilde{\rho}(t, x, p, q) |J| \delta(\phi_1) \delta(\phi_2) dp dq.$$

Note that by the use of absolute value for J is required since the Jacobian changes sign if singularities are formed.

A combination of (4.21) and (4.22) gives

$$L(\tilde{\rho}(\pm J)) = 0,$$

away from singularities. Then we have, away from the singular points,

$$L(f) = 0, \quad f := \tilde{\rho}|J|,$$

where the absolute sign is used to ensure the same nonnegative sign of f before and after the blow-up time when $J = 0$. Thus we just need to compute the quantity f by solving the field transport equation

$$\partial_t f + p\partial_x f + Kq\partial_p f - c(x)p\partial_q f = 0, \tag{4.23}$$

subject to initial data

$$f(0, x, p, q) = \rho_0(x)J(0, x, p, q) = \rho_0(x). \tag{4.24}$$

Note that by choice of (4.16) and (4.17), $J(0, x, p, q) \equiv 1$. With this quantity f the singularities in density ρ is canceled out by $J(\Phi)$. Thus, we are able to locally evaluate the density in physical space by projection of f onto the manifold $\{(p, q) : \quad \Phi(x, p, q) = 0\}$

$$\bar{\rho}(t, x) = \int_{\mathbb{R}^2} f(t, x, p, q)\delta(\phi_1)\delta(\phi_2)dpdq. \tag{4.25}$$

Note that in field space the effective manifold for single valued fields is given by $\{(x, p, q)|\ p = u(t, x),\ q = E(t, x)\}$. For multi-valued velocity and electric fields, we have

$$(u, E) \in \{(p, q) : \phi_1(t, x, p, q) = 0, \quad \phi_2(t, x, p, q) = 0\}.$$

We can evaluate their averages by

$$\bar{u}(t, x) = \int_{\mathbb{R}^2} pf(t, x, p, q)\delta(\Phi)dpdq/\bar{\rho}, \tag{4.26}$$

$$\bar{E}(t, x) = \int_{\mathbb{R}^2} qf(t, x, p, q)\delta(\Phi)dpdq/\bar{\rho}. \tag{4.27}$$

Superposition of Multi-valued Quantities

This section is devoted to the issue of how to relate the computed averaged physical observables such as $\bar{\rho}$, $\bar{u}$ and $\bar{E}$ to exact multi-valued quantities predicted by the characteristic method.

We start with the observed mean density computed from the formula (4.25). We shall show that if multi-valued densities are given, the above calculated mean density is simply a superposition of all multi-valued densities. This result is summarized below.

Theorem 4.0.5 (**Superposition principle for the density**). Let $\{\rho_i\}_{i=1}^N$ be multi-valued densities corresponding to multi-valued fields (u_i, E_i) determined by

$$(u_i, E_i) \in \{(p,q) : \phi_l(t,x,p,q) = 0, l = 1,2\}.$$

Then

$$\bar{\rho}(t,x) = \sum_{i=1}^{N} \rho_i(t,x). \tag{4.28}$$

Proof. In order to evaluate the integral (4.25), we assume that all (u_i, E_i) lie in a bounded domain and use a partition of unity so that we just need to evaluate

$$\int\int f\sigma\delta(\phi_1)\delta(\phi_2)dpdq,$$

where $\sigma \in C_0^\infty$ vanishes near (p_i, q_i), with $\sigma(p_i, q_i) = 1$. Recall that for any smooth function $g(p)$ with only one zero $p = p^*$ we have

$$\delta(g(p)) = \frac{\delta(p-p^*)}{|g'(p^*)|}.$$

In the neighborhood of (p_i, q_i), the implicit function theorem suggests that the zero level set $\phi_1 = 0$ can be explicitly expressed by $p = h(q)$ for each q near q_i, with $p_i = h(q_i)$. Thus

$$\begin{aligned}
\int\int f\sigma(p,q)\delta(\phi_1)\delta(\phi_2)dpdq =& \int\int f\sigma\frac{\delta(p-h(q))}{|\partial_p\phi_1|_{p=h(q)}}\delta(\phi_2)dpdq \\
=& \int \frac{f(t,x,h(q),q)\sigma(h(q),q)\delta(\phi_2(t,x,h(q),q))}{|\partial_p\phi_1|_{p=h(q)}|}dq \\
=& \int \frac{f(t,x,h(q),q)\sigma(h(q),q)\delta(q-q_i)}{|\partial_p\phi_1|_{p=h(q)}||\frac{d}{dq}\phi_2|_{q_i}}dq \\
=& \frac{f(t,x,p_i,q_i)}{|\partial_p\phi_1||\partial_p\phi_2 h'(q) + \partial_q\phi_2|_{(p_i,q_i)}}.
\end{aligned} \tag{4.29}$$

Furthermore, for any q near q_i we have

$$\phi_1(h(q),q) \equiv 0,$$

which leads to

$$\partial_p\phi_1 h'(q) + \partial_q\phi_1 = 0.$$

This when inserted into the denominator in (4.29) gives the Jacobian of (ϕ_1, ϕ_2):

$$|\partial_p\phi_1\partial_q\phi_2 - \partial_q\phi_1\partial_p\phi_2| = |J|.$$

Note that $f(t, x, u_i, E_i) = \rho_i(t, x)|J|$, we thus have

$$\int\int f\sigma(p, q)\delta(\phi_1)\delta(\phi_2)dpdq = \rho_i(t, x).$$

This when combined with the partition of unity gives the asserted (4.28). □

This theorem shows that the linear superposition principle holds for the density of the nonlinear Euler-Poisson system in the sense that direct summation of all multi-valued densities gives the physical observed density. To our knowledge, this is the first rigorous proof via the field space configuration. It would be interesting to see whether this could be justified using the usual Wigner transform in the phase space.

Similar results hold for velocity and electric fields and are stated in the following.

Theorem 4.0.6 (**Weighted superposition for field quantities**). Let $\{\rho_i\}_{i=1}^N$ be multi-valued densities corresponding to multi-valued fields (u_i, E_i) determined by

$$(u_i, E_i) \in \{(p, q) : \phi_l(t, x, p, q) = 0, l = 1, 2\}.$$

Then

$$\bar{u}(t, x) = \frac{\sum_{i=1}^N u_i(t, x)\rho_i(t, x)}{\bar{\rho}}, \tag{4.30}$$

$$\bar{E}(t, x) = \frac{\sum_{i=1}^N E_i(t, x)\rho_i(t, x)}{\bar{\rho}}. \tag{4.31}$$

Proof. Replacing f by fp and fq respectively in the proof of Theorem 4.0.5 we obtain the desired $\bar{u}$ and $\bar{E}$. □

Finally, we remark that the multi-valued quantities predicted by the characteristic method are nothing but those expressed implicitly by the zero level sets of ϕ_1 and ϕ_2 defined above.

Kinetic and Quantum Descriptions

In the following we discuss a kinetic formulation in field space for Euler-Poisson equations, and its connections with Schrödinger-Poisson equations, as well as Vlasov-Poisson equations in phase space.

Kinetic equation in field space

Since both Φ and f solve a linear homogeneous transport equation (4.23), so does $\eta = f\delta(\Phi)$. For smooth initial velocity and electric fields, the density distribution η thus evolves according to

$$\partial_t \eta + p\partial_x \eta + Kq\partial_p \eta - c(x)p\partial_q \eta = 0, \tag{4.32}$$

$$\eta(0, x, p, q) = \rho_0(x)\delta(p - u_0(x))\delta(q - E_0(x)). \tag{4.33}$$

This is a kinetic type equation in field space with non-negative measure data. If we formally set

$$\rho = \int \eta dpdq, \quad \rho u^i E^j = \int p^i q^j \eta dpdq \quad 0 \le i + j \le 2.$$

Multiplying $\{1, p, q\}$ to (4.32) and integrating over $\mathsf{IR}^2_{p,q}$ we obtain

$$\partial_t \rho + \partial_x(\rho u) = 0,$$

$$\partial_t(\rho u) + \partial_x(\rho u^2) - K\rho E = 0,$$

$$\partial_t(\rho E) + \partial_x(\rho u E) + c(x)\rho u = 0,$$

which, for smooth solutions, recovers the expected Euler-Poisson system (4.1),(4.2) and (4.13). In order to recover (4.3), we let

$$W = E_x - (\rho - c).$$

By the choice of E_0 in (4.18) and (4.19), we have

$$W(0, x) = E_x(0, x) - \rho(0, x) + c = 0. \tag{4.34}$$

Using (4.1) and (4.13), we find that W solves the following transport equation

$$W_t + (uW)_x = 0. \tag{4.35}$$

By the uniqueness of the zero solution to (4.35) and (4.34), we conclude

$$W \equiv 0,$$

which gives (4.3).

Wigner transformation

Consider the one-dimensional Schrödinger-Poisson equation of the form

$$i\epsilon\partial_t\psi^\epsilon = -\frac{\epsilon^2}{2}\partial_x^2\psi^\epsilon + V^\epsilon\psi^\epsilon, \quad x \in \mathsf{IR}, \quad t \geq 0 \tag{4.36}$$

$$\partial_x^2 V^\epsilon = c(x) - |\psi^\epsilon|^2. \tag{4.37}$$

The electric field is determined by $E = -V_x$. Seeking the WKB-type solution of the form

$$\psi = \sqrt{\rho(t,x)}\exp(iS(t,x)/\epsilon),$$

we obtain, to the leading order, the Euler-Poisson system for $(\rho, u = S_x)$, i.e., (4.1)-(4.3).

Another path for semiclassical approximation of quantum mechanics is to use the Wigner transformation from "physical space" into "phase space", which was introduced by Wigner Wigner (1932) and can be written as

$$w^\epsilon(t,x,p) = \frac{1}{2\pi}\int_{\mathsf{IR}} e^{-ipy}\psi(t,x+\frac{\epsilon y}{2})\overline{\psi(t,x-\frac{\epsilon y}{2})}dy.$$

We use the overbar to represent the complex conjugate. Wigner transform has been widely used in the study of high frequency, homogenization limits of various equations, see e.g., Gérard et al. (1997); Ryzhik et al. (1996); Gosse and Mauser (2006a); Lions and Paul (1993); Sparber et al. (2003). In the current setting, a direct calculation by applying the Wigner transform to the Schrödinger-Poisson system (4.36)-(4.37) shows that $w^\epsilon(t,x,p)$ satisfies the so-called Wigner equation

$$\partial_t w^\epsilon + p\partial_x w^\epsilon + \theta^\epsilon[V^\epsilon]w^\epsilon = 0, \tag{4.38}$$

where the pseudo-differential operator (local in x and nonlocal in p) is defined as

$$\theta^\epsilon[V^\epsilon]w^\epsilon := \frac{i}{2\pi}\int\int \frac{V^\epsilon(x+\frac{\epsilon y}{2}) - V^\epsilon(x-\frac{\epsilon y}{2})}{\epsilon} w^\epsilon(t,x,\xi)e^{-i(p-\xi)y}d\xi dy.$$

The macroscopic density $\rho(t,x)$ is usually computed through the zero moment in the kinetic variable p

$$\rho^\epsilon(t,x) = \int w^\epsilon(t,x,p)dp.$$

Formally passing $\epsilon \to 0$ in the quantum Wigner equation (4.38) one obtains the Vlasov-Poisson system

$$\partial_t w + p\partial_x w + KE\partial_p w = 0, \quad K = 1 \tag{4.39}$$

$$E_x = \int_{\mathbb{R}_p} w(t,x,p)dp - c(x). \tag{4.40}$$

For the WKB type initial data

$$\psi_0(x) = \sqrt{\rho_0(x)}\exp(iS_0(x)/\epsilon),$$

the limit of the corresponding Wigner function becomes

$$w_0(x,p) = \rho_0(x)\delta(p - u_0(x)).$$

The classical limit from the Schrödinger-Poisson to the Vlasov-Poisson equations in one - dimensional case has been justified by Zhang, Zheng and Mauser Zhang et al. (2002) for bounded integrable data. This V-P system is also a model for collisionless plasma of ions and corresponding electrons. The transport is uni-directional so that the problem can be formulated in one-space dimension. Here the particle motion is governed solely by induced electrostatic forces, while electromagnetic interactions are neglected.

In contrast the classical moment closure approach offers

$$\bar{\rho} = \int w dp, \qquad \overline{\rho u} = \int pw dp.$$

In an interesting earlier work Li et al. (2004), the authors propose a moment closure approach based on the Vlasov-Poisson equation (4.39). From our study in Liu and Wang (2007a) and in this work, we see that the electric field E generally becomes multi-valued simultaneously with velocity field except in the case with null background. Thus solving problem (4.32)-(4.33) in field space serves as an appropriate kinetic formulation to interpret multi-valuedness encountered .

From field space to phase space

We may also formally derive the Vlasov-Poisson equation from (4.32)-(4.33). Assume the closure assumption as $\eta = w(t,x,p)\delta(q - E(t,x))$ we set

$$w(t,x,p) = \int \eta dq, \quad E^i w(t,x,p) = \int q^i \eta dq, i = 1,2.$$

Integration of the $\eta-$equation (4.32) against $\{1, q\}$ leads to

$$\partial_t w + p\partial_x w + KE\partial_p w = 0,$$
$$\partial_t (Ew) + p\partial_x (Ew) + K\partial_p (E^2 w) + c(x)pw = 0.$$

The combination of the two gives

$$\partial_t E + p\partial_x E + c(x)p = 0,$$

this coincides with (4.13) when projection onto the physical space is via $p = u(t,x)$.

Numerical Procedures and Implementation

In this section we discuss the numerical procedures of the new field space based level set method. High dimension level set method was studied in Burchard et al. (2001) for motion of curves.

The main task encountered in this work is to evaluate the density $\bar{\rho}$ accurately. Based on the level set formulation, for evaluation of the density

$$\bar{\rho}(t,x) = \int_{\mathsf{IR}_q} \int_{\mathsf{IR}_p} f(t,x,p,q)\delta(\phi_1)\delta(\phi_2) dpdq, \tag{4.41}$$

we need to first compute two level set functions ϕ_1, ϕ_2 and the function f, all solve the field transport equation (4.15) of the compact form

$$\Phi_t + \overrightarrow{V}(X) \cdot \nabla_X \Phi = 0, \quad t \in \mathsf{IR}^+, \quad X \in \mathsf{IR}^3, \tag{4.42}$$

where $X = (x,p,q)$ and

$$\overrightarrow{V} = (V_1, V_2, V_3) = (p, Kq, -c(x)p).$$

The initial data are chosen to embed the given initial data of the Euler-Poisson equation. One simple choice is

$$\Phi|_{t=0} = (p - u_0(x), q - E_0(x), \rho_0(x))^\top,$$

for smooth u_0, E_0. Following Liu and Wang (2007a), we discretize the gradient $\nabla_X \Phi$ by a first order upwind approximation or a higher order ENO approximation Shu (1999), and then discretize time by a forward Euler method or a higher order Runge-Kutta method. Let $\{t_n, x_i, p_j, q_k\}$ be uniform grids in the $tX-$plane with mesh sizes Δt, Δx, Δp and Δq, respectively. The simplest first order upwind scheme can be formulated as

$$\frac{\Phi^{n+1}_{(i,j,k)} - \Phi^n_{(i,j,k)}}{\Delta t} + V_1(i,j,k)\Phi^{\pm}_x + V_2(i,j,k)\Phi^{\pm}_p + V_3(i,j,k)\Phi^{\pm}_q = 0, \tag{4.43}$$

where $\Phi^n_{(i,j,k)} \approx \Phi(t_n, x_i, p_j, q_k)$, $V_m(i,j,k) := V_m(x_i, p_j, q_k)(m = 1,2,3)$ and

$$\Phi^+_x = \frac{\Phi^n_{(i+1,j,k)} - \Phi^n_{(i,j,k)}}{\Delta x}, \quad \Phi^-_x = \frac{\Phi^n_{(i,j,k)} - \Phi^n_{(i-1,j,k)}}{\Delta x},$$

similar notations are adopted for Φ^+_p,Φ^-_p,Φ^+_q and Φ^-_q. For $m = 1,2$ or 3, if $V_m(i,j,k) > 0$, we use Φ^-; otherwise, Φ^+ is applied. Under the CFL condition

$$\Delta t \max\left(\frac{|\, V_1 \,|}{\Delta x} + \frac{|\, V_2 \,|}{\Delta p} + \frac{|\, V_3 \,|}{\Delta q}\right) \le 1, \tag{4.44}$$

this scheme is stable in both L^∞ and L^1 norm, which, to be stated below, were shown in Liu and Wang (2007a) for more general V.

- **[Discrete Maximum Principle]** Assume that $V_m(x,p,q)(m = 1,2,3)$ are bounded functions in the computational domain. Let Φ^n be a numerical solution produced by the first order upwind scheme subject to the initial data Φ^0, then

$$||\Phi^n||_\infty \le ||\Phi^0||_\infty. \tag{4.45}$$

- **[L^1 Stability]** Assume that $V_m(x,p,q)(m = 1,2,3)$ are bounded and Lipschitz continuous in its i-th argument in the computational domain. Let Φ^n be a numerical solution produced by the first order upwind scheme subject to the initial data Φ^0, then for finite time T, there exists a constant M, such that

$$||\Phi^n||_1 \le e^{MT}||\Phi^0||_1, \tag{4.46}$$

where $||\Phi^n||_1 := \sum_{i,j,k} |\Phi^n_{(i,j,k)}| \Delta x \Delta p \Delta q$.

In our numerical simulation, this first order upwind scheme is mostly adopted for computing $\Phi = (\phi_1, \phi_2, f)^\top$, with which we discuss the evaluation of density via (4.41).

Since the integration (4.41) involves the Dirac $\delta-$function in its integrand, as usual we first regularize the Dirac $\delta-$function by a smooth bounded function δ_ϵ in such a way that $\delta_\epsilon \rightharpoonup \delta$ as $\epsilon \to 0^+$. The error introduced in this regularization step depends on the choice of the approximation, whose accuracy is indicated by a so called moment condition Beyer and LeVeque (1992) of the regularization. δ_ϵ is said to satisfy r^{th} order of moment condition if $\int_{\mathsf{IR}} \delta_\epsilon(x) = 1$ and $\int_{\mathsf{IR}} \delta_\epsilon(x) x^k = 0$ for $1 \le k \le r$. It is known that the higher the order of moment condition, the smaller the regularization error. The choice of regularization δ_ϵ could be any smooth function with the above properties. However, considering the concentration of the Delta function, it suffices to choose δ_ϵ to have a compact support:

$$\delta_\epsilon(x) = \begin{cases} \frac{1}{\epsilon}\Psi(\frac{x}{\epsilon}), & |x| \le \epsilon \\ 0, & |x| > \epsilon. \end{cases}$$

One of well accepted choices of this type of δ_ϵ is the cosine kernel, $\Psi(\eta) = \frac{1}{2}(1 + \cos(\pi\eta))$, i.e.,

$$\delta^{\cos}_\epsilon(x) = \frac{1}{2\epsilon}\left(1 + cos\left(\frac{\pi x}{\epsilon}\right)\right) I_{[-\epsilon,\epsilon]}, \tag{4.47}$$

which has first order moment condition. Here $I_{[-\epsilon,\epsilon]}$ is the standard indicator function.

Replacing $\delta(\phi_1)\delta(\phi_2)$ by $\delta_\epsilon(\phi_1)\delta_\epsilon(\phi_2)$, we thus have the first approximation of $\bar\rho$,

$$\bar\rho_\epsilon(t,x) = \int_{\mathsf{IR}_q}\int_{\mathsf{IR}_p} f(t,x,p,q)\delta_\epsilon(\phi_1)\delta_\epsilon(\phi_2)dpdq, \tag{4.48}$$

to which standard quadrature rules can be applied. In our simulation, the rectangle rule is chosen and the numerical density is further evaluated by

$$\bar\rho_{\epsilon h}(t,x) = \sum_{\{|\phi_i(t,x,p_j,q_k)|\le\epsilon, i=1,2\}} f(t,x,p_j,q_k)\delta^{\cos}_\epsilon(\phi_1)\delta^{\cos}_\epsilon(\phi_2)\Delta p\Delta q. \tag{4.49}$$

In this two-step procedure, total error is bounded by the sum of regularization error $|\bar\rho - \bar\rho_\epsilon|$ and quadrature error $|\bar\rho_\epsilon - \bar\rho_{\epsilon h}|$. For example, if the cosine kernel and the rectangle rule are used, $|\bar\rho - \bar\rho_\epsilon|$ is of order ϵ and $|\bar\rho_\epsilon - \bar\rho_{\epsilon h}|$ is of order h/ϵ, where $h = \max\{\Delta x, \Delta p, \Delta q\}$. Using the

similar analysis as in Raviart (1983), it is clear that the total error is minimized as of order $\sqrt{h}$ when an optimal ϵ^* is chosen to be of order $\sqrt{h}$. Thus the convergence rate of the numerical integration is at least of order 1/2, i.e.,

$$|\bar{\rho} - \bar{\rho}_{\epsilon h}| \leq C h^{\frac{1}{2}},$$

for some constant C. For details on convergence rates in general cases, see (Tornberg and Engquist, 2003, Theorem 3).

Though, theoretically, ϵ^* is optimal, it is impractical to determine it exactly. Thus, we choose to run numerical experiments with a wide range of ϵ to circumvent this numerical difficulty. In our simulation the support of δ_ϵ is tested with $\epsilon = h, 2h, 3h, \cdots$. Based on many experiments on ϵ, we found that the smaller ϵ, the sharper of density at the cost of oscillation. So we have to pick proper ϵ to balance the resolution and smoothness. Through our simulation, we also found that usually we get best results when ϵ is within [1.5h, 4.5h] depending on examples being tested. In short, the choice of ϵ plays a crucial role in the evaluation of density. An interesting phenomenon is that the choice of ϵ as mh while using the signed distance function in multi-dimensional setting may lead to $O(1)$ error Tornberg and Engquist (2004). However, in our case, a product of $\delta-$functions is being approximated. Thus convergence is guaranteed with $\epsilon^* \in [h, mh]$ for some constant m. We also notice that the geometry of the level set function also affects the choice of ϵ, as observed in Jin et al. (2005c,a). And we refer to Engquist et al. (2005) for more regularization techniques related to level set methods.

Here we remark that one could also compute the density $\bar{\rho}$ by solving the field transport equation (4.32) :

$$\partial_t \eta + p\partial_x \eta + Kq\partial_p \eta - c(x)p\partial_q \eta = 0,$$

but subject to initial data involving delta functions,

$$\eta(0, x, p, q) = \rho_0(x)\delta(p - u_0(x))\delta(q - E_0(x)). \tag{4.50}$$

The density is then evaluated by

$$\bar{\rho} = \int \eta dp dq. \tag{4.51}$$

Here, $\bar{\rho}$ is still evaluated by a post-processing step, i.e. integration over field configuration, but with no involvement of the Dirac $\delta-$function. However, in order to utilize (4.51), one needs to regularize the $\delta-$function in the initial condition (4.50), and such an initial regularization error will surely evolve and accumulate, reducing accuracy of the final integration. Therefore, the evaluation of $\bar{\rho}$ by post-processing in (4.49) is preferred to solving the kinetic equation with (4.50) directly.

We now discuss several technical details to be involved in our numerical tests.

Firstly, we need to specify an appropriate computational domain. The guiding principle is that the extreme values of u and E should be covered in the computation domain. Thus, if the example has an exact solution, we choose to prescribe a domain containing the range of the exact solution for all t before the desired time T. In the case of no exact solution available, based on the initial condition, we first choose a relatively large domain with coarse meshes to get a rough solution in order to determine the computation domain. Then we can refine our mesh to get better resolution.

Secondly, the computational boundary condition should be enforced in such a way that no artificial and spurious waves are propagated into the computational domain. In our simulation, if the initial data are periodic in an argument, we use a periodic boundary data in the direction of that argument. For other cases, we use a Neumann boundary condition.

Finally, we show how to realize multi-valued u and E. The projection of common zeros onto xp and xq spaces gives the visualization of multi-valued $u(T,x)$ and $E(T,x)$:

$$(u,E)(T,x) \in \{(p,q)|\phi_1(T,x,p,q)=0\} \cap \{(p,q)|\phi_1(T,x,p,q)=0\}, \quad \forall x \in \mathsf{IR}.$$

Numerically, we interpolate only grid points satisfying

$$\{(x_i,p_j,q_k) \in \Omega| \quad |\phi_1(T,x_i,p_j,q_k)| < \tilde{\epsilon}, \quad |\phi_2(T,x_i,p_j,q_k)| < \tilde{\epsilon}\},$$

where $\tilde{\epsilon}$ is chosen in such a way that a unique grid point can be identified along the zero level set. Computationally, a $\tilde{\epsilon}$ which is much smaller than h works well. We point out that a larger

$\tilde{\epsilon}$ may be necessary for the case when level set functions are rough. Meanwhile the density $\bar{\rho}$ is approximated by (4.49) using ϕ_1 and ϕ_2.

Using the multi-valued density predicted by the characteristic method and the superposition principle (4.28), we construct an exact averaged density

$$\bar{\rho}_{ea} = \sum_{i=1}^{N} \rho_i(t,x). \tag{4.52}$$

Based on this, we show the numerical accuracy and convergence for averaged density obtained by our level set method (4.49). Numerical convergence test with L^2 error of (4.49) and (4.52) is performed.

Exact Solution and Breakdown Time

We now recall some solution formulas given in Engelberg et al. (2001) by using the characteristic system

$$\frac{dx}{dt} = u, \tag{4.53}$$
$$\frac{du}{dt} = KE, \tag{4.54}$$
$$\frac{dE}{dt} = -c(x)u \tag{4.55}$$

of (4.1)-(4.3) subject to the initial condition

$$x(0) = \alpha, \quad u(0) = u_0(\alpha), \quad E(0) = E_0(\alpha).$$

1. Zero background charge $c(x) \equiv 0$.

Integration of the characteristic system (4.53)-(4.55) leads to

$$x(t,\alpha) = \alpha + u_0 t + KE_0 t^2/2, \tag{4.56}$$
$$u(t, x(t,\alpha)) = u_0 + KE_0 t, \tag{4.57}$$
$$E(t, x(t,\alpha)) = E_0. \tag{4.58}$$

The density is conserved along characteristics, see (4.11). As shown in Engelberg et al. (2001), the necessary and sufficient condition for the break down of smooth solution is $\Gamma(t,\alpha) = 0$ for

some time t and initial position α. This condition also gives the exact time when breakdown occurs, which in current setting gives

$$T^* = \min_{\alpha} \left\{ t : \frac{-u_0' - \sqrt{u_0'^2 - 2K\rho_0}}{K\rho_0}, \quad u_0' < -\sqrt{2K\rho_0} \right\}, \tag{4.59}$$

where $\{\alpha : u_0' < -\sqrt{2K\rho_0}\}$ denotes the set of initial points which will lead to finite time breakdown.

2. Constant background charge $c > 0$.

By the characteristic equations (4.54) and (4.55), we have

$$u'' + cKu = 0.$$

If the force is repulsive, $K > 0$, solutions are

$$x(t,\alpha) = \alpha + u_0 \sin(\sqrt{cK}t) + E_0 \cos(\sqrt{cK}t) - E_0, \tag{4.60}$$

$$u(t, x(t,\alpha)) = u_0 \cos(\sqrt{cK}t) + E_0 \sin(\sqrt{cK}t), \tag{4.61}$$

$$E(t, x(t,\alpha)) = E_0 \cos(\sqrt{cK}t) - u_0 \sin(\sqrt{cK}t), \tag{4.62}$$

where the density is still given by $\rho(t, x(t,\alpha)) = \frac{\rho_0(\alpha)}{\Gamma(t,\alpha)}$, but with

$$\Gamma(t,\alpha) = 1 + u_0' \sin(\sqrt{cK}t) + E_0' \cos(\sqrt{cK}t) - E_0'. \tag{4.63}$$

Finite time breakdown is unavoidable if

$$|u_0'(\alpha)| \geq \sqrt{K(2\rho_0 - c)}$$

for some $\alpha \in \mathbb{R}$. Under this condition, the first breakdown time is

$$T^* = \min_{\alpha} \left\{ t, \Gamma(t,\alpha) = 0, |u_0'(\alpha)| \geq \sqrt{K(2\rho_0 - c)} \right\}.$$

If the force is attractive, i.e. $K < 0$, then

$$\begin{aligned} x(t,\alpha) &= \alpha + \frac{C_1}{-\lambda}(e^{-\lambda t} - 1) + \frac{C_2}{\lambda}(e^{\lambda t} - 1), && (4.64)\\ u(t,x(t,\alpha)) &= C_1 e^{-\lambda t} + C_2 e^{\lambda t}, && (4.65)\\ E(t,x(t,\alpha)) &= \frac{-C_1\lambda}{K} e^{-\lambda t} + \frac{C_2\lambda}{K} e^{\lambda t}, && (4.66)\\ \rho(t,x(t,\alpha)) &= \frac{\rho_0(\alpha)}{\Gamma(t,\alpha)}, && (4.67) \end{aligned}$$

where $\lambda = \sqrt{-cK}$, $C_1 = \frac{\lambda u_0 - E_0 K}{2\lambda}$, $C_2 = \frac{\lambda u_0 + E - 0K}{2\lambda}$ and

$$\Gamma(t,\alpha) = 1 + \frac{C_1'}{-\lambda}(e^{-\lambda t} - 1) + \frac{C_2'}{\lambda}(e^{\lambda t} - 1).$$

In this case, the necessary and sufficient condition for smooth solutions to experience finite time breakdown is

$$u_0'(\alpha) \le -\left(1 - \frac{\rho_0(\alpha)}{c}\right)\sqrt{-Kc}$$

for some $\alpha \in \mathbb{R}$. Under this condition, T^* can be found by solving $\Gamma(t,\alpha) = 0$.

These parameterized solution formulas give multi-valued solutions of u, E and ρ after interaction of characteristic curves, i.e. $t > T^*$. Thus, we can compare our numerical solution with exact solutions to verify the accuracy of our method.

Numerical Examples

In this section, we demonstrate the accuracy and capacity of our level set method by testing several numerical examples and compare the numerical solution with the parameterized exact solution when available. In the following experiments, the first order up-wind scheme is employed.

1. Numerical Test One: 5 Branches

Our first example is the model with zero background with $c = 0$, $K = 0.01$. The initial condition is given by

$$\begin{aligned} u(0,x) &= \sin^3(x),\\ \rho(0,x) &= \frac{1}{\pi} e^{-(x-\pi)^2}. \end{aligned}$$

In this case, since c is zero, the initial electric field $E_0(x)$ is determined from $\rho_0(x)$ by

$$E_0(x) := E(0,x) = \frac{1}{2}\left(\int_{-\infty}^{x} \rho_0 dx - \int_{x}^{-\infty} \rho_0 dx\right).$$

In this example, (4.11) gives

$$\Gamma(t,\alpha) = 1 + 3sin^2(\alpha)cos(\alpha)t + \frac{1}{2\pi}Kt^2e^{-(\alpha-t)^2}.$$

A calculation based on (4.59) shows that $T^* < 3$. So we compare our numerical results with exact solution at time t after 3. Our computation domain is $\Omega = [0, 2\pi] \times [-1.2, 1.2] \times [-0.5, 0.5]$, which is chosen to include the range of u, E, ρ at $t \approx 3$. The discretization parameters $\Delta x, \Delta p, \Delta q$ are chosen to be $0.02, 0.01, 0.01$ respectively, with $\tilde{\epsilon} = 0.0025$, $\epsilon = 1.5\Delta x$ and CFL number 0.8. In Fig.4.1 and other following figures, unless specified otherwise, solid line is exact solution while dots are our numerical results. We see that results from our level set method match the exact solution, though only a first order upwind scheme has been used.

Now, we perform the numerical convergence test for the averaged density. $\bar{\rho}_{\epsilon h}$ is calculated with $\epsilon = mh$ via (4.49) for $m = 1, 2, 3, 4$. Then the numerical L^2 error between $\bar{\rho}_{\epsilon h}$ and $\bar{\rho}_{ea}$ obtained in (4.52) is computed as

$$\int (\bar{\rho}_{ea} - \bar{\rho}_{\epsilon h})^2 dx \approx \sum_{\{x_i\}} \left(\bar{\rho}_{ea}(t, x_i) - \bar{\rho}_{\epsilon h}(t, x_i)\right)^2 \Delta x.$$

In Table 4.1, one sees that the L^2 error becomes small as the step size decreases for some selected ϵ. This is also visually shown in Fig.4.2. Thus the numerical convergence is obtained, which shows the validity of our level set approach in computing averaged density.

2. Numerical Test Two: 7 Branches

We now test the model with zero background with $c = 0$, $K = 0.01$, but subject to initial condition,

$$\begin{aligned} u(0,x) &= \sin(2x)\cos(x), \\ \rho(0,x) &= \frac{1}{\pi}e^{-(x-\pi)^2}. \end{aligned}$$

Though this example is similar to the first one, the solution has richer structures. Note that from the numerical convergence test in example 1, we are assured that the level set approach

{dx,dp,dq,t}	m	L^2 error
{0.06,0.03,0.03,3.0149}	1	0.1018
	2	0.1345
	3	0.1464
	4	0.1693
{0.05,0.02,0.02,3.0021}	1	0.0513
	2	0.0714
	3	0.0790
	4	0.0901
{0.02,0.01,0.01,3.0017}	1	0.0412
	2	0.0626
	3	0.0776
	4	0.0895

Table 4.1 L^2 error for averaged density at various spatial step sizes and support $\epsilon = mh$

developed here will give correct multi-valued u, E and averaged $\bar{\rho}$. Thus from this example on, we choose not to do the numerical convergence test. Instead, we will just show the averaged density obtained from the level set method, and exact multi-valued density predicated by the characteristic method.

As in the first example, the initial condition $E_0(x)$ is given by

$$E_0(x) = \frac{1}{2}\left(\int_{-\infty}^{x} \rho_0 dx - \int_{x}^{-\infty} \rho_0 dx\right).$$

Then the exact solution can be found using (4.56)-(4.11).

Using the same formula (4.59) as in the previous example in determining the critical time T^*, we find that multi-valued solution will appear before $t = 4$. Our computation domain is $\Omega = [0, 2\pi] \times [-1, 1] \times [-0.5, 0.5]$, which is chosen to include the range of u, E, ρ at desired time. The discretization parameters $\Delta x, \Delta p, \Delta q$ are chosen to be $0.02, 0.01, 0.01$ respectively, with $\tilde{\epsilon} = 0.0025$, $\epsilon = 4.5\Delta x$ and CFL number 0.8. In Fig.4.3, once again, by comparing with the exact solution, we see that results from our level set method match the exact solution. In this example, when we used smaller ϵ, some oscillations for $x \in [2, 4]$ are observed. Thus, we pick relatively bigger $\epsilon = 4.5\Delta x$ to smear the observed oscillation.

3. Numerical Test Three: Negative K

In the previous two examples, multi-valuedness is induced by the decreasing initial velocity in finite time. However, if the force is attractive, $K < 0$, even for constant initial velocity, breakdown still occurs at finite time. This can be seen from the following example. If we consider zero background case, i.e. $c = 0$, the solution for x and Γ are given by

$$x(t, \alpha) = \alpha + u_0(\alpha)t + E_0(\alpha)Kt^2/2,$$

$$\Gamma(t, \alpha) = 1 + u_0'(\alpha)t + \rho_0 Kt^2/2.$$

Thus even if $u_0(\alpha)$ is nondecreasing, as long as K is negative, there will be some time t such that $\Gamma = 0$ provided that $\rho_0 \geq 0$. This tells us that multi-valued solutions must appear in the case of $K < 0$.

Now we test our method with $c = 0$ and $K = -1$, subject to initial condition,

$$\begin{aligned} u(0, x) &= 0.01, \\ \rho(0, x) &= \frac{1}{\pi} e^{-(x-\pi)^2}. \end{aligned}$$

In this case, $\Gamma = 1 - \frac{1}{2\pi} e^{(\alpha-\pi)^2} t^2$, which starts to become zero at $\alpha = \pi$, $t = T^* = \sqrt{2\pi}$. Thus when $t > \sqrt{2\pi}$, multi-valued solutions need to be considered. In order to see more structures, we will test our algorithm at time t around 4. Our computation domain is $\Omega = [0, 2\pi] \times [-1.5, 1.5] \times [-0.5, 0.5]$, which is chosen to include the range of u, E, ρ at desired time. The discretization parameters $\Delta x, \Delta p, \Delta q$ are chosen to be $0.02, 0.01, 0.01$ respectively, with $\tilde{\epsilon} = 0.002$, $\epsilon = 1.5\Delta x$ and CFL number 0.8. In Fig.4.4, we see that though the structure of the solution is not so rich as in previous one, this example does validate the physical situation that attractive force always induces multi-valued solutions in finite time.

4. Numerical Test Four: Nonzero Background

We now test an example with nonzero background with $c = 1$, $K = 1$ and initial condition,

$$\begin{aligned} u(0, x) &= 2 \sin^4 x \\ \rho(0, x) &= 1. \end{aligned}$$

In this case, as in (4.60)-(4.63) the exact solution can be found explicitly. Here the choice of constant initial density is to simplify the identification of when multi-valuedness happens.

Since $\Gamma(t,\alpha) = 1 + 4\sin\alpha\sin 2\alpha\sin t$,

$$T^* = \min_{\alpha} sin^{-1}\left\{-\frac{1}{4sin2\alpha\sin^2\alpha}\right\} \approx 0.5.$$

We visualize our numerical simulation at $t = 1$. Our computation domain is $\Omega = [0, 2\pi] \times [-2.5, 2.5] \times [-2.5, 2.5]$, which is chosen to include the range of u, E, ρ at desired time. The discretization parameters $\Delta x, \Delta p, \Delta q$ are chosen to be $0.02, 0.02, 0.02$ respectively, with $\tilde{\epsilon} = 0.01$, $\epsilon = 2.5\Delta x$ and CFL number 0.8. In Fig.4.5, we see the results in two periods. Looking at the graph for ρ at x near 2π, one may wonder why the peak is not complete. This is caused by the fact that the wave is shifting to right while our computation domain is fixed in $[0, 4\pi]$.

5. Numerical Test Five: Discontinuous Background $c(x)$

In previous examples, all parameters and initial conditions are smooth. Thus the exact solution can be expressed in terms of the initial position parameter α. By comparing with exact solution within the same graph, we have verified the accuracy of our method. We now present an example with piecewise smooth background charge.

Consider the model with discontinuous background with $c = \frac{1}{2}I_{[-1,1]}$, $K = 0.01$, with initial condition,

$$\begin{aligned} u(0,x) &= 4sin(x), \\ \rho(0,x) &= \frac{1}{2\sqrt{\pi}}\Big(e^{-(x+\frac{\pi}{2})^2} + e^{-(x-\frac{\pi}{2})^2}\Big), \end{aligned}$$

where $I_{[-1,1]}$ is the usual indicator function in $[-1, 1]$.

Our computation domain is $\Omega = [-2\pi, 2\pi] \times [-5, 5] \times [-1, 1]$, which is chosen to be large in order to include the range of u, E, ρ at $t \approx 1$. The discretization parameters $\Delta x, \Delta p, \Delta q$ are chosen to be $0.04, 0.02, 0.02$ respectively, with $\tilde{\epsilon} = 0.009$, $\epsilon = 3\Delta x$ and CFL number 0.8. In Fig.4.6, multi-valued u and E are shown along with averaged density with peaks.

Conclusion

Together with Liu and Wang (2007a) we have developed a field space based level set method for computing multi-valued solutions to 1D Euler-Poisson equations. In field space multi-valued

velocity and electric fields are naturally incorporated into the configuration, and represented implicitly by common zeros of two level set functions. Using those level set functions as building blocks, we further develop an implicit projection method to evaluate the multi-valued density as well as averaged velocity and electric fields. The main advantage of the proposed approach over phase space based method is its ability to unfold singularities in both velocity and electric fields. Moreover, the use of level set formulation enables us to easily treat any number of multi-valued branches, and the topology of multi-valued solutions is handled automatically.

Furthermore, we prove that the averaged density is simply a superposition of all multi-valued densities predicated by the characteristic method. Averaged field quantities are weighted superposition of corresponding multi-valued ones. This is remarkable since the underlying Euler-Poisson system is nonlinear!

The application of our method is not restricted to the computation of the semiclassical approximation of Schrödinger-Poisson equations. Similar problems arise in plasma oscillations, beam propagation, to which the techniques discussed in this paper is expected to be useful.

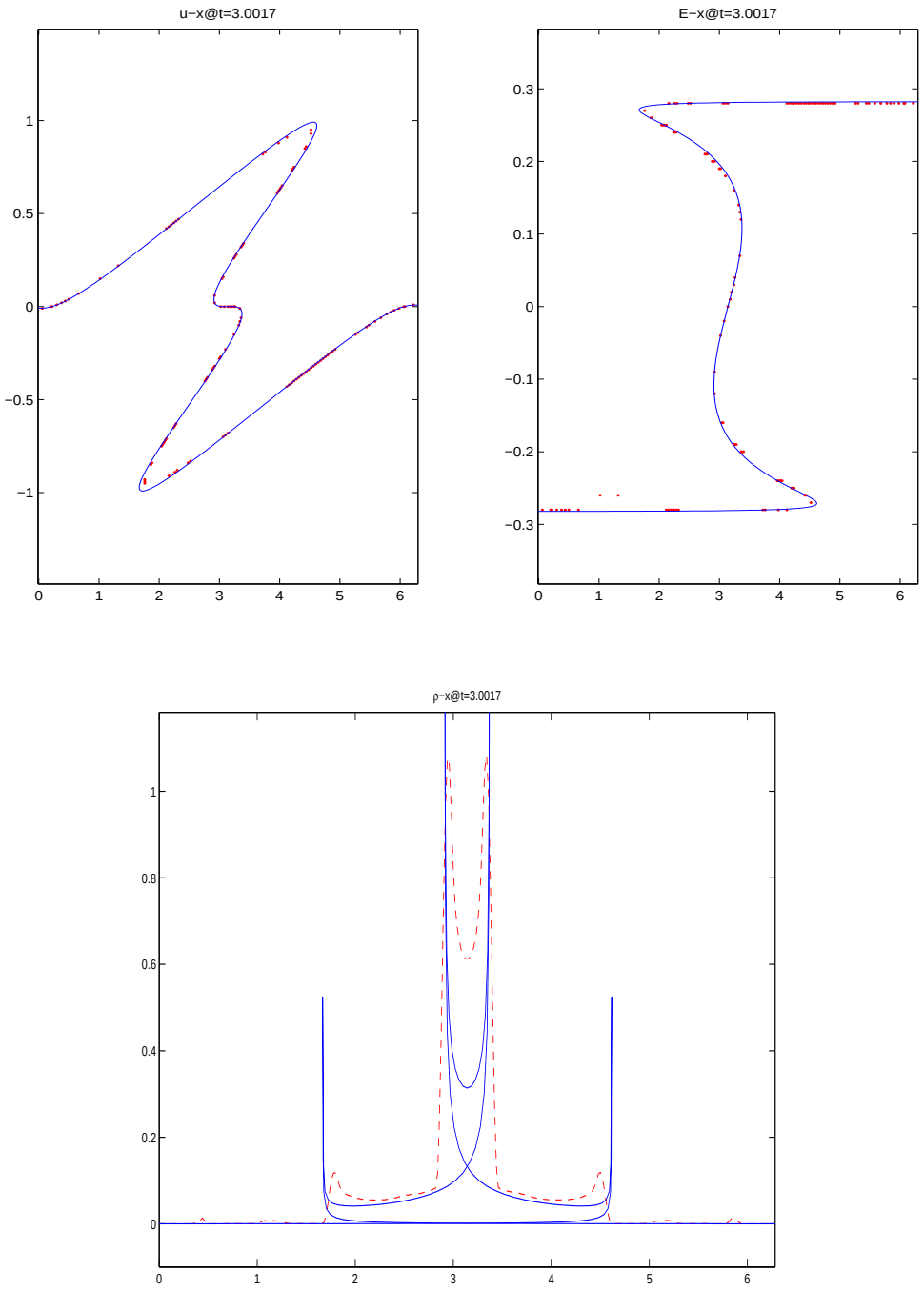

Figure 4.1 Multi-valued solution for 1D Euler-Poisson equation at time about 3.

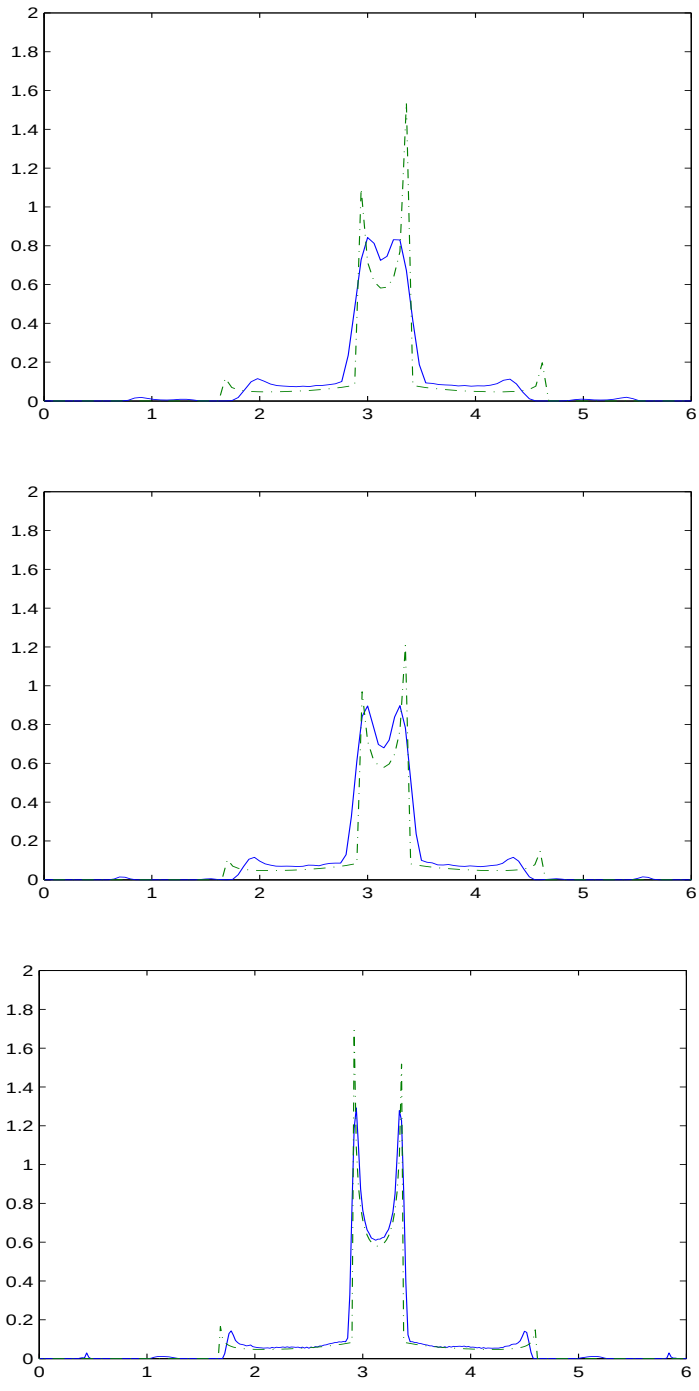

Figure 4.2 Comparison of averaged $\rho_{\epsilon h}$(solid blue) and ρ_{ea}(dotted green) at various spatial step size and time about 3. Spatial step size decreases from top to bottom as in Table 4.1

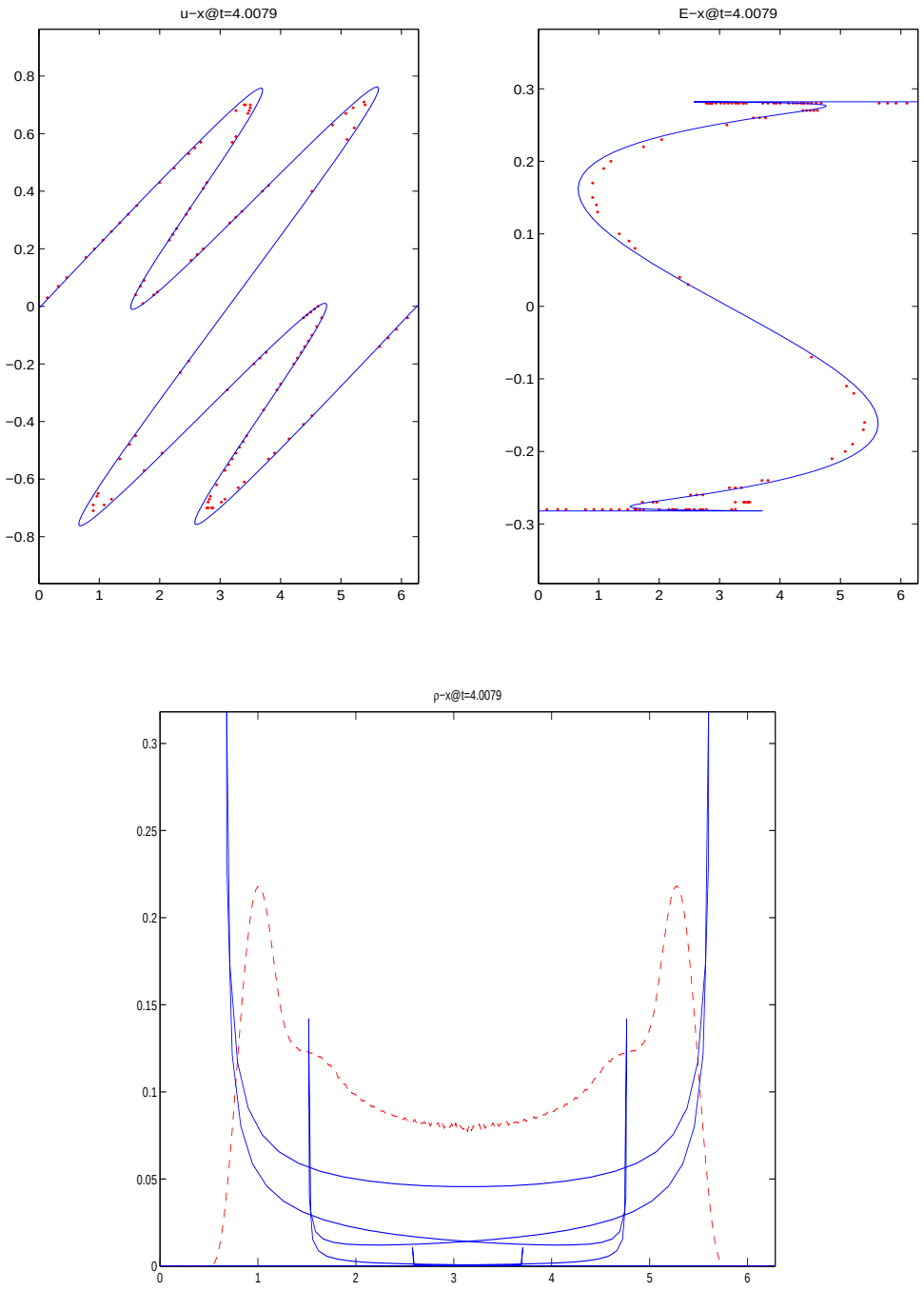

Figure 4.3 Multi-valued solution for 1D Euler-Poisson equation at $t = 4.0079$.

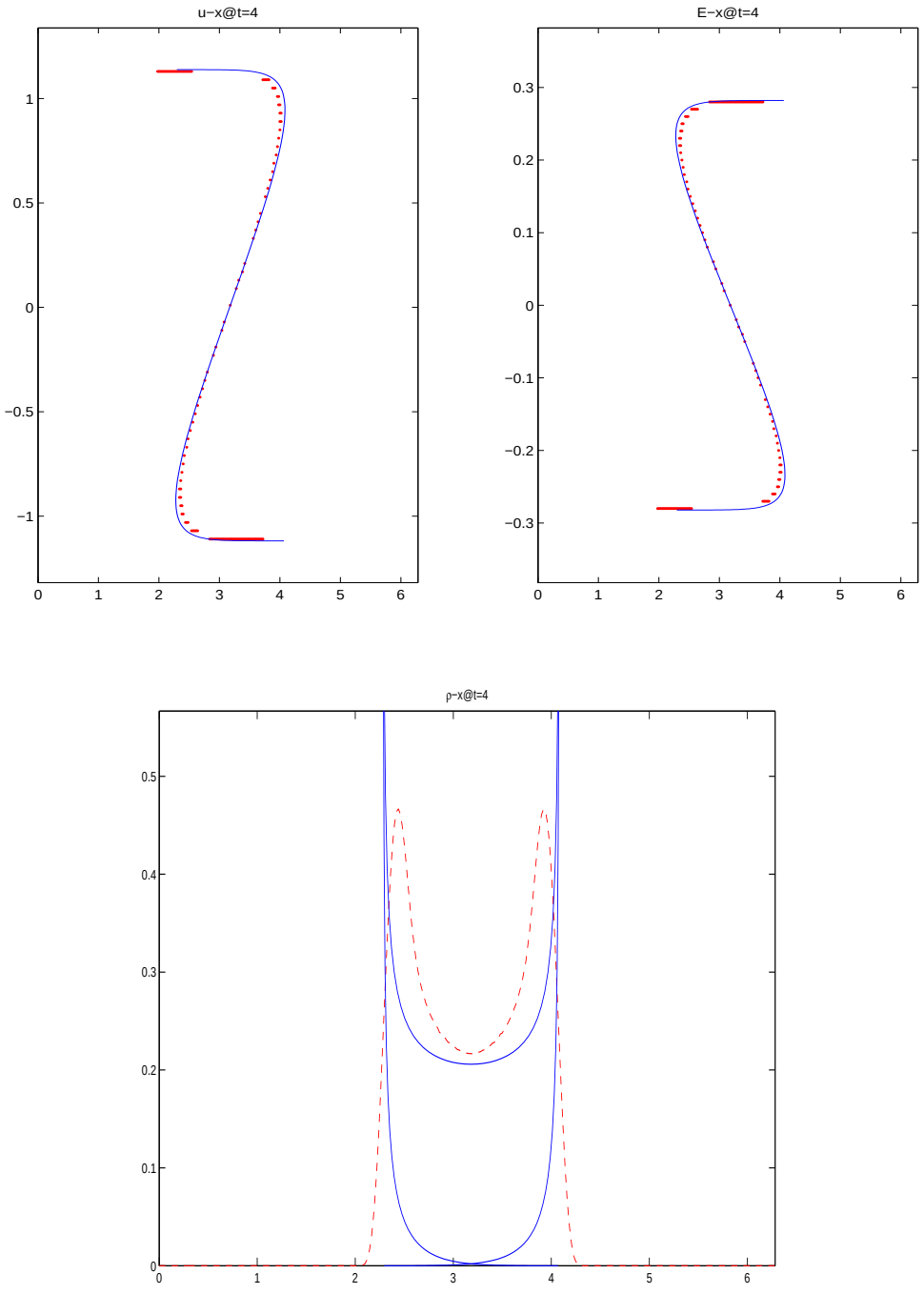

Figure 4.4 Multi-valued solution for 1D Euler-Poisson equation at time around 4.

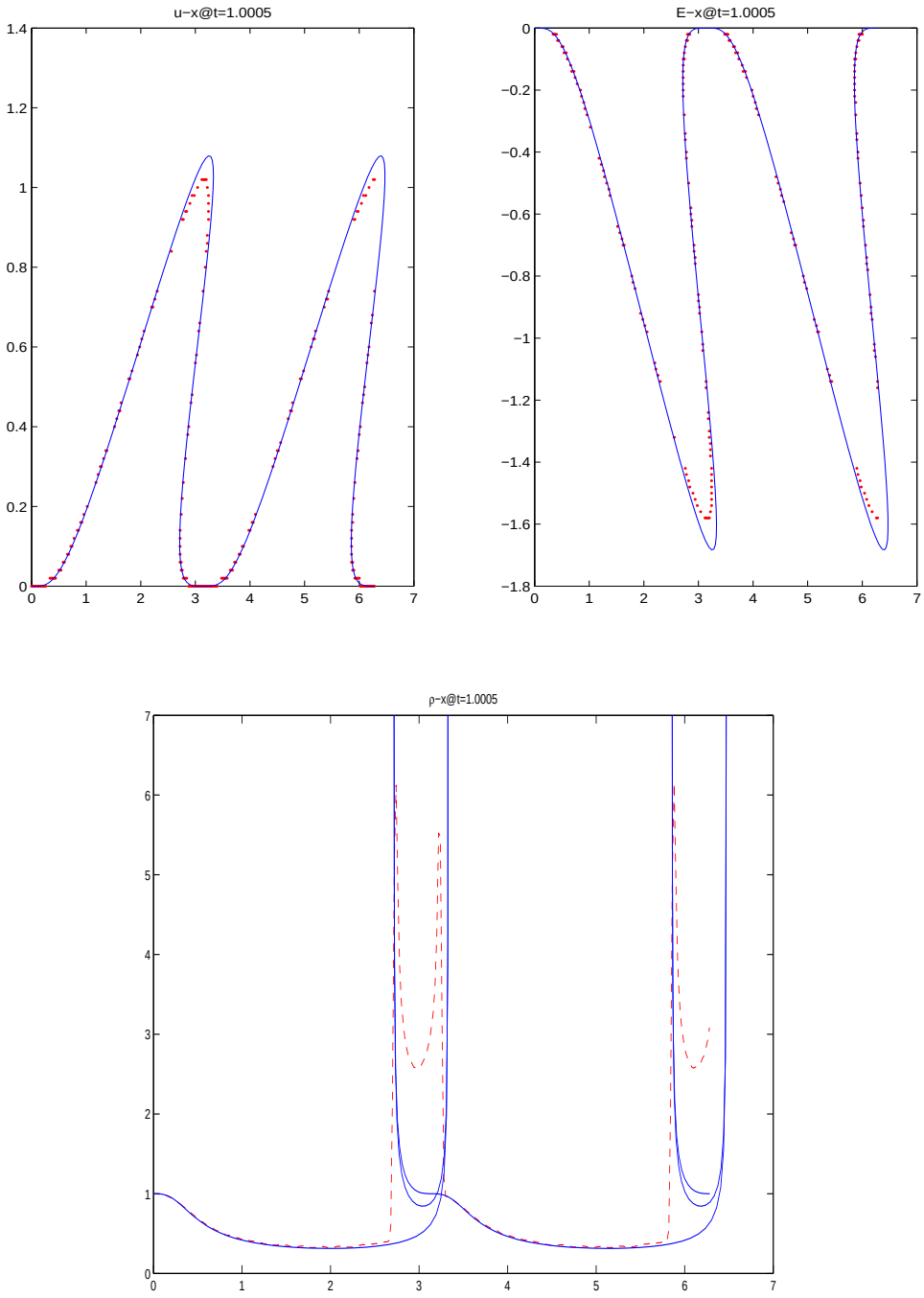

Figure 4.5 Multi-valued solution for 1D Euler-Poisson equation at time around 1.

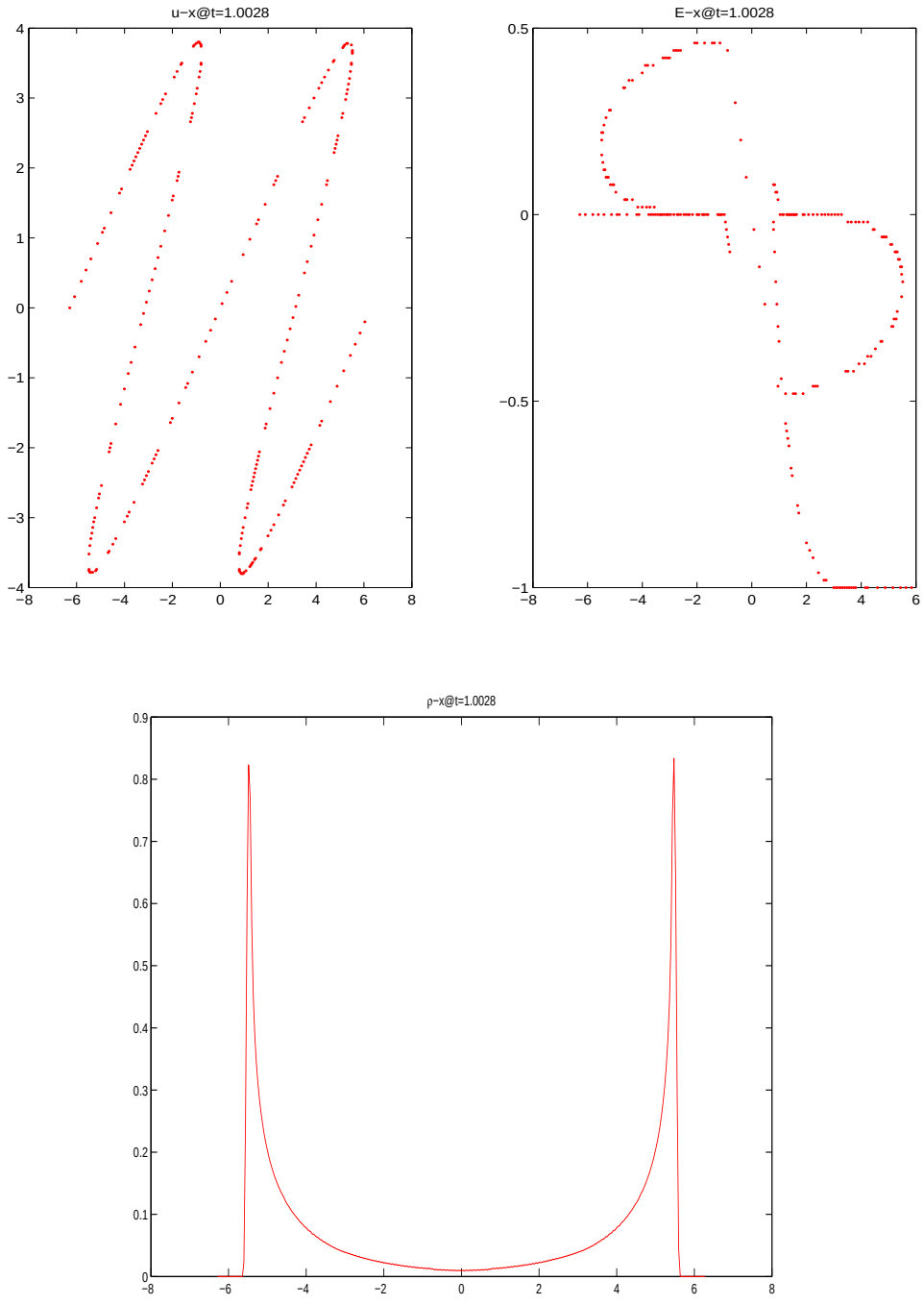

Figure 4.6 Multi-valued solution for 1D Euler-Poisson equation at time around 1.

CHAPTER 5. A BLOCH BAND BASED LEVEL SET METHOD FOR COMPUTING THE SEMICLASSICAL LIMIT OF SCHRÖDINGER EQUATIONS

A paper to be submitted to Journal on Scientific Computation

Hailiang Liu, Zhongming Wang

Abstract

A Bloch band based level set method is developed for computing the semiclassical limit of one-dimensional Schrödinger equations in periodic medium. A hybrid of the WKB approximation and homogenization leads to the Bloch eigenvalue problem and an associated Hamilton-Jacobi system for the phase, with Hamiltonian being the Bloch eigenvalues. Following the level set methodology explored in Cheng et al. (2003); Liu and Wang (2008b), we develop a Bloch band based level set method, which is a hybrid numerical scheme – splitting the solution process into several steps: i) initialize the level set function from the band decomposition of the initial data; ii) solve the Bloch eigenvalue problem to compute Bloch waves; iii) evolve the band level set equation to compute multi-valued velocity and density on each Bloch band; iv) evaluate the total position density over a sample set of bands using Bloch waves and band densities obtained in step ii) and iii), respectively. Numerical results with different number of bands are provided to demonstrate the good quality of the method.

Introduction

We are interested in developing an efficient numerical method to solve the linear Schrödinger equation

$$i\epsilon\frac{\partial\psi^\epsilon}{\partial t} = -\frac{\epsilon^2}{2}\frac{\partial}{\partial x}\left(a\left(\frac{x}{\epsilon}\right)\frac{\partial\psi^\epsilon}{\partial x}\right) + V\left(\frac{x}{\epsilon}\right)\psi^\epsilon + V_e(x)\psi^\epsilon, \quad x \in \mathbb{R},\ t \in \mathbb{R}^+, \tag{5.1}$$

where ψ^ϵ is the complex wave field, and ϵ is a re-scaled Planck constant. Both $a(y) > 0$ and $V(y)$ are smooth and periodic with respect to the regular lattice $\Gamma = 2\pi\mathbb{Z}$, i.e.,

$$a(y + 2\pi) = a(y), \quad V(y + 2\pi) = V(y), \quad \forall y \in \mathbb{R}. \tag{5.2}$$

The external potential V_e is a given smooth function.

This type of Schrödinger equations is a fundamental model in solid-state physics Ashcroft and Mermin (1976) and also appears as a model for motion of electrons in small-scale periodic potentials. This problem has been studied from both physical and mathematical aspects in the literature, see e.g. Asch and Knauf (1998); Blount (1962); Luttinger (1951); Panati et al. (2003); Zak (1968). The mathematical asymptotic analysis as $\epsilon \to 0$ combining both semiclassical and homogenization limits has been of interest in many references Bal et al. (1999); Bensoussan et al. (1978); Gérard et al. (1997); Lions and Paul (1993); Markowich et al. (1994); Sparber et al. (2003).

We consider (5.1) subject to the high frequency initial data

$$\psi^\epsilon(0, x) = e^{iS_0(x)/\epsilon} f\left(x, \frac{x}{\epsilon}\right), \quad \epsilon \ll 1, \tag{5.3}$$

where $f(x, y) \in C_0^\infty(\mathbb{R} \times 2\pi\mathbb{Z})$ is allowed to be complex valued and $S_0(x) \in C^\infty(\mathbb{R})$ is real valued.

In the semiclassical regime, where ϵ is small, the external potential $V_e(x)$ varies at larger spatial scales than periodic potential $V(y)$ does and can be considered weak compared with periodic field. The wave function ψ^ϵ and the related physical observables become oscillatory of wave length $O(\epsilon)$. A direct simulation of (5.1) requies time steps and mesh sizes to be of order $O(\epsilon)$, see e.g. Huang et al. (2007), making the computation of solutions extremely costly when ϵ becomes very small.

A more realistic approach is to explore an asymptotic model by passing $\epsilon \to 0$. The periodic structure requires the use of the modified WKB ansatz

$$\psi^\epsilon = A^\epsilon \left(t, x, \frac{x}{\epsilon}\right) e^{iS(t,x)/\epsilon},$$

in which the amplitude A^ϵ is assumed to admit an asymptotic expansion of the form

$$A^\epsilon(t,x,y) \sim A(t,x,y) + \epsilon A_1(t,x,y) + \epsilon^2 A_2(t,x,y) + \cdots .$$

The main gain of this modified WKB-approach is that it yields a *seperation of scales* within the appearing fast amplitude, $\epsilon-$oscillatory, and slowly varying amplitude.

The insertion of the above ansatz into (5.1) gives, to the leading orders of ϵ, a band Hamilton-Jacobi equation for the phase $S(t,x)$ and the transport equation for the amplitude $\rho = \int_0^{2\pi} |A|^2 dy$:

$$S_t + E(S_x) + V_e(x) = 0, \tag{5.4}$$

$$\rho_t + (E'(S_x)\rho)_x = 0, \tag{5.5}$$

where $E(k)$ is determined by solving the Bloch eigenvalue problem

$$H(k,y)z(k,y) = E(k)z(k,y), \quad z(k,y+2\pi) = z(k,y), \tag{5.6}$$

where

$$H(k,y) := \frac{1}{2}(-i\partial_y + k)[a(y)(-i\partial_y + k)] + V(y)$$

is a differential operator parameterized by k.

Singularity formation(S_x becomes discontinuous) in solutions of (5.4) is a generic phenomena even when the initial phase is smooth. Before the singularity formation, the classical theory in Bensoussan et al. (1978) asserts that the wave function can be recovered by a superposition of wave patterns on each band

$$\left\| \psi^\epsilon(t,\cdot) - \sum_n \sqrt{\rho_n}(t,\cdot) z_n \left((S_n)_x, \frac{x}{\epsilon}\right) \exp\left(\frac{iS_n(t,\cdot)}{\epsilon}\right) \right\|_{L^2(\mathbb{R})} \sim \mathcal{O}(\epsilon).$$

After the singularity formation standard shock capturing schemes will select the viscosity solution Crandall and Lions (1983, 1984), which is inadequate in this context for describing

the relevant physical phenomena since it violates the local superposition principle. Multi-valued solutions become of interest for (5.4). The first attempt to compute multi-valued solutions for (5.1) with $a(y) \equiv 1$ was due to Gosse and Markowich (2004), see also subsequent works Gosse and Mauser (2006a,b).

Recently, the level set method has been developed to compute the semiclassical limit of the Schrödinger equations Cheng et al. (2003); Jin et al. (2005c). The idea of the level set method is to build the phase gradient $u = S_x$ into the intersection of zero level sets of the phase space functions, which can be shown to satisfy the linear Liouville equation.

The aim of this paper is to extend the level set method of Cheng et al. (2003); Jin et al. (2005c) to solve the banded WKB system (5.4)–(5.5) and then compute physical observables for (5.1)-(5.3) accordingly. To illustrate the level set method developed in this paper, we let $\phi(t, x, k)$ be a function in phase space $(x, k) \in \mathbb{R}^2$, whose zero level set determines the multi-valued phase gradient $u = S_x$, i.e.,

$$u(t, x) \in \{k| \quad \phi(t, x, k) = 0\}, \quad (t, x) \in \mathbb{R}^+ \times \mathbb{R}.$$

It is shown that on n^{th} Bloch band, ϕ solves

$$\phi_t + E_n'(k)\phi_x - V_e'(x)\phi_k = 0.$$

The initial data for the level set function $\phi(t, x, k)$ is selected to uniquely imbed the initial phase into its zero set, say $\phi(0, x, k) = k - \partial_x S_0(x)$.

Following Liu and Wang (2008b), we compute the multi-valued density by

$$\rho_n^j(t, x) \in \left\{ \frac{f(t, x, k)}{|\partial_k \phi|} \Big| \quad \phi(t, x, k) = 0 \right\}, \quad (t, x) \in \mathbb{R}^+ \times \mathbb{R},$$

where f is determined by solving the Liouville equation on the n^{th} band

$$f_t + E_n'(k) f_x - V_e'(x) f_k = 0, \tag{5.7}$$
$$f(0, x, k) = \rho_n(0, x).$$

Here $E_n(k)$ is obtained from the associated Bloch eigenvalue problem (5.6), for which we apply a standard Fourier method.

The initial density on each band is calculated from $\psi^\epsilon(0,x)$ in (5.3) through a projection procedure,

$$\rho_n(x) = |a_n(x)|^2,$$

where

$$a_n(x) = \int_0^{2\pi} f(x,y)\bar{z}_n(\partial_x S_0, y)dy.$$

Note that this $f(x,y)$ is from the initial condition (5.3) and should not be confused with $f(t,x,k)$ in (5.7).

Considering the possible phase shift, the wave profile in each Bloch band takes the form

$$\psi_n^\epsilon(t,x) = \sum_{j=1}^{K_n} \sqrt{\rho_n^j(t,x)} z_n\left(u_n^j(t,x), \frac{x}{\epsilon}\right) \exp\left(\frac{iS_n^j(t,x)}{\epsilon}\right) \exp\left(\frac{i\pi}{4}\mu_n^j\right) + \mathcal{O}(\epsilon),$$

where the phase shift μ_n^j corresponds to the usual Keller-Maslov phase shift Maslov and Fedoriuk (1981) in the absence of periodic potentials.

Finally, the total position density over all bands is evaluated using Bloch waves and multi-valued densities obtained on each band:

$$\bar{\rho}(t,x) = \sum_n \sum_{j=1}^{K_n} \rho_n^j \sum_m |\hat{z}_{n,m}(u_n^j)|^2,$$

where $\hat{z}_{n,m}$ denotes the Fourier transform of $z_n(k,y)$ evaluated at $k = u_n^j$.

Although the level set equation is formulated in phase space, the computational cost, when using a local level set method such as those in Min (2004); Osher et al. (2002); Peng et al. (1999), is almost linear in the number of grid points in physical domain. Compared with the method in Gosse and Markowich (2004) using K-branch solutions, the level set method is simple and more robust in the case of large K.

This paper is organized as follows: in §2, we develop the level set method and show how to evaluate the position density. §3 describes the numerical procedures followed by a series of numerical tests in §4.

Level Set Formulation

In this section we follow a standard hybrid of semiclassical approximation and the homogenization to derive the Bloch eigenvalue problem and the Bloch banded WKB system for phase and amplitude, and then explore the level set method at each Bloch band, followed by evaluation of the position density over a sample set of Bloch bands.

Semiclassical homogenization and Bloch decomposition

We now sketch the asymptotic procedure Bensoussan et al. (1978) to derive limiting models for the Schrödinger equation

$$i\epsilon\frac{\partial\psi^\epsilon}{\partial t} = -\frac{\epsilon^2}{2}\frac{\partial}{\partial x}\left(a\left(\frac{x}{\epsilon}\right)\frac{\partial\psi^\epsilon}{\partial x}\right) + V\left(\frac{x}{\epsilon}\right)\psi^\epsilon + V_e(x)\psi^\epsilon, \quad x \in \mathsf{IR}, t \in \mathsf{IR}^+ \tag{5.8}$$

$$\psi^\epsilon(x,0) = e^{iS_0(x)/\epsilon} f\left(x, \frac{x}{\epsilon}\right). \tag{5.9}$$

A standard WKB ansatz

$$\psi^\epsilon(t,x) = A^\epsilon(t,x)\exp(iS(t,x)/\epsilon), \quad A^\epsilon = A + \epsilon A_1 + \epsilon^2 A_2 + \cdots,$$

when applied to the above Schrödinger equation, with a separation of real and imaginary parts, yields the following WKB system

$$S_t + a\left(\frac{x}{\epsilon}\right)\frac{(S_x)^2}{2} + V\left(\frac{x}{\epsilon}\right) + V_e(x) = 0, \tag{5.10}$$

$$(A^2)_t + a'\left(\frac{x}{\epsilon}\right)(A^2)_x + a\left(\frac{x}{\epsilon}\right)(A^2 S_x)_x = 0. \tag{5.11}$$

In this way the phase still oscillates on $O(\epsilon)$ scale, which is inconsistent with the $S \sim O(1)$ assumption.

As illustrated in Bensoussan et al. (1978); Guillot et al. (1988), a modified WKB ansatz with a two-scale amplitude needs to be considered

$$A^\epsilon(t,x,y := \frac{x}{\epsilon}) = A(t,x,y) + \epsilon A_1(t,x,y) + \cdots, \tag{5.12}$$

where $A^\epsilon(t,x,y)$ is a $2\pi-$periodic function in y. A substitution of this refined ansatz into (5.8), extracting $\mathcal{O}(1)$ terms, gives

$$\begin{aligned} &A\left(S_t+\tfrac{1}{2}a\left(y\right)\left(S_x\right)^2-\tfrac{i}{2}a'\left(y\right)S_x+V(y)+V_e(x)\right) \\ &=\tfrac{1}{2}\left(a'\left(y\right)A_y+a\left(y\right)A_{yy}+2ia\left(y\right)S_xA_y\right). \end{aligned} \tag{5.13}$$

This formulation allows for a separation of slow and fast variables as $A(t,x,y)=a(t,x)z(k,y)$ through $k=S_x$, which can be regarded as a parameter for each fixed x:

$$S_t+V_e(x)=-H(k,y)z(k,y)/z(k,y)=-E(k), \tag{5.14}$$

where

$$H(k,y)=-\frac{1}{2}(\partial_y+ik)[a(y)(\partial_y+ik)(\cdot)]+V(y)\cdot,\quad k=S_x.$$

Here $-E(k)$ stands for a parameter depending only on $k=S_x$.

Note that the shifted cell operator $H(k,y)$ when equipped with a periodic boundary condition forms a standard eigenvalue problem

$$H(k,y)z_n(k,y)=E_n(k)z_n(k,y), \tag{5.15}$$

$$z_n(k,y+2\pi)=z_n(k,y),\quad k\in\mathcal{B},\quad y\in\mathbb{R}.$$

It is known Wilcox (1978) that for a mild condition upon $V(y)$ and $a(y)>0$, $H(k.y)$ admits a complete set of eigenfunctions z_n for each fixed k, in the sense that $\{z_n(k,y)\}_{n=1}^{\infty}$ form an orthonormal basis in $L^2(0,2\pi)$ for any fixed k. Without loss of generality k is confined to the cell $\mathcal{B}=[-0.5,0.5]$, called reciprocal cell of $\mathcal{Y}=[0,2\pi]$ (or a Brillouin zone in physical literature)Bensoussan et al. (1978); Wilcox (1978). Correspondingly there exists a countable family of real eigenvalues which can be ordered according to

$$E_1(k)\le E_2(k)\le\cdots\le E_n(k)\le\cdots,\quad n\in\mathbb{N},$$

including the respective multiplicity. The set $\{E_n(k)|\quad k\in\mathcal{B}\}$ is called the n^{th} energy band, which together with the corresponding Bloch functions characterizes the spectral properties of the operator $H(k,y)$.

The superposition principle for linear Schrödinger equations suggests that the wave function have an asymptotic description of the form

$$\psi^\epsilon(t,x) = \sum_{n=1}^{\infty} a_n(t,x) z_n \left(\partial_x S_n, \frac{x}{\epsilon}\right) e^{iS_n(t,x)/\epsilon} + \mathcal{O}(\epsilon),$$

where $S_n(t,x)$ satisfies the n^{th} band Hamilton-Jacobi equation

$$S_t + E_n(S_x) + V_e(x) = 0. \tag{5.16}$$

Substitution of the ansatz $A = a_n z_n$ into (5.13) leads to the following equation:

$$\partial_t a_n + \frac{1}{2} a_n \partial_x E_n'(S_x) + \partial_x a_n E_n'(S_x) + \beta a_n = 0, \tag{5.17}$$

with

$$\beta = (\partial_t z_n, z_n) - \frac{1}{2}\partial_x E_n'(S_x) - \frac{i}{2}((\partial_y + iS_x)[a(y)\partial_x z_n] + a(y)\partial_x(\partial_y + iS_x)[z_n], z_n).$$

As shown in Appendix that β_n is purely imaginary, therefore $\rho_n = |a_n|^2$ satisfies

$$(\rho_n)_t + (E_n'(S_x)\rho_n)_x = 0. \tag{5.18}$$

Upon these equations for density, phase as well as the Bloch waves we preceed to formulate our Bloch band based level set method.

Bloch band based level set equation

Once we obtain the WKB system on n^{th} Bloch band

$$S_t + E_n(S_x) + V_e(x) = 0,$$
$$\rho_t + (E_n'(S_x)\rho)_x = 0,$$

the next task is to solve them numerically to obtain multi-valued solutions (in this section, for simplicity, band indexes for ρ is dropped). Here, multi-valued solutions shall be sought in order to capture the relevant physical phenomenon.

Let $\phi(t,x,k)$ be a function in phase space, whose zero level set implicitly describes the phase gradient $\partial_x S(t,x)$, where $S(t,x)$ solves (5.16), then ϕ is proven to satisfy

$$\phi_t + E_n'(k)\phi_x - V_e'(x)\phi_k = 0, \tag{5.19}$$

$$\phi(0,x,k) = k - \partial_x S_0(x), \tag{5.20}$$

with $E_n'(k)$ solved from (5.15). The multi-valued velocity is then given by

$$u_n^j(t,x) \in \{k| \quad \phi(t,x,k) = 0\}, \quad \forall (t,x) \in \mathbb{R}^+ \times \mathbb{R}.$$

The corresponding multi-valued density can be evaluated as proposed in Liu and Wang (2008b)

$$\rho_n^j(t,x) \in \left\{ \frac{f(t,x,k)}{|\det(\nabla_k \phi)|} \middle| \quad \phi(t,x,k) = 0 \right\}, \quad \forall (t,x) \in \mathbb{R}^+ \times \mathbb{R} \tag{5.21}$$

where f solves

$$f_t + E_n'(k) f_x - V_e'(x) f_k = 0, \tag{5.22}$$

$$f(0,x,p) = \rho_0(x), \tag{5.23}$$

where $\rho_0(x)$ is to be determined from the initial data $\psi^\epsilon(0,x)$, see (5.28).

Note that we need to compute $E_n'(k)$ in the level set equation, which can also be evaluated based on $\{z_n\}$. Differentiating the identity

$$H(k,y) z_n = E_n(k) z_n,$$

with respect to k and taking inner product with z_n, we have

$$E_n'(k) = (H_k z_n, z_n) + ((H-E)\partial_k z_n, z_n)\,. \tag{5.24}$$

The fact that H is self-adjoint gives

$$((H-E)\partial_k z_n, z_n) = (\partial_k z_n, (H-E) z_n) = 0.$$

This along with (5.24) gives

$$\begin{aligned} E_n'(k) &= (H_k z_n, z_n) \\ &= k \int_0^{2\pi} a(y) |z_n|^2 dy + \int_0^{2\pi} a(y) \mathrm{Im}(\bar{z}_n \partial_y z_n) dy. \end{aligned} \tag{5.25}$$

Remark 5. The above procedure is extendable to more general cases, say the case with coefficient $a(x, x/\epsilon)$ and potential $V(x, x/\epsilon)$. The formulation is analogous. However, in this case the Bloch eigenvalue problem becomes

$$H(k,x,y)z(k,x,y) = E(k,x)z(k,x,y), \quad z(k,x,y) = z(k,x,y+2\pi), \quad \forall (k,x) \in \mathcal{B} \times \mathbb{R}.$$

A level set formulation in multi-dimensional case can also be derived similarly.

Initial band configuration

We now discuss the recovery of the initial band density $\rho_n(0,x)$ from the given initial data

$$\psi_0^\epsilon\left(x, \frac{x}{\epsilon}\right) = f\left(x, \frac{x}{\epsilon}\right) \exp(iS_0(x)/\epsilon), \tag{5.26}$$

with a real-valued phase $S_0 \in C^\infty(\mathbb{R})$ and a possible complex-valued amplitude $f(x,\cdot) \in L^2(\mathbb{R})$.

For each fixed x, we also have $\psi_0(x,\cdot) \in L^2(\mathbb{R})$. Using the Bloch expansion theorem in (Bensoussan et al., 1978§3.2 of Chapter 4), $\psi_0^\epsilon(x,\cdot)$ can be decomposed in terms of Bloch waves, i.e.,

$$\psi_0^\epsilon(x,y) = \sum_{n=1}^{\infty} \int_{\mathcal{B}} \hat{\psi}_n(x;k) e^{iky} z_n(k,y) dk,$$

where the n^{th} band Bloch coefficients

$$\hat{\psi}_n(x;k) := \int_{\mathbb{R}} \psi_0^\epsilon(x,\xi) e^{-ik\xi} \bar{z}_n(k,\xi) d\xi.$$

Furthermore, one has Parseval's Identity:

$$\int_R |\psi_0(x,y)|^2 dy = \sum_{n=1}^{\infty} \int_B |\hat{\psi}_n(x;k)|^2 dk. \tag{5.27}$$

Using the stationary phase method, we have

$$\psi_0^\epsilon(x,y) = \sum_{n=1}^{\infty} a_n(x) z_n(\partial_x S_0, y) \exp(iS_0(x)/\epsilon) + \mathcal{O}(\epsilon).$$

Thus we have

$$f(x,y) \approx \sum_{n=1}^{\infty} a_n(x) z_n(\partial_x S_0, y).$$

Using the orthonormality of $z_n(\partial_x S_0, y)$, we have the following approximation for a_n

$$a_n(x) \approx \int_0^{2\pi} f(x,y)\bar{z}_n(\partial_x S_0, y)dy.$$

Then $\rho_n(x)$ is naturally approximated by

$$\rho_n = |a_n(x)|^2 \approx \left| \int_0^{2\pi} f(x,y)\bar{z}_n(\partial_x S_0, y)dy \right|^2. \tag{5.28}$$

Evaluation of position density

In previous sections, we compute the multi-valued velocities $u_n := \partial_x S_n$, and density ρ_n in n^{th} band. To recover the wave function ψ_n^ϵ, it is necessary to incorporate the so called Keller-Maslov phase shift Maslov and Fedoriuk (1981) as a caustic correction.

Let $\{u_n^j, j = 1, \cdots, K_n\}$ be the multi-valued velocities, $\{S_n^j, j = 1, \cdots, K_n\}$ and $\{\rho_n^j, j = 1, \cdots, K_n\}$ be the corresponding phases and densities on n^{th} band, the original wave function ψ_n^ϵ, with a possible phase shift $\frac{\pi}{4}\mu_n^j$, has the following form

$$\psi_n^\epsilon(t,x) = \sum_{j=1}^{K_n} \sqrt{\rho_n^j} z_n\left(u_n^j, \frac{x}{\epsilon}\right) \exp\left(\frac{iS_n^j}{\epsilon}\right) \exp\left(\frac{i\pi}{4}\mu_n^j\right) + \mathcal{O}(\epsilon), \tag{5.29}$$

where $\exp(\frac{i\pi}{4}\mu_n^j)$ is the phase shift at j^{th} caustic point of n^{th} band. Note that this phase shift does not affect the position density to be computed here.

Theorem 5.0.7. Let $\rho^\epsilon = \sum_n \rho_n^\epsilon$ be the total position density, where $\rho_n^\epsilon = \psi_n^\epsilon \overline{\psi_n^\epsilon}$ is the position density on the n^{th} band, with ψ_n^ϵ given in (5.29), and ρ_n^j, u_n^j be the multi-valued density and velocity on n^{th} band respectively, then

$$\rho^\epsilon \rightharpoonup \bar{\rho} := \sum_n \sum_{j=1}^{K_n} \rho_n^j \sum_m |\hat{z}_{n,m}(u_n^j)|^2 \quad as \quad \epsilon \to 0, \tag{5.30}$$

where $\hat{z}_{n,m}$ satisfies

$$z_n(k,y) = \sum_m \hat{z}_{n,m}(k)e^{imy}.$$

Proof. Since $z_n(k, x/\epsilon)$ is $2\pi-$periodic function in x/ϵ, Fourier series gives that

$$\begin{aligned} z_n(u_n^j, y) &= \sum_m \hat{z}_{n,m}(u_n^j)e^{imy}, \\ \overline{z_n(u_n^{j'}, y)} &= \sum_{m'} \overline{\hat{z}_{n,m'}(u_n^{j'})}e^{-im'y}. \end{aligned}$$

Thus the position density ρ_n^ϵ can be calculated as

$$\rho_n^\epsilon = \psi_n^\epsilon \overline{\psi_n^\epsilon} = \sum_{j=1}^{K_n} \rho_n^j \sum_m |\hat{z}_{n,m}(u_n^j)|^2 + O_1 + \mathcal{O}(\epsilon),$$

where O_1 refers to the *oscillatory terms* given by

$$\begin{aligned} O_1 = &\sum_{j\neq j'}^{K_n} \sqrt{\rho_n^j \rho_n^{j'}} \exp\left(i\frac{S_n^j - S_n^{j'}}{\epsilon}\right) \exp\left(\frac{i\pi(\mu_n^j - \mu_n^{j'})}{4}\right) z_n\left(u_n^j, \frac{x}{\epsilon}\right) \overline{z_n\left(u_n^{j'}, \frac{x}{\epsilon}\right)} \\ &+ \sum_{j=1}^{K_n} \rho_n^j \sum_{m\neq m'} \hat{z}_{n,m}(u_n^j) \overline{\hat{z}_{n,m'}(u_n^j)} \exp(i(m-m')x/\epsilon) := O_{11} + O_{12}. \end{aligned}$$

Now we formally show that O_1 weakly converges to zero as ϵ goes to zero. For any test function $\Phi \in C_0^\infty$,

$$\begin{aligned} &\int_{\mathbb{R}} O_{11}\Phi(x)dx \\ &= \sum_{j\neq j'}^{K_n} \sum_{m,m'} \int_{\mathbb{R}} \sqrt{\rho_n^j \rho_n^{j'}} \exp\left(i\frac{S_n^j - S_n^{j'} + (m-m')x}{\epsilon}\right) \exp\left(\frac{i\pi(\mu_n^j - \mu_n^{j'})}{4}\right) \hat{z}_m(u_n^j) \overline{\hat{z}_{m'}(u_n^{j'})} \Phi(x)dx. \end{aligned}$$

Let $S_{jj'mm'}(x) := S_n^j(x) - S_n^{j'}(x) + (m-m')x$, by the stationary phase method, as $\epsilon \to 0$, the main contribution comes from the points set

$$\mathcal{A} := \{x | \partial_x S_{jj'mm'}(x) = 0, S_{jj'mm'}(x) \neq 0, \quad j \neq j' \in 1, \cdots, K_n, \quad m, m' \in \mathbb{Z}\}. \tag{5.31}$$

This only happens when the difference of velocities in two branches is an integer. Since the velocities on all branches are continuous, $\mathcal{A}$ contains at most countable isolated points. Hence

$$measure(\mathcal{A}) = 0. \tag{5.32}$$

Let

$$h(x) = \sqrt{\rho_n^j \rho_n^{j'}} \exp\left(\frac{i\pi(\mu_n^j - \mu_n^{j'})}{4}\right) \hat{z}_m(u_n^j) \overline{\hat{z}_m(u_n^{j'})} \Phi(x),$$

and suppose $S_{jj'mm'}$ has a single and non-degenerate critical point x^*, then Theorem 1.1 in Maslov and Fedoriuk (1981) implies

$$\int h(x) \exp\left(i\frac{S_{jj'mm'}(x)}{\epsilon}\right) dx = \epsilon^{\frac{1}{2}} \exp\left(i\frac{S_{jj'mm'}(x^*)}{\epsilon}\right) h(x^*) + \mathcal{O}(\epsilon^{\frac{3}{2}}), \tag{5.33}$$

which converges to zero as $\epsilon \to 0$. Suppose $\mathcal{A}$ contains only non-degenerate points, (5.33), combined with (5.32), we obtain

$$\int_{\mathbb{R}} O_{11}\Phi dx \sim \sum_{x^*\in\mathcal{A}} \epsilon^{\frac{1}{2}} \exp\left(i\frac{S_{jj'mm'}(x^*)}{\epsilon}\right) h(x^*) \to 0 \quad as \quad \epsilon \to 0. \tag{5.34}$$

In a similar manner

$$\int_{\mathbb{R}} O_{12}\Phi(x)dx = \int_{\mathbb{R}} \sum_{j=1}^{k_n} \rho_n^j \sum_{m\neq m'} \hat{z}_{n,m}(u_n^j)\overline{\hat{z}_{n,m'}(u_n^j)} \exp(i(m-m')x/\epsilon)\Phi(x)dx.$$

It is obvious that $\partial_x \frac{(m-m')x}{\epsilon} \neq 0$ for all x if $m \neq m'$. Thus

$$\int_{\mathbb{R}} O_{12}\Phi(x) \to 0 \quad as \quad \epsilon \to 0. \tag{5.35}$$

Then combining (5.34) and (5.35), we have

$$\rho_n^\epsilon \rightharpoonup \bar{\rho}_n = \sum_{j=1}^{K_n} \rho_n^j \sum_m |\hat{z}_{n,m}(u_n^j)|^2 \quad as \quad \epsilon \to 0. \tag{5.36}$$

Finally, by a superposition of all Bloch bands, we have

$$\psi^\epsilon = \sum_n \sum_{j=1}^{K_n} \sqrt{\rho_n^j} z_n(u_n^j, \frac{x}{\epsilon}) \exp\left(\frac{iS_n^j}{\epsilon}\right) \exp\left(\frac{i\pi}{4}\mu_n^j\right) + \mathcal{O}(\epsilon). \tag{5.37}$$

The overall position density is thus given by

$$\rho^\epsilon = \psi^\epsilon\overline{\psi^\epsilon} = \sum_n \sum_{j=1}^{K_n} \rho_n^j \sum_m |\hat{z}_{n,m}(u_n^j)|^2 + O_2 + \mathcal{O}(\epsilon), \tag{5.38}$$

where O_2 refers to all oscillatory terms within one band and crossing-bands terms.

Similarly, we formally show that O_2 converges to zero weakly as ϵ goes to zero. By Fourier expansion of $z_n(u_n^j, y)$ and $\overline{z_{n'}(u_{n'}^{j'}, y)}$ and let

$$S_{jj'mm'} = S_n^j(x) - S_{n'}^{j'}(x) + (m-m')x,$$

$$h'(x) = \sqrt{\rho_n^j \rho_{n'}^{j'}} \exp\left(\frac{i\pi(\mu_n^j - \mu_{n'}^{j'})}{4}\right) z_m(u_n^j)\overline{z_m(u_{n'}^{j'})}\Phi(x).$$

Semiclassically the only non-vanishing contributions comes from the points

$$\mathcal{B} := \{x | \partial_x S_{jj'mm'} = 0, \quad S_{jj'mm'} \neq 0, \quad j \neq j' \in 1, \cdots, K_n, \quad n, n', m, m' \in \mathbb{Z}\},$$

which is a measure-zero set of at most countable isolated points. Hence we have

$$\int_{\mathbb{R}} O_2 \Phi dx \sim \sum_{x^* \in \mathcal{B}} \epsilon^{\frac{1}{2}} \exp\left(i \frac{S_{jj'mm'}(x^*)}{\epsilon} \right) h'(x^*) \to 0 \quad as \quad \epsilon \to 0. \tag{5.39}$$

This upon institution into (5.38) gives the asserted (5.30). □

Therefore, in our numerical simulation the total position density $\bar{\rho}(x)$ is evaluated by

$$\bar{\rho}(x) = \sum_n \sum_{j=1}^{K_n} \rho_n^j \sum_m |\hat{z}_{n,m}(u_n^j)|^2. \tag{5.40}$$

Numerical Procedures

In this section, we first study the Bloch decomposition numerically and then show how to implement the level set method described. We characterize our approach mainly in the following steps.

Step 1. Solving Bloch eigenvalue problem

We first evaluate $E_n(k)$ from a sequence of the eigenvalue problems (5.15)

$$V(y) z_n + \frac{1}{2}(-i\partial_y + k)\left[a(y)(-i\partial_y + k) z_n\right] = E_n(k) z_n, \tag{5.41}$$

where $E_n(k)$ is the n^{th} energy band, and $e^{iky} z_n$ is a n^{th} Bloch function with $k \in [-\frac{1}{2}, \frac{1}{2}]$. Since $z_n, a(y)$ and $V(y)$ are $2\pi-$periodic functions, we can use Fourier series to approximate them and plug into (5.41). By expanding $V(y)$, $a(y)$ and $z_n(k, y)$ in Fourier series about y

$$V(y) = \sum_{q \in \mathbb{Z}} \hat{V}_q \exp(iqy), \quad \hat{V}_q = \frac{1}{2\pi} \int_0^{2\pi} V(y) \exp(-iqy) dy, \tag{5.42}$$

$$a(y) = \sum_{q \in \mathbb{Z}} \hat{a}_q \exp(iqy), \quad \hat{a}_q = \frac{1}{2\pi} \int_0^{2\pi} a(y) \exp(-iqy) dy, \tag{5.43}$$

$$z_n(k, y) = \sum_{q \in \mathbb{Z}} \hat{z}_{n,q} \exp(iqy), \quad \hat{z}_{n,q} = \frac{1}{2\pi} \int_0^{2\pi} z_n(k, y) \exp(-iqy) dy. \tag{5.44}$$

Insertion of these into (5.41), we obtain

$$\frac{1}{2} \sum_{q \in \mathbf{Z}} (k+m)(k+q) \hat{a}_{m-q} \hat{z}_{n,q} + \sum_{q \in \mathbf{Z}} \hat{V}_{m-q} \hat{z}_{n,q} = E_n(k) \hat{z}_{n,m}, \quad \forall m \in \mathbb{Z}. \tag{5.45}$$

Extracting $2N+1$ terms for $q \in \{-N, \cdots, N\}$, we have the corresponding matrix H of the eigenvalue problem as

$$H_{m,q} = \frac{1}{2}(k+m)(k+q)\hat{a}_{m-q} + \hat{V}_{m-q}, \quad -N \le m, q \le N$$

which is a Hermitian matrix satisfying

$$H \begin{bmatrix} (\hat{z}_n)_{-N} \\ \vdots \\ (\hat{z}_n)_N \end{bmatrix} = E_n(k) \begin{bmatrix} (\hat{z}_n)_{-N} \\ \vdots \\ (\hat{z}_n)_N \end{bmatrix}.$$

Note that by a transform of $\tilde{z}_n(y) = z_n(y)e^{imy}$ in (5.41), we obtain an equivalent eigenvalue problem to (5.45) for $\tilde{z}_n$, which shows that the eigenvalue problem is invariant under any integer shift in k. Taking $m = 1$, we have the following relation,

$$E_n(k+1) = E_n(k), \quad z_n(k+1, y) = z_n(k, y), \tag{5.46}$$

which implies that the fundamental domain of dual lattice, $\overline{\mathcal{B}} = [-0.5, 0.5]$, is not restricted.

Remark 6. The complexity of eigenvalue problem for general $N \times N$ matrix is of order N^3 Horn and Johnson (1985), which is considerably huge for large N. However, since the eigen-matrix is independent with respect to spatial grids and evolution, we only have to solve it once. Moreover, due to the special property of the matrix H, the complexity of finding eigenvalues will be dramatically reduced. Thus it is not a major issue in our computation.

After solving the above Bloch eigenvalue problem at each uniform grid point $\{k_i \in [-0.5, 0.5], i = -M, \cdots, M\}$ with mesh size Δk, we are equipped with discrete function values of $E_n(k_i)$. We now evaluate $\{E_n'(k_i), i = -M \cdots M\}$ for any grid point k_i. A natural way of computing first order derivative to a certain order accuracy is by polynomial interpolation using nearby grid points. Note that, periodic boundary conditions are used due to the 1-periodicity of $E(k)$, (5.46). A second order approximation is central difference

$$E'(k_i) = \frac{E(k_{i+1}) - E(k_{i-1})}{2\Delta k}, \tag{5.47}$$

and a fourth order approximation is given by

$$E'(k_i) = \frac{E(k_{i-2}) - 8E(k_{i-1}) + 8E(k_{i+1}) - E(k_{i+2})}{12\Delta k}. \tag{5.48}$$

Note that in this case, $E_n'(k)$ can also be computed from $z_n(k,y)$ by the integral (5.25).

Step 2. Bloch band based decomposition of initial data if needed

After solving the eigenvalue problem, we study the effects of number of energy bands, i.e., to answer the question: given an L^2 WKB-type wave function

$$\psi^\epsilon\left(x,\frac{x}{\epsilon}\right) = f\left(x,\frac{x}{\epsilon}\right)\exp(iS_0(x)/\epsilon)$$

and a desired accuracy, how many eigen-modes are needed to recover the density $\rho = \int_0^{2\pi}|\psi^\epsilon(x,y)|^2dy$? We will measure the accuracy by L^2 error

$$error = ||\rho - \sum_{n=1}^{M}\rho_n||_{L^2}, \quad M = 2,4,6,8,10,\cdots \tag{5.49}$$

with ρ_n defined in (5.28).

Step 3. Solving the level set equation

$$\phi_t + E'(k)\phi_x - V_e'(x)\phi_k = 0, \tag{5.50}$$

subject to initial data (5.20).

We discretize space with uniform mesh size Δx and Δk, and use $\phi(t,x_i,k_j)$ to denote the grid function value. Let $\phi_{ij}(t) \approx \phi(t,x_i,k_j)$ be the numerical solution, then the upwind semi-discrete scheme gives

$$\frac{d}{dt}\phi_{ij}(t) = L(\phi_{ij}), \tag{5.51}$$

$$\begin{aligned} L(\phi_{ij}) := & -A\frac{(\phi_{ij})_x^+ + (\phi_{ij})_x^-}{2} + |A|\frac{(\phi_{ij})_x^+ - (\phi_{ij})_x^-}{2} \\ & -V_e'\frac{(\phi_{ij})_k^+ + (\phi_{ij})_k^-}{2} + |V_e'|\frac{(\phi_{ij})_k^+ - (\phi_{ij})_k^-}{2}, \end{aligned} \tag{5.52}$$

where $A = E'(k)$ was evaluated in **Step 1**. High order spatial approximation can be achieved by high order ENO reconstruction applied to both $\phi_x^\pm$ and $\phi_k^\pm$ respectively, see Osher and Sethian (1988). Here we use a second order ENO scheme in our simulation.

In time, a two-stage, second order SSP Runge-Kutta method Gottlieb et al. (2001) is used

$$\begin{aligned} \phi_{ij}^* &= \phi_{ij}^n + \Delta t L(\phi_{i,j}^{(n)}), \\ \phi_{ij}^{n+1} &= \frac{1}{2}\phi_{ij}^n + \frac{1}{2}\left(\phi_{ij}^* + \Delta t L(\phi_{ij}^*)\right). \end{aligned} \tag{5.53}$$

Now,we briefly summarize the procedure here:

(i) Find high order approximation of $(\phi_{ij})^{\pm}_{x,k}$ using ENO, and $E'(k_j)$ using (5.47) or (5.48) at each grid point,

(ii) Solve (5.50) by using (5.51) and (5.53),

(iii) Project $\phi = 0$ onto $x - k$ plane to get S_x.

Note that in (ii), the grid point of $E'(k_j)$ might not be coincided with the grid point obtained in (5.47) or (5.48). In this case, we need to use interpolation. In our computation, we choose the same grid points for simplicity

Step 4. Computing the density ρ

We solve (5.22) with initial condition (5.23) using methods described in **step 3** in each band for f_n. We compute the total density by (5.40)

$$\bar{\rho}(x) = \sum_n \sum_{j=1}^{K_n} \rho_n^j \sum_m |\hat{z}_{n,m}(u_n^j)|^2,$$

where ρ_n^j and u_n^j are given by (5.21) as discussed in Liu and Wang (2008b).

Numerical Examples

Bloch band based initial decomposition

We first examine the accuracy of the Bloch band decomposition of the initial data

$$\psi_0(x) = f(x, x/\epsilon)e^{iS_0(x)/\epsilon}, \quad \epsilon \ll 1,$$

in terms of Bloch functions $\{z_n\}$ obtained from (5.41) with $V(y) = \cos(y)$ and $a(y) \equiv 1$. This internal potential $V(y) = \cos(y)$ aries in Mathieu's model.

The eigen-structure of this potential $V(y)$ and $a(y)$ is shown in Fig.5.1, in which we observe that all 5 eigenvalues are distinct for any k. It meets the assumption of the Bloch Band expansion in Section 2.

In the numerical simulation of this subsection, for simplicity, we are confining our initial condition $\psi_0(x, y)$ in $\mathbb{R} \times [0, 2\pi]$. In all examples the computation domain is $(x, k) \in [0, 2\pi] \times$

$[-0.5, 0.5]$ with 151×101 grid points and 101×101 eigen-matrix.

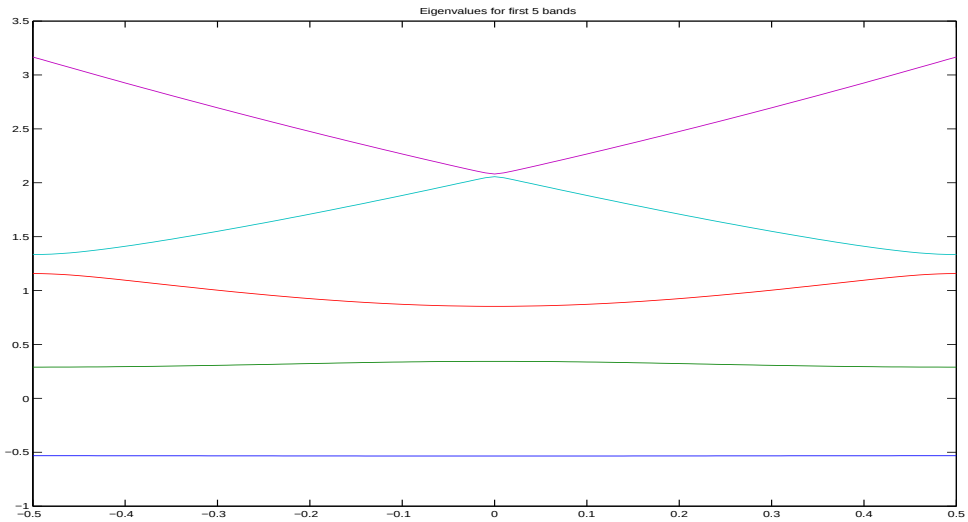

Figure 5.1 Eigenvalues for $V(y) = cos(y)$ and $a \equiv 1$ of band 1, 2, $\cdots$, 5 (bottom to top).

Example 1. We first consider initial data with

$$f\left(x, \frac{x}{\epsilon}\right) = \exp\left(\frac{-(x-\pi)^2}{2}\right), \quad S_0(x) = 0. \tag{5.54}$$

L^2 error defined in (5.49) is shown in Table 5.1.

# of bands	4	6	8	10	12
L^2 error	0.017099	0.001555	0.001547	0.001547	0.001547

Table 5.1 L^2 of decomposition of initial condition given in (5.54)

Example 2. We now consider the initial data with periodic phase, i.e.,

$$f\left(x, \frac{x}{\epsilon}\right) = \exp\left(\frac{-(x-\pi)^2}{2}\right), \quad S_0(x) = -0.3\cos(x). \tag{5.55}$$

# of bands	4	6	8	10	12
L^2 error	0.005762	0.001179	0.001177	0.001177	0.001177

Table 5.2 L^2 of decomposition of initial condition given in (5.55)

Similarly, L^2 error is listed in Table 5.2.

Example 3. We then consider a general initial amplitude with

$$f\left(x, \frac{x}{\epsilon}\right) = \exp\left(\frac{-(x-\pi)^2}{2}\right)\cos\left(\frac{x}{\epsilon}\right), \quad S_0(x) = 0. \tag{5.56}$$

Similarly, L^2 error is shown in Table 5.3.

# of bands	4	6	8	10	12
L^2 error	0.190590	0.001572	0.001404	0.001404	0.001404

Table 5.3 L^2 of decomposition of initial condition given in (5.56)

From these three examples, we see that 8 bands will give good approximation with L^2 error in the order of 10^{-3}, while $\Delta x = 2\pi/150$ and $\Delta k = 1/100$. More bands will not improve the accuracy of decomposition. Therefore, we need only a few bands in evolution to capture the physical quantities.

One figure comparing the exact density and decomposition approximation using 8 bands of Example 3 is listed in Fig.5.2. We see that they match very well. This tells that, in solving level set equations (5.50), only a few bands are needed, which makes the desired level set method more practical.

Solving Level Set Equation

We test our algorithm using the Mathieu's potential

$$V = \cos(x).$$

Case I: $a \equiv 1$ **and** $V_e = 0$

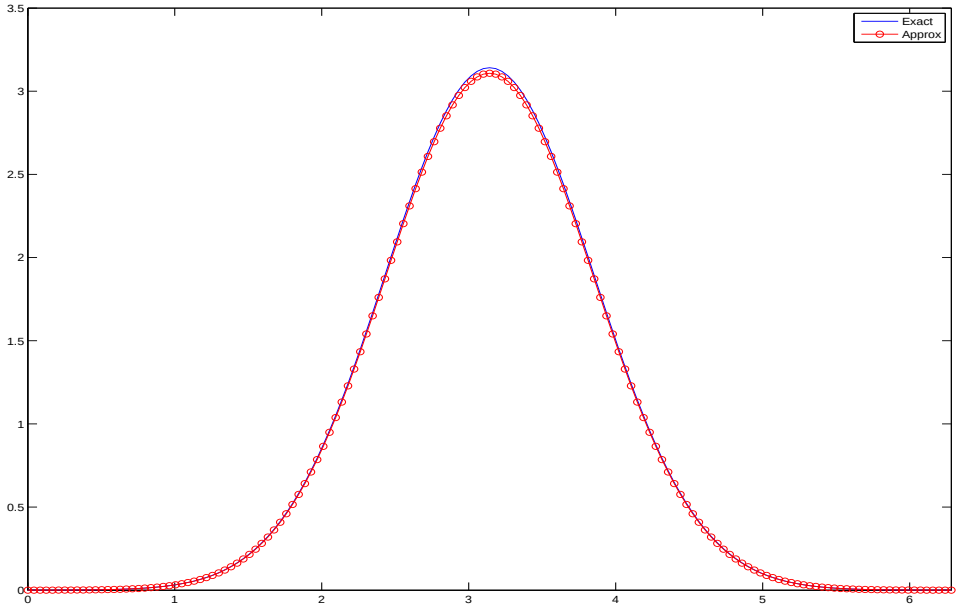

Figure 5.2 Example 3, Bloch Decomposition of initial density, exact density vs approximation with 8 bands.

Example 1.

$$\psi^{\epsilon}(0,x) = \exp(\frac{-0.3i\cos(x)}{\epsilon})\exp(-(x-\pi)^2)z_3(0.3\sin(x), x/\epsilon)$$

When initial velocity is a sine profile, both the third and fifth bands will lead to multi-valued solutions, since $E'_{3,5}(k)$ is positive when $k > 0$ and negative when $k < 0$. For the third band, the $|E'_3(k)|$ is approximately a parabola. Thus it has a finite time singularity. See Fig.5.3 for multi-valued velocity and density at different time. Here the density is calculated as

$$\sum_n \sum_{j=1}^{K_n} \rho_n^j \sum_m |\hat{z}_{n,m}(u_n^j)|^2.$$

From these figures we see that the density becomes unbounded(peak) where the velocity has turns.

Example 2.

$$\psi^\epsilon(0,x) = \exp(\frac{-0.3i\cos(x)}{\epsilon})\exp(-(x-\pi)^2)z_5(0.3\sin(x), x/\epsilon)$$

For fifth band, $|E_5'(k)|$ is like $|k|$; thus the sine profile just moves left/right when the velocity is negative/positive. Moreover, we observe multi-valuedness in velocity immediately after the evolution starts. See Fig.5.4 and Fig.5.5 for details.

Example 3.

$$\psi^\epsilon(0,x) = \exp(\frac{-0.3i\cos(x)}{\epsilon})\exp(-(x-\pi)^2)\left(z_4(0.3\sin(x), x/\epsilon)\right)$$

Previous examples show the formation of multi-valued solutions due to caustics. In this example, the case of rarefaction is also studied. In Fig. 5.6 and 5.7, we see that as the rarefaction appears around $x = \pi$, a vacuum is created there. Note that the multi-valued velocity at the boundaries are the waves from adjacent period, since we are assuming the velocity field is periodic.

Case II: $a \equiv 1$**,** $V_e \neq 0$

Example 4.

Now we test an example of harmonic external potential $V_e = \frac{|x-\pi|^2}{2}$ with initial data

$$\psi^\epsilon(0,x) = \exp(\frac{-0.3i\cos(x)}{\epsilon})\exp(-(x-\pi)^2)\left(z_5(0.3\sin(x), x/\epsilon)\right).$$

Due to V_e, the velocity increases while shock forms immediately after evolution. This phenomenon is observed in Fig.5.8. Besides the increment of velocity, we observe the motion of peak in intensity, which corresponds to the location of turning point in velocity. Clearly, the level set method is capable of dealing with any nonzero external potential V_e. However, in the case of $V_e \neq 0$, one needs to choose proper computation domain since the velocity may increase and exceed the computation domain.

Case III: general a **and** $V_e = 0$

Example 5.

$$a\left(\frac{x}{\epsilon}\right) = \frac{3}{2} + \sin\left(\frac{x}{\epsilon}\right)$$

$$\psi_0 = \exp\left(-\frac{(x-\pi)^2}{2}\right)\exp\left(\frac{-0.3i\cos(x)}{\epsilon}\right).$$

Here we test this initial data with Mathieu's potential. The eigen-structure for this potential and $a(y) = \frac{3}{2} + \sin(y)$ is shown in Fig. 5.9.

We first do the initial Bloch decomposition with error shown in Table 5.4. Here, we see that with $\Delta x = 2\pi/100$ and $\Delta k = 1/100$, decomposition with 8 bands already gives good approximation, i.e., L^2 error is 0.000950 and introducing more band would not increase the accuracy, either. So in our simulation, we only use 8 bands, in which there are at least 3 caustics and 3 rarefactions. In Fig. 5.10 and 5.11 with 201×101 grid points, we clearly see the movement of the wave, where peaks are corresponding to turning points of our multi-valued solution while valleys are corresponding to the rarefaction waves. Near $x = \pi$ there are oscillations due to the interactions of caustics and rarefactions.

# of bands	4	6	8	10	12
L^2 error e_2	0.004515	0.000967	0.000950	0.000950	0.000950

Table 5.4 L^2 error table for initial Bloch decomposition of example 5 with 101×101 grid points and 101 eigen-matrix.

Appendix

Here we show the derivation of the continuity equation of the density $\rho_n = |a_n|^2$

$$(\rho_n)_t + (E_n'(S_x)\rho_n)_x = 0. \tag{A.1}$$

For simplicity of presentation, we assume that $z_n(k, y)$ is differentiable in k(For general case, an integration argument is necessary).

By the solvability condition shown in Bensoussan et al. (1978), we have

$$(L_2 A, z_n) = 0, \tag{A.2}$$

where

$$L_2 = i\partial_t - \frac{1}{2}(\partial_y + iS_x)[a(y)\partial_x \cdot] - \frac{1}{2}\partial_x[a(y)(\partial_y + iS_x)\cdot].$$

By defining $L[\cdot] = (\partial_y + iS_x)(\cdot)$, we have

$$\partial_t a_n + \alpha_n(\partial_t z_n, z_n) + a_n E_k - \frac{i}{2} a_n \beta_1 = 0, \tag{A.3}$$

with

$$\beta_1 = \frac{\partial_x a_n}{2}(L[a(y)z_n] + a(y)L[z_n], z_n) + \frac{a_n}{2}(L[a(y)\partial_x z_n] + a(y)\partial_x L[z_n], z_n).$$

Differentiating $H(k,y)z_n(k,y) = E(k)z_n(k,y)$ both sides with respect to k and taking inner product with z_n, we obtain

$$((H_k - E_k)z_n, z_n) = ((E - H)\partial_k z_n, z_n).$$

Since H is self-adjoint,

$$((E - H)\partial_k z_n, z_n) = (\partial_k z_n, (E - H)z_n) = (\partial_k z_n, 0) \equiv 0,$$

which implies that

$$(L[a(y)z_n] + a(y)L[z_n], z_n) = 2iE_k.$$

Therefore, (A.3) becomes

$$\partial_t a_n + \frac{1}{2} a_n E_{kx} + \partial_x a_n E_k + \beta a_n = 0, \tag{A.4}$$

with

$$\beta = (\partial_t z_n, z_n) - \frac{1}{2}E_{kx} - \frac{i}{2}(L[a(y)\partial_x z_n] + a(y)\partial_x L[z_n], z_n).$$

Now we define

$$\beta_1 = (\partial_t z_n, z_n),$$
$$\beta_2 = -\frac{1}{2}E_{kx} + (L[a(y)\partial_x z_n] + a(y)\partial_x L[z_n], z_n).$$

Then

$$\beta_1 \in i\mathbb{R} \tag{A.5}$$

follows immediately from

$$0 \equiv \partial_t(z_n, z_n) = (\partial_t z_n, z_n) + (z_n, \partial_t z_n) = (\partial_t z_n, z_n) + \overline{(\partial_t z_n, z_n)}.$$

By differentiating $(H_k z_n, z_n) = E_k$ with respect to x on both sides, we can further expand β_2 as

$$\begin{aligned}\beta_2 = -\frac{i}{2}\{ &-\frac{1}{2}(\partial_x(L[a(y)z_n] + a(y)L[z_n]), z_n) \\ &-\frac{1}{2}(L[a(y)z_n] + a(y)L[z_n], \partial_x z_n) \\ &+ (L[a(y)\partial_x z_n] + a(y)\partial_x L[z_n], z_n)\} := -\frac{i}{2}\tilde{\beta}_2.\end{aligned}$$

Further calculation gives that

$$\begin{aligned}\tilde{\beta}_2 =&(a_y\partial_x z_n, z_n) + (a\partial_{xy} z_n, z_n) + iS_x[(a\partial_x z_n, z_n) - (az_n, \partial_x z_n)] \\ =&((a\partial_x z_n)_y, z_n) - (a\partial_y z_n, \partial_x z_n) + iS_x[(a\partial_x z_n, z_n) - \overline{(a\partial_x z_n, z_n)}].\end{aligned}$$

Integrating by parts in $((a\partial_x z_n)_y, z_n)$ and using the fact that $a(y)$ and $z(k, y)$ are $2\pi-$periodic functions in y, we have

$$\begin{aligned}\tilde{\beta}_2 =&iS_x[(a\partial_x z_n, z_n) - \overline{(a\partial_x z_n, z_n)}] - (a\partial_x z_n, \partial_y z_n) - (a\partial_y z_n, \partial_x z_n) \\ =&iS_x[(a\partial_x z_n, z_n) - \overline{(a\partial_x z_n, z_n)}] - [(a\partial_x z_n, \partial_y z_n) + \overline{(a\partial_x z_n, \partial_y z_n)}] \in \mathbb{IR},\end{aligned}$$

which implies that $\beta_2 = -\frac{i}{2}\tilde{\beta}_2 \in i\mathbb{IR}$.

Therefore, combining (A.5)

$$\beta = \beta_1 + \beta_2 \in i\mathbb{IR},$$

which leads to the continuity equation (A.1).

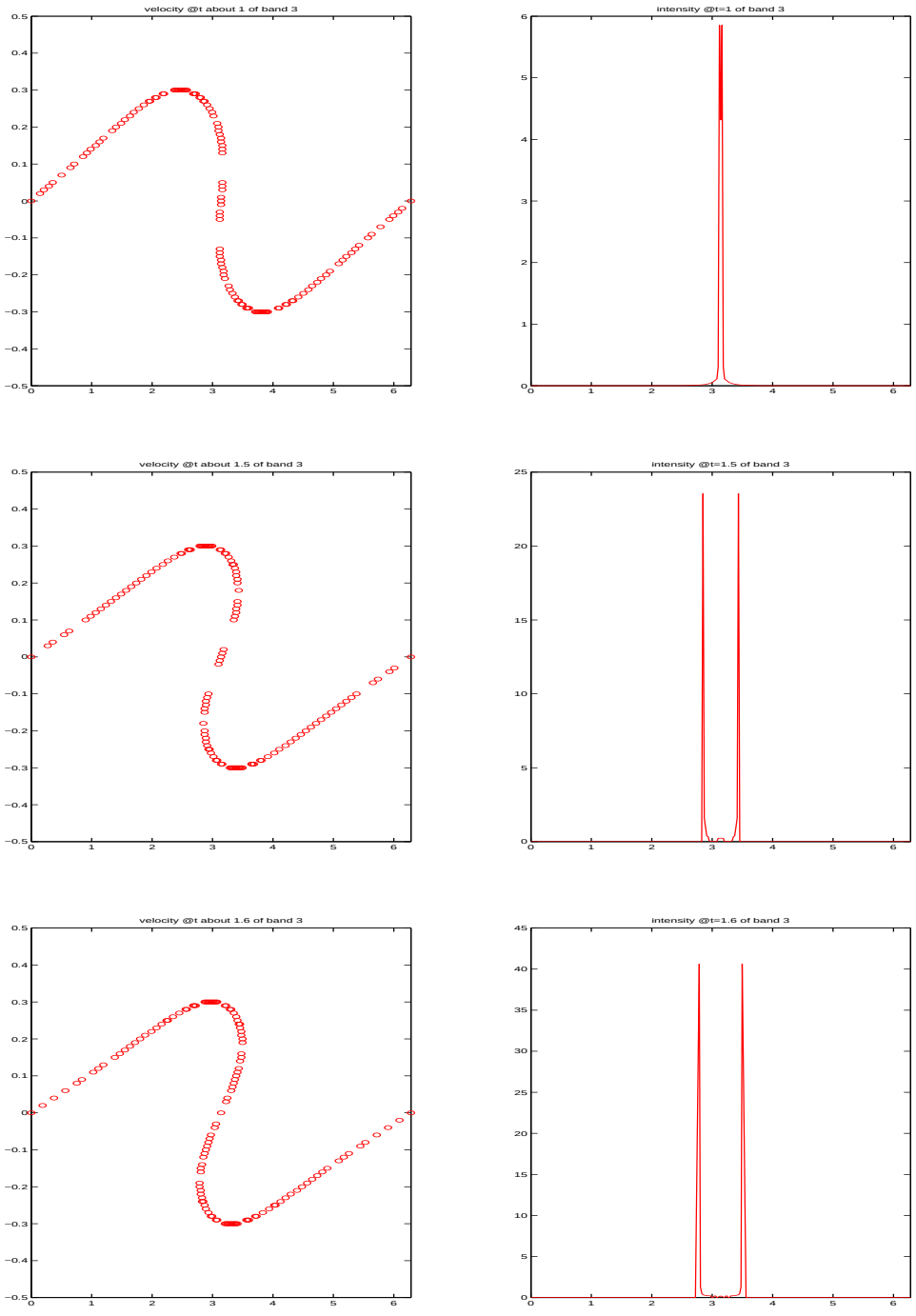

Figure 5.3 Example 1, velocity and density of band 3 at different times.

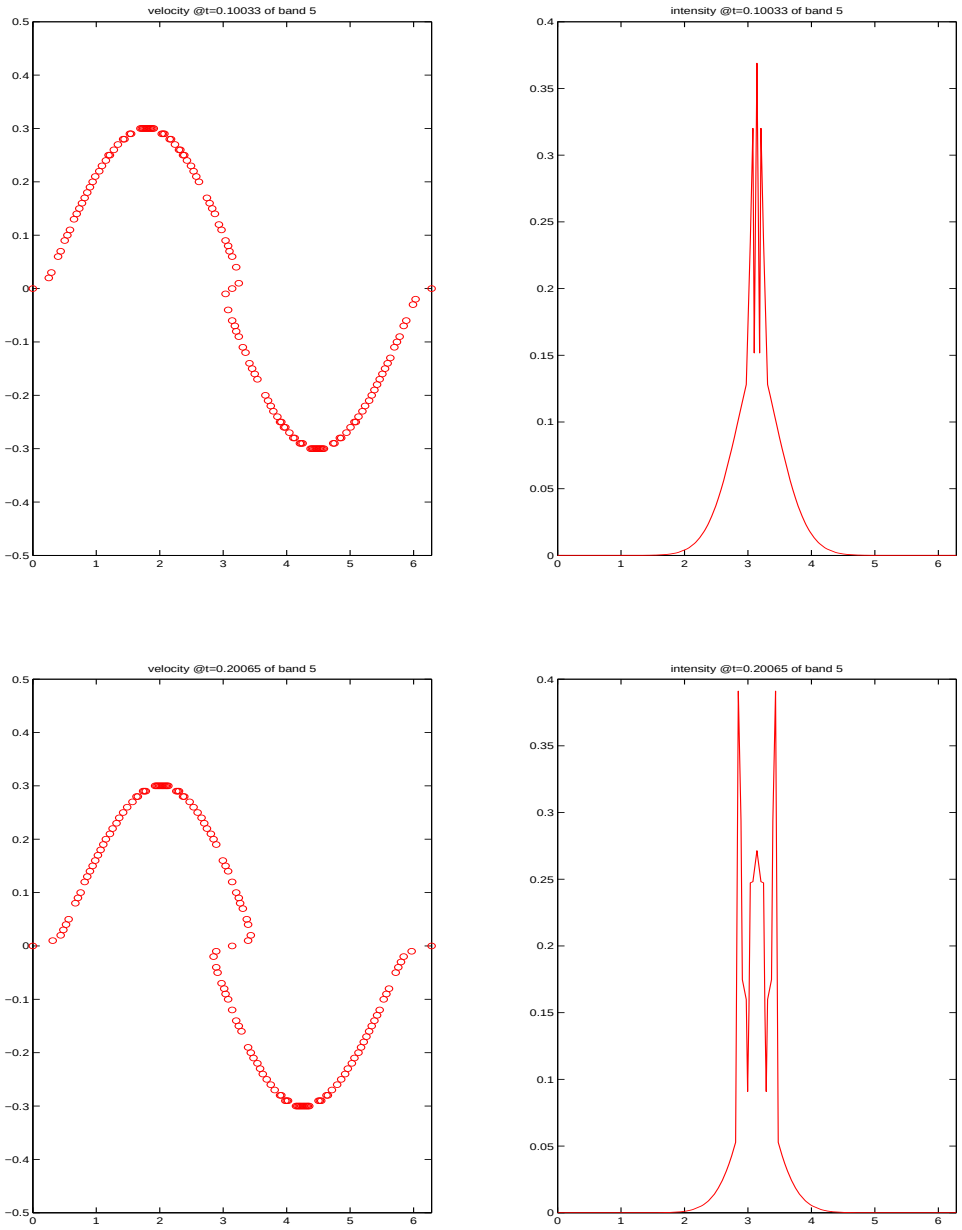

Figure 5.4 Example 2, velocity and density of band 5 at time about 0.1 and 0.2.

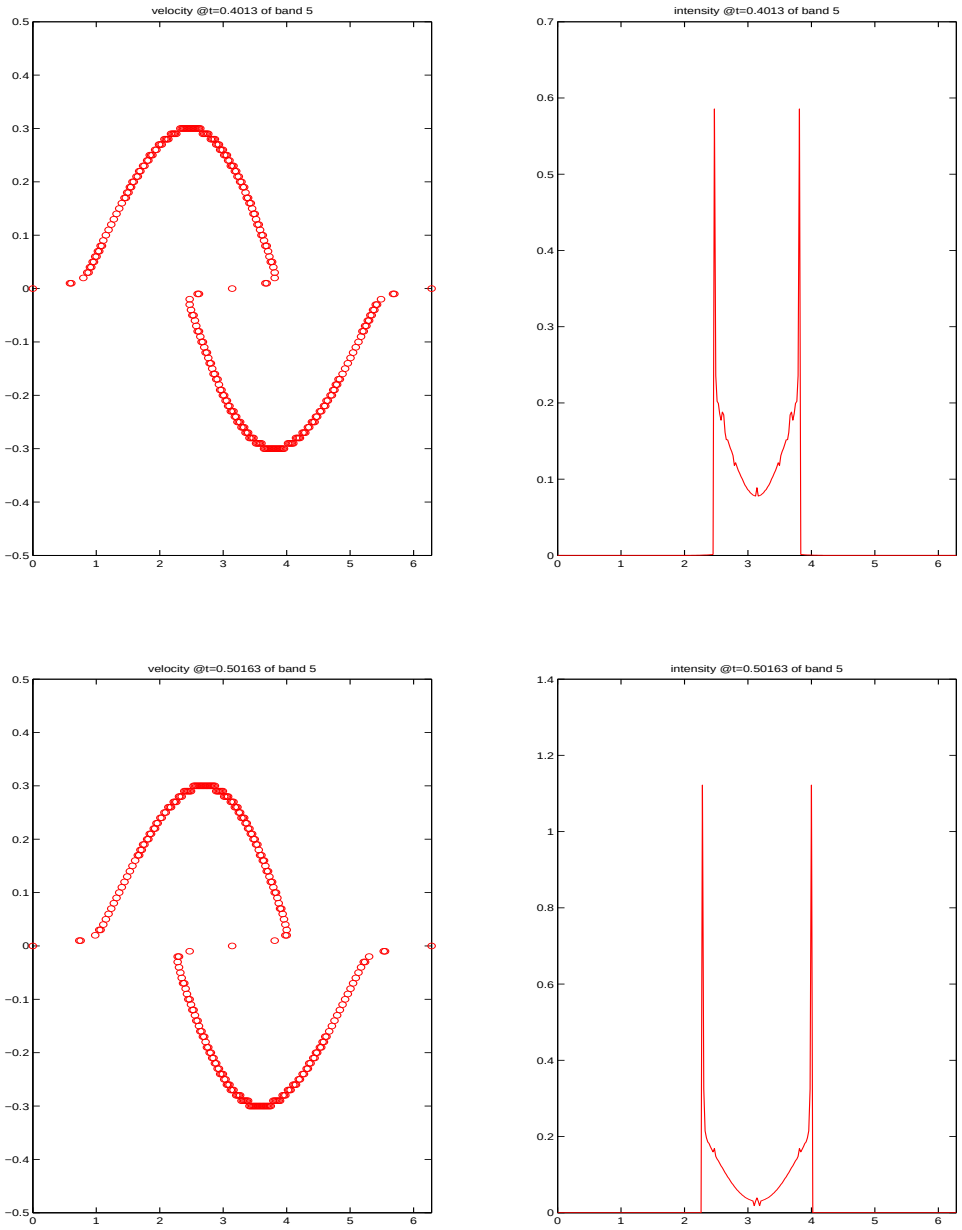

Figure 5.5 Example 2, velocity and density of band 5 at time about 0.4 and 0.5.

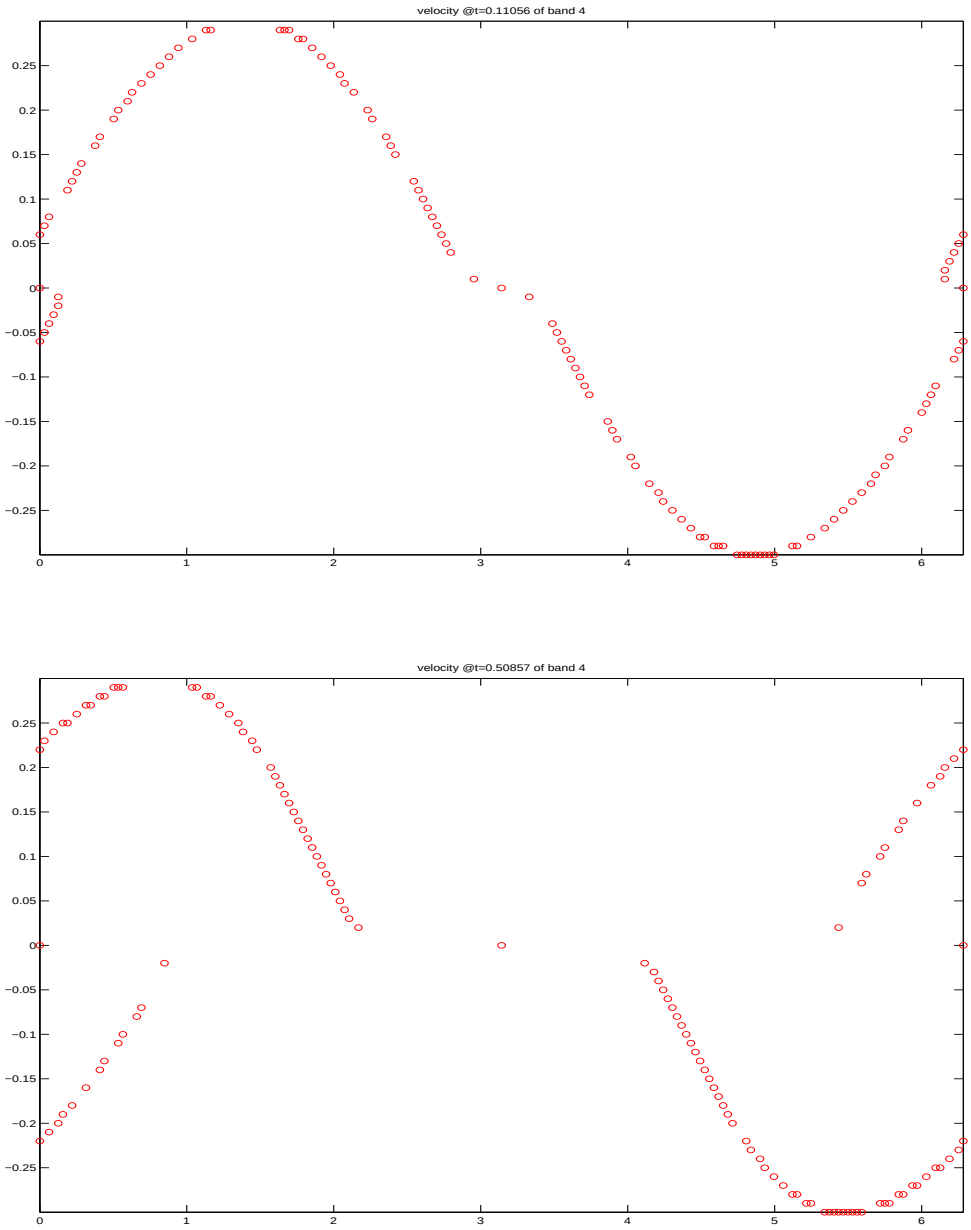

Figure 5.6 Example 3, velocity of band 4 at different time.

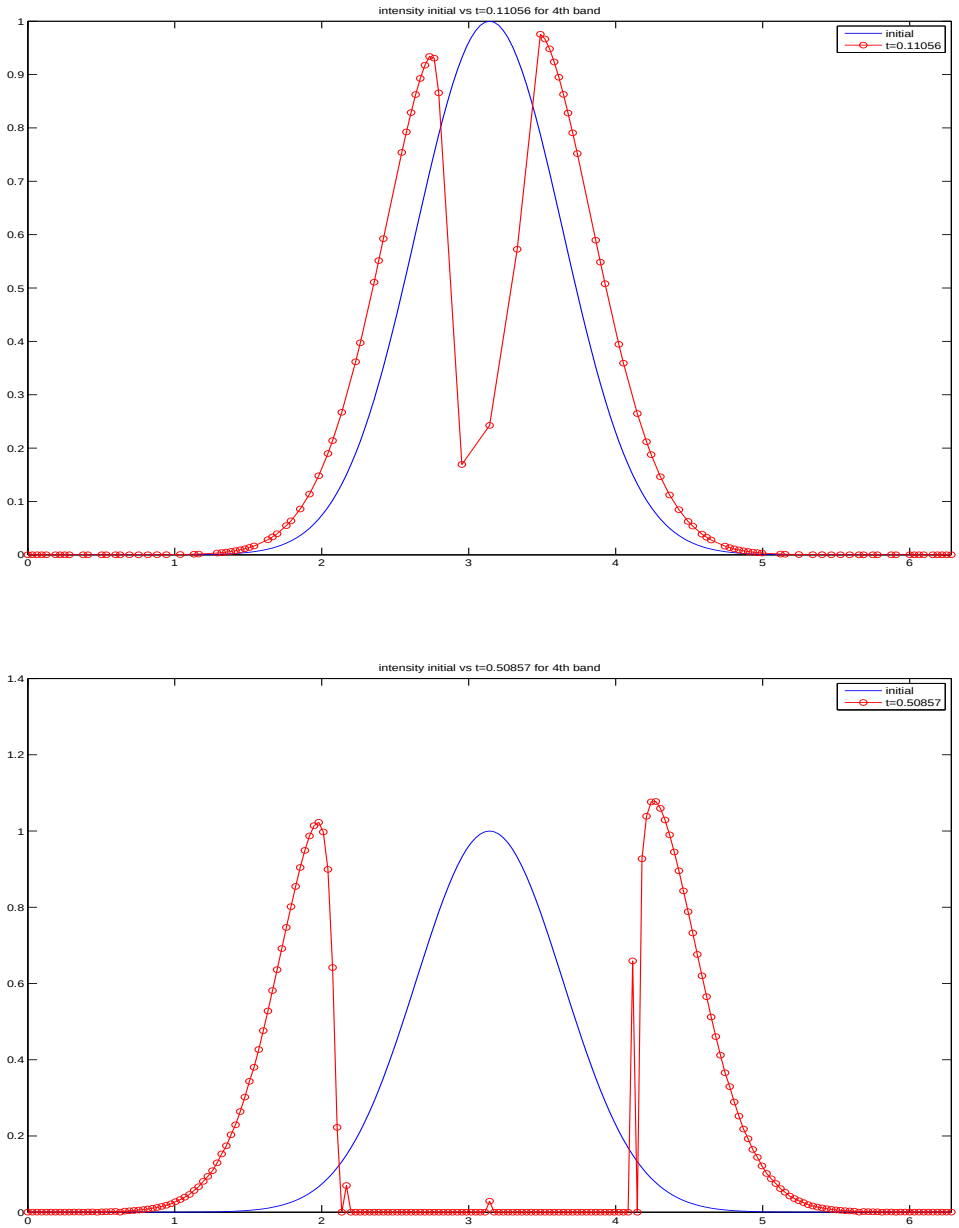

Figure 5.7 Example 3, density of band 4 at different time.

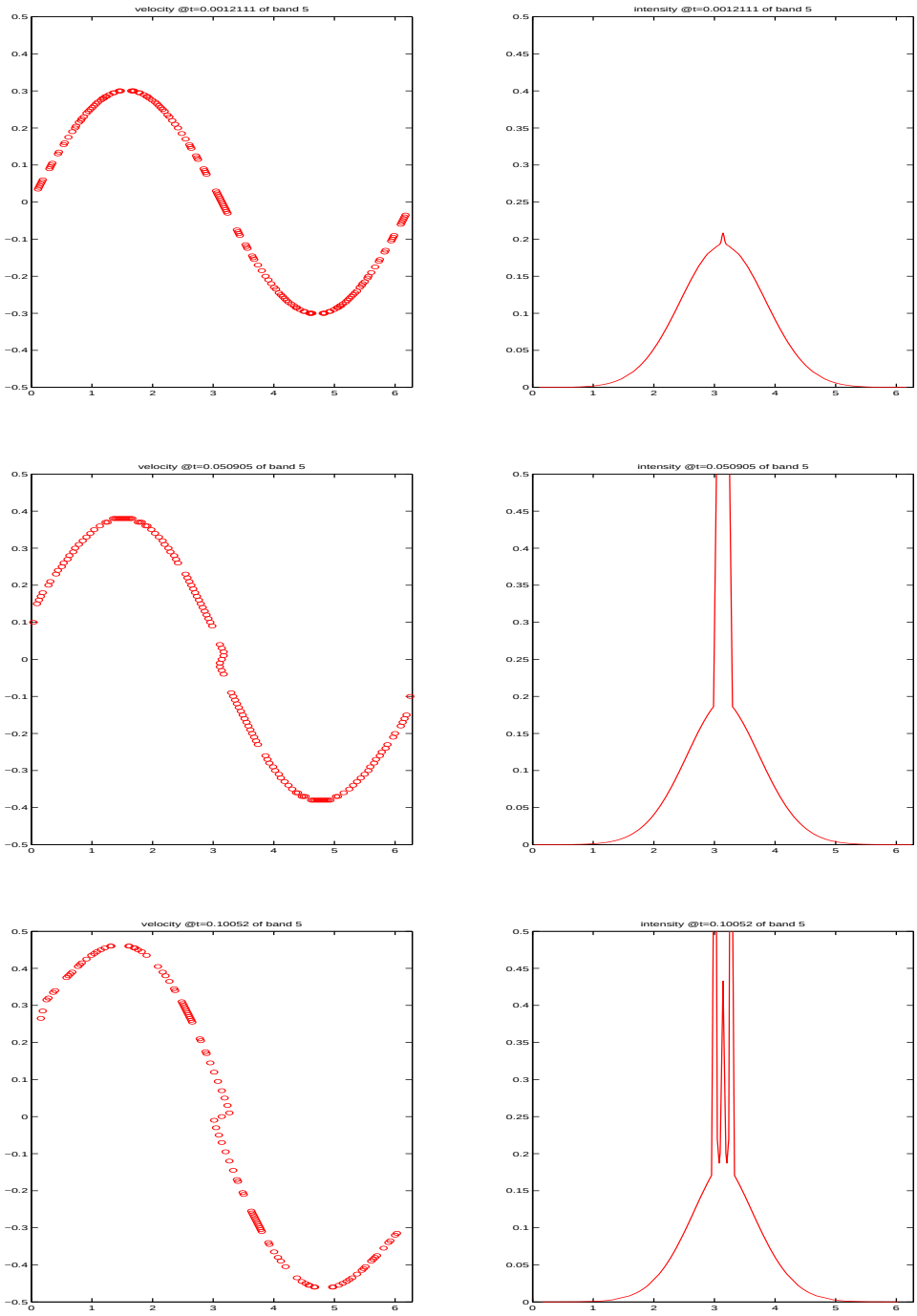

Figure 5.8 Example 4, velocity and density of band 5 with $V_e = \frac{|x-\pi|^2}{2}$ at different times.

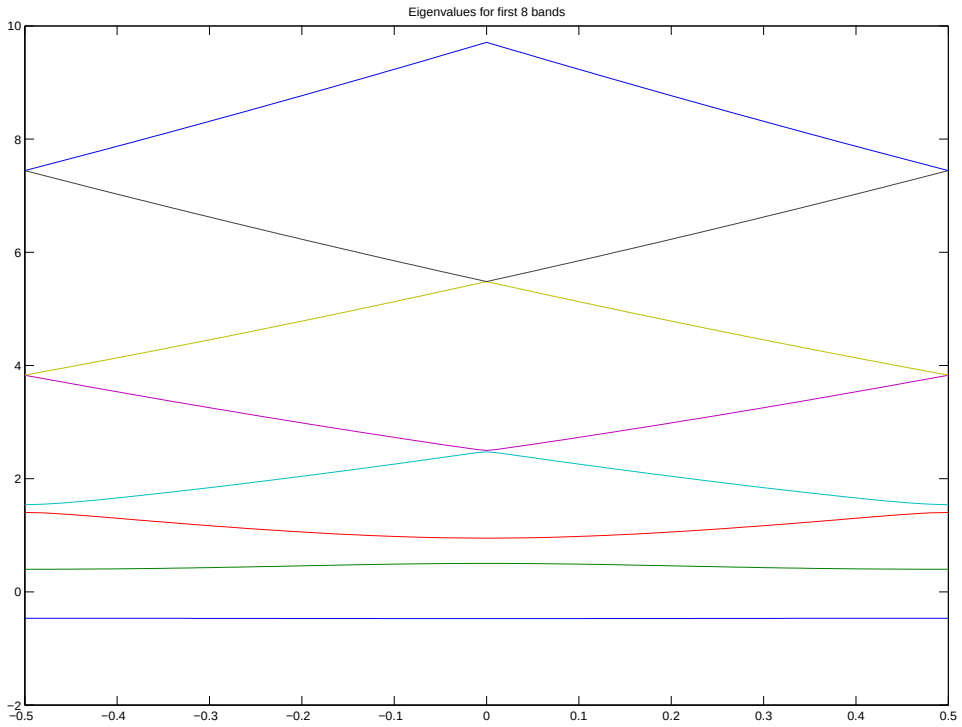

Figure 5.9 Eigenvalues for $V(y) = cos(y)$ and $a(y) = \frac{3}{2} + \sin(y)$ of band 1, 2, $\cdots$, 8 (bottom to top).

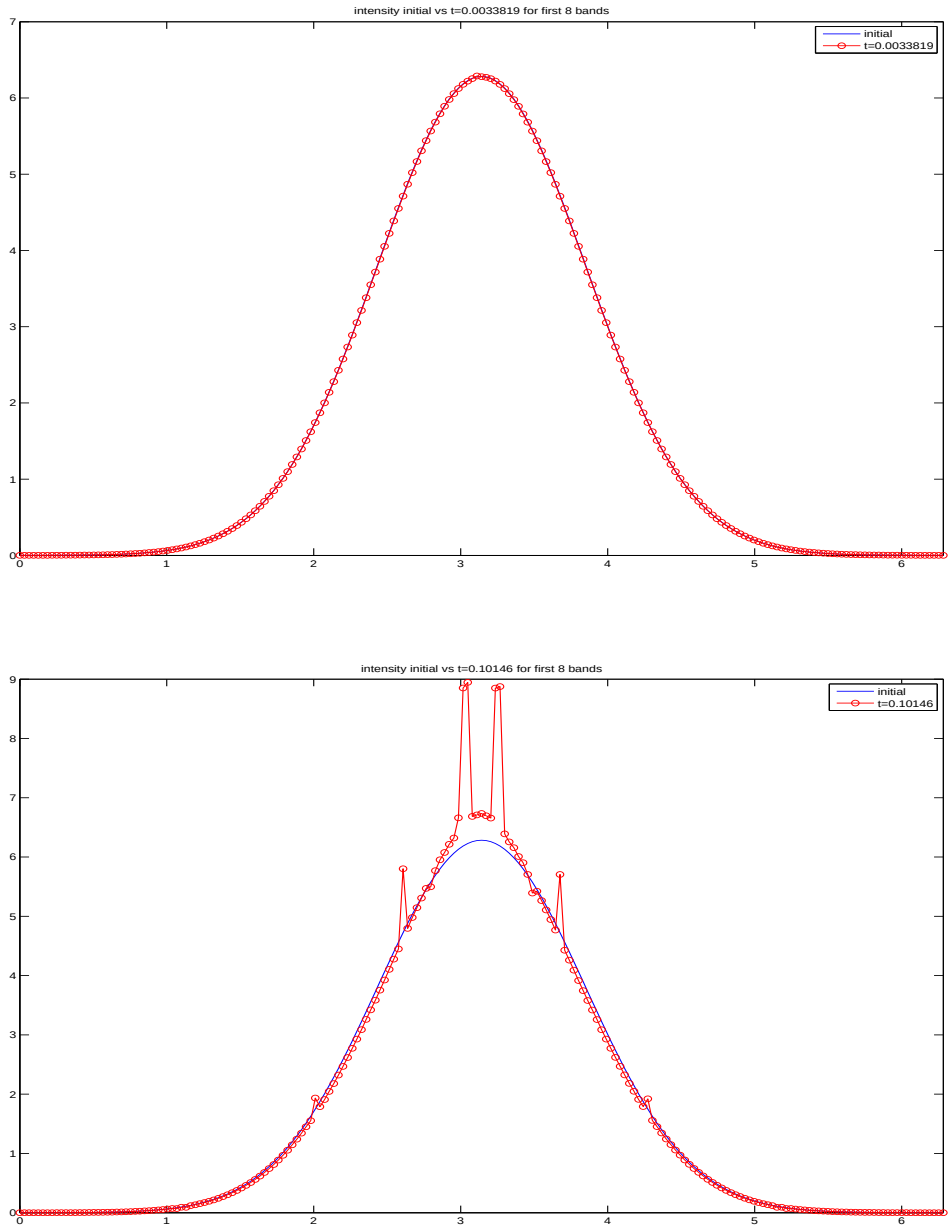

Figure 5.10 Example 5, approximation density with 8 bands at time about 0.003 and 0.1.

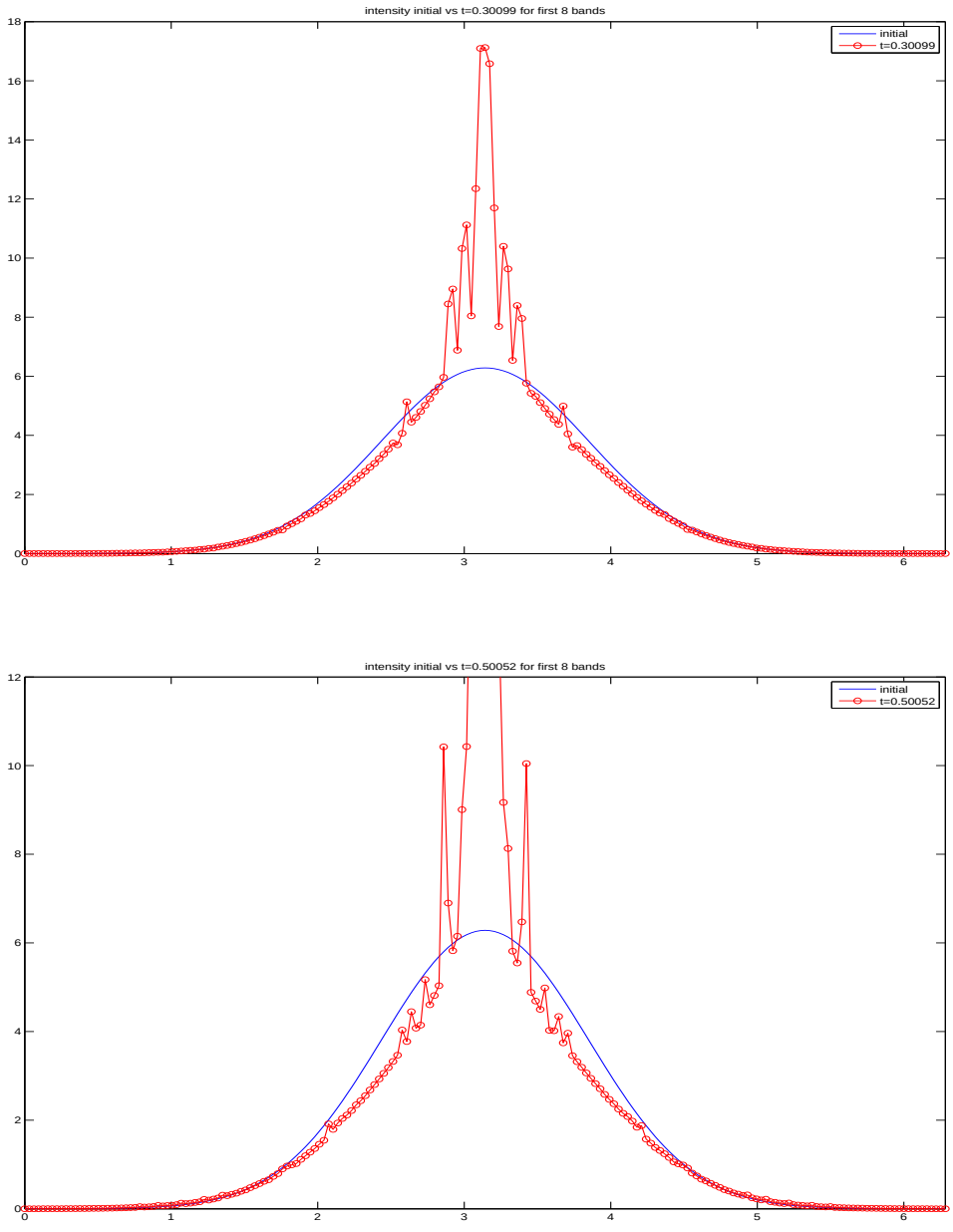

Figure 5.11 Example 5, approximation density with 8 bands at time about 0.3 and 0.5.

CHAPTER 6. GENERAL CONCLUSION

General Conclusion

In this thesis, we study numerical solutions of various problems including semiclassical limit of Schrödinger equation, Euler-Poisson equations and semiclassical limit of Schrödinger equation with periodic structures. In the nonlinear semiclassical models of these problems, singularity formation is generic and standard shock capturing numerical methods fail to capture the physical relevant solutions. We have developed several level set methods in phase space or field space to capture multi-valued solutions to those semiclassical equations after singularity. Within the level set method framework, besides the multi-valued quantities such as velocity, other physical observable quantities such as density, momentum and energy can be evaluated in a post processing step. The advantage of this level set approach is that it can automatically handle the multi-valuedness by an implicit representation of the solution in higher dimensional space. This is a robust method and can be applied to the cases where solutions have complicated structures. A series of numerical tests illustrates the capability and accuracy of our method in describing the solutions. One of the theoretical results is the superposition in the nonlinear semiclassical models. By semiclassical limits, the original linear equations become nonlinear Hamilton-Jacobi-type equations and the superposition is lost. By our level set method, the superposition is obtained for physical quantities such as density, momentum and energy.

Future Research

We plan to continue the development of level set methods in Schrödinger-type equations. It includes the following projects.

- For the Euler-Poisson system, since it can be regarded as the semiclassical limit of Schrödinger-Poisson equations, one future work is to recover the original wave field in Schrödinger-Poisson equations. To this end, besides the level set method developed in Chapter 3 and Chapter 4, we need following steps.

  1. Recover the multi-valued phases from the velocity field and electric field
  2. Figure out a proper phase shift corresponding to each of the multi-valued phases

- The level set method developed in Chapter 3 and Chapter 4 works only for 1D Euler-Poisson system, a continuation is to generalize the method to for multi-dimensional Euler-Poisson equations. We have not been able to derive a closed dynamic system for multi-dimensional case, and further investigation is needed.

- A continuation of the Bloch band based level set method in Chapter 5 is to study the effect of the number of Bloch bands used. This involves an error analysis of the initial decomposition in terms of number of Bloch bands for a fixed Bloch shifted cell operator. This analysis will give an estimate in determining how many level set equations are needed in numerical simulations.

- Multi-valued solutions are computed for the semiclassical limit of the wave equation subject to highly oscillatory initial data using level set method. In order to solve the original wave equation, next step is to recover the wave function by using a proper phase shift via level set method framework.

Besides the above projects, we also intend to develop level set methods in equations or models arising in other applications, such as biology, material science, chemistry, etc.

BIBLIOGRAPHY

Asch, J. and Knauf, A. (1998). Motion in periodic potentials. *Nonlinearity*, 11(1):175–200.

Ashcroft, N. and Mermin, N. (1976). *Solid-state Physics*. Rinehart and Winston, Holt.

Bal, G., Fannjiang, A., Papanicolaou, G., and Ryzhik, L. (1999). Radiative transport in a periodic structure. *J. Statist. Phys.*, 95(1-2):479–494.

Benamou, J.-D. (1999). Direct computation of multivalued phase space solutions for Hamilton-Jacobi equations. *Comm. Pure Appl. Math.*, 52(11):1443–1475.

Benamou, J.-D., Castella, F., Katsaounis, T., and Perthame, B. (2002). High frequency limit of the Helmholtz equations. *Rev. Mat. Iberoamericana*, 18(1):187–209.

Bensoussan, A., Lions, J.-L., and Papanicolaou, G. (1978). *Asymptotic analysis for periodic structures*, volume 5 of *Studies in Mathematics and its Applications*. North-Holland Publishing Co., Amsterdam.

Beyer, R. P. and LeVeque, R. J. (1992). Analysis of a one-dimensional model for the immersed boundary method. *SIAM J. Numer. Anal.*, 29(2):332–364.

Blount, E. I. (1962). Formalisms of band theory. In *Solid State Physics, Vol. 13*, pages 305–373. Academic Press, New York.

Brenier, Y. and Corrias, L. (1998). A kinetic formulation for multi-branch entropy solutions of scalar conservation laws. *Ann. Inst. H. Poincaré Anal. Non Linéaire*, 15(2):169–190.

Burchard, P., Cheng, L.-T., Merriman, B., and Osher, S. (2001). Motion of curves in three spatial dimensions using a level set approach. *J. Comput. Phys.*, 170(2):720–741.

Cheng, L.-T. (2006). Efficient level set methods for constructing wave fronts in three dimensions. *UCLA CAM report.*

Cheng, L.-T., Kang, M., Osher, S., Shim, H., and Tsai, Y.-H. (2004). Reflection in a level set framework for geometric optics. *CMES Comput. Model. Eng. Sci.*, 5(4):347–360.

Cheng, L.-T., Liu, H., and Osher, S. (2003). Computational high-frequency wave propagation using the level set method, with applications to the semi-classical limit of Schrödinger equations. *Commun. Math. Sci.*, 1(3):593–621.

Cockburn, B., Qian, J., Reitich, F., and Wang, J. (2005). An accurate spectral/discontinuous finite-element formulation of a phase-space-based level set approach to geometrical optics. *J. Comput. Phys.*, 208(1):175–195.

Courant, R. and Hilbert, D. (1962). *Methods of mathematical physics. Vol. II: Partial differential equations.* (Vol. II by R. Courant.). Interscience Publishers (a division of John Wiley & Sons), New York-Lon don.

Crandall, M. G. and Lions, P.-L. (1983). Viscosity solutions of Hamilton-Jacobi equations. *Trans. Amer. Math. Soc.*, 277(1):1–42.

Crandall, M. G. and Lions, P.-L. (1984). Two approximations of solutions of Hamilton-Jacobi equations. *Math. Comp.*, 43(167):1–19.

Engelberg, S., Liu, H., and Tadmor, E. (2001). Critical thresholds in Euler-Poisson equations. *Indiana Univ. Math. J.*, 50(Special Issue):109–157. Dedicated to Professors Ciprian Foias and Roger Temam (Bloomington, IN, 2000).

Engquist, B. and Runborg, O. (1996). Multi-phase computations in geometrical optics. *J. Comput. Appl. Math.*, 74(1-2):175–192. TICAM Symposium (Austin, TX, 1995).

Engquist, B. and Runborg, O. (2003). Computational high frequency wave propagation. *Acta Numer.*, 12:181–266.

Engquist, B., Runborg, O., and Tornberg, A.-K. (2002). High-frequency wave propagation by the segment projection method. *J. Comput. Phys.*, 178(2):373–390.

Engquist, B., Tornberg, A.-K., and Tsai, R. (2005). Discretization of Dirac delta functions in level set methods. *J. Comput. Phys.*, 207(1):28–51.

Fatemi, E., Engquist, B., and Osher, S. (1995). Numerical solution of the high frequency asymptotic expansion for the scalar wave equation. *J. Comput. Phys.*, 120(1):145–155.

Flaschka, H., Forest, M. G., and McLaughlin, D. W. (1980). Multiphase averaging and the inverse spectral solution of the Korteweg-de Vries equation. *Comm. Pure Appl. Math.*, 33(6):739–784.

Fomel, S. and Sethian, J. A. (2002). Fast-phase space computation of multiple arrivals. *Proc. Natl. Acad. Sci. USA*, 99(11):7329–7334 (electronic).

Gasser, I., Levermore, C. D., Markowich, P. A., and Schmeiser, C. (2001). The initial time layer problem and the quasineutral limit in the semiconductor drift-diffusion model. *European J. Appl. Math.*, 12(4):497–512.

Gérard, P., Markowich, P. A., Mauser, N. J., and Poupaud, F. (1997). Homogenization limits and Wigner transforms. *Comm. Pure Appl. Math.*, 50(4):323–379.

Gosse, L. (2002). Using K-branch entropy solutions for multivalued geometric optics computations. *J. Comput. Phys.*, 180(1):155–182.

Gosse, L. (2004). Multiphase semiclassical approximation of an electron in a one-dimensional crystalline lattice. II. Impurities, confinement and Bloch oscillations. *J. Comput. Phys.*, 201(1):344–375.

Gosse, L., Jin, S., and Li, X. (2003). Two moment systems for computing multiphase semiclassical limits of the Schrödinger equation. *Math. Models Methods Appl. Sci.*, 13(12):1689–1723.

Gosse, L. and Markowich, P. A. (2004). Multiphase semiclassical approximation of an electron in a one-dimensional crystalline lattice. I. Homogeneous problems. *J. Comput. Phys.*, 197(2):387–417.

Gosse, L. and Mauser, N. J. (2006a). Multiphase semiclassical approximation of an electron in a one-dimensional crystalline lattice. III. From ab initio models to WKB for Schrödinger-Poisson. *J. Comput. Phys.*, 211(1):326–346.

Gosse, L. and Mauser, N. J. (2006b). Multiphase semiclassical approximation of an electron in a one-dimensional crystalline lattice. III. From ab initio models to WKB for Schrödinger-Poisson. *J. Comput. Phys.*, 211(1):326–346.

Gottlieb, S., Shu, C.-W., and Tadmor, E. (2001). Strong stability-preserving high-order time discretization methods. *SIAM Rev.*, 43(1):89–112 (electronic).

Guillot, J.-C., Ralston, J., and Trubowitz, E. (1988). Semi-classical approximations in solid state physics. In *Partial differential equations (Rio de Janeiro, 1986)*, volume 1324 of *Lecture Notes in Math.*, pages 263–269. Springer, Berlin.

Guo, Y. (1998). Smooth irrotational flows in the large to the Euler-Poisson system in $\mathbf{R}^{3+1}$. *Comm. Math. Phys.*, 195(2):249–265.

Harten, A. (1987). Preliminary results on the extension of ENO schemes to two-dimensional problems. In *Nonlinear hyperbolic problems (St. Etienne, 1986)*, volume 1270 of *Lecture Notes in Math.*, pages 23–40. Springer, Berlin.

Harten, A. (1989). ENO schemes with subcell resolution. *J. Comput. Phys.*, 83(1):148–184.

Horn, R. A. and Johnson, C. R. (1985). *Matrix analysis*. Cambridge University Press, Cambridge.

Huang, Z., Jin, S., Markowich, P. A., and Sparber, C. (2007). A Bloch decomposition-based split-step pseudospectral method for quantum dynamics with periodic potentials. *SIAM J. Sci. Comput.*, 29(2):515–538 (electronic).

Hutter, R. (1960). *Beam and wave electronics in microwave tubes*. D. Van Nostrand Company, Inc. Princeton.

Jiang, G.-S. and Wu, C.-C. (1999). A high-order WENO finite difference scheme for the equations of ideal magnetohydrodynamics. *J. Comput. Phys.*, 150(2):561–594.

Jin, S. and Li, X. (2003). Multi-phase computations of the semiclassical limit of the Schrödinger equation and related problems: Whitham vs. Wigner. *Phys. D*, 182(1-2):46–85.

Jin, S., Liu, H., Osher, S., and Tsai, R. (2005a). Computing multi-valued physical observables for the high frequency limit of symmetric hyperbolic systems. *J. Comput. Phys.*, 210(2):497–518.

Jin, S., Liu, H., Osher, S., and Tsai, R. (2005b). Computing multi-valued physical observables for the high frequency limit of symmetric hyperbolic systems. *J. Comput. Phys.*, 210(2):497–518.

Jin, S., Liu, H., Osher, S., and Tsai, Y.-H. R. (2005c). Computing multivalued physical observables for the semiclassical limit of the Schrödinger equation. *J. Comput. Phys.*, 205(1):222–241.

Jin, S. and Osher, S. (2003). A level set method for the computation of multivalued solutions to quasi-linear hyperbolic PDEs and Hamilton-Jacobi equations. *Commun. Math. Sci.*, 1(3):575–591.

Kružkov, S. N. (1970). First order quasilinear equations with several independent variables. *Mat. Sb. (N.S.)*, 81 (123):228–255.

Lax, P. D. and Levermore, C. D. (1983a). The small dispersion limit of the Korteweg-de Vries equation. I. *Comm. Pure Appl. Math.*, 36(3):253–290.

Lax, P. D. and Levermore, C. D. (1983b). The small dispersion limit of the Korteweg-de Vries equation. II. *Comm. Pure Appl. Math.*, 36(5):571–593.

Lax, P. D. and Levermore, C. D. (1983c). The small dispersion limit of the Korteweg-de Vries equation. III. *Comm. Pure Appl. Math.*, 36(6):809–829.

Leung, S., Qian, J., and Osher, S. (2004). A level set method for three-dimensional paraxial geometrical optics with multiple point sources. *Commun. Math. Sci.*, 2(4):643–672.

Li, X., Wöhlbier, J. G., Jin, S., and Booske, J. H. (2004). An eulerian method for computing multi-valued solutions of the euler-poisson equations and applucaions to wave breaking in klystrons. *Phys Rev E*, 70.

Lions, P.-L. and Paul, T. (1993). Sur les mesures de Wigner. *Rev. Mat. Iberoamericana*, 9(3):553–618.

Liu, H., Cheng, L.-T., and Osher, S. (2005). A level set framework for capturing multi-valued solutions to nonlinear first-order equations. *J. Comput. Phys.*

Liu, H. and Tadmor, E. (2002). Semiclassical limit of the nonlinear Schrödinger-Poisson equation with subcritical initial data. *Methods Appl. Anal.*, 9(4):517–531.

Liu, H. and Wang, Z. (2007a). Computing multi-valued velocity and electric fields for 1D Euler-Poisson equations. *Appl. Numer. Math.*, 57(5-7):821–836.

Liu, H. and Wang, Z. (2007b). A fieled-space based level set method for computing mult-valued solutions to 1D Euler-Poisson equations. *J. Comput. Phys.*, 225:591–614.

Liu, H. and Wang, Z. (2008a). A bloch band based level set method for computing the semiclassical limits in schrödinger equations. *Preprint*.

Liu, H. and Wang, Z. (2008b). Superposition of multi-valued solutions in high frequency wave dynamics. *Accepted by J. Sci. Comput.*

Luttinger, J. M. (1951). The effect of a magnetic field on electrons in a periodic potential. *Physical Rev. (2)*, 84:814–817.

Markowich, P. A. and Mauser, N. J. (1993). The classical limit of a self-consistent quantum-Vlasov equation in 3D. *Math. Models Methods Appl. Sci.*, 3(1):109–124.

Markowich, P. A., Mauser, N. J., and Poupaud, F. (1994). A Wigner-function approach to (semi)classical limits: electrons in a periodic potential. *J. Math. Phys.*, 35(3):1066–1094.

Markowich, P. A., Ringhofer, C. A., and Schmeiser, C. (1990). *Semiconductor equations*. Springer-Verlag, Vienna.

Maslov, V. P. and Fedoriuk, M. V. (1981). *Semiclassical approximation in quantum mechanics*, volume 7 of *Mathematical Physics and Applied Mathematics*. D. Reidel Publishing Co., Dordrecht. Translated from the Russian by J. Niederle and J. Tolar, Contemporary Mathematics, 5.

Min, C. (2004). Local level set method in high dimension and codimension. *J. Comput. Phys.*, 200(1):368–382.

Montarnal, P. and Shu, C.-W. (1999). Real gas computation using an energy relaxation method and high-order WENO schemes. *J. Comput. Phys.*, 148(1):59–80.

Osher, S., Cheng, L.-T., Kang, M., Shim, H., and Tsai, Y.-H. (2002). Geometric optics in a phase-space-based level set and Eulerian framework. *J. Comput. Phys.*, 179(2):622–648.

Osher, S. and Fedkiw, R. (2003). *Level set methods and dynamic implicit surfaces*, volume 153 of *Applied Mathematical Sciences*. Springer-Verlag, New York.

Osher, S. and Sethian, J. A. (1988). Fronts propagating with curvature-dependent speed: algorithms based on Hamilton-Jacobi formulations. *J. Comput. Phys.*, 79(1):12–49.

Osher, S. and Shu, C.-W. (1991). High-order essentially nonoscillatory schemes for Hamilton-Jacobi equations. *SIAM J. Numer. Anal.*, 28(4):907–922.

Panati, G., Spohn, H., and Teufel, S. (2003). Effective dynamics for Bloch electrons: Peierls substitution and beyond. *Comm. Math. Phys.*, 242(3):547–578.

Peng, D., Merriman, B., Osher, S., Zhao, H., and Kang, M. (1999). A PDE-based fast local level set method. *J. Comput. Phys.*, 155(2):410–438.

Qian, J., Cheng, L.-T., and Osher, S. (2003). A level set-based Eulerian approach for anisotropic wave propagation. *Wave Motion*, 37(4):365–379.

Qian, J. and Leung, S. (2004). A level set based Eulerian method for paraxial multivalued traveltimes. *J. Comput. Phys.*, 197(2):711–736.

Raviart, P.-A. (1983). On the numerical analysis of particle simulations in plasma physics. In *Nonlinear partial differential equations and their applications. Collège de France Seminar, Vol. IV (Paris, 1981/1982)*, volume 84 of *Res. Notes in Math.*, pages 173–193. Pitman, Boston, Mass.

Runborg, O. (2000). Some new results in multiphase geometrical optics. *M2AN Math. Model. Numer. Anal.*, 34(6):1203–1231.

Ryzhik, L., Papanicolaou, G., and Keller, J. B. (1996). Transport equations for elastic and other waves in random media. *Wave Motion*, 24(4):327–370.

Sethian, J. A. (1999). *Level Set Methods and Fast Marching Methods : Evolving Interfaces in Computational Geometry, Fluid Mechanics, Computer Vision, and Materials Science.* Cambridge.

Shu, C.-W. (1999). High order ENO and WENO schemes for computational fluid dynamics. In *High-order methods for computational physics*, volume 9 of *Lect. Notes Comput. Sci. Eng.*, pages 439–582. Springer, Berlin.

Shu, C.-W. and Osher, S. (1989). Efficient implementation of essentially nonoscillatory shock-capturing schemes. II. *J. Comput. Phys.*, 83(1):32–78.

Sparber, C., Markowich, P. A., and Mauser, N. J. (2003). Wigner functions versus WKB-methods in multivalued geometrical optics. *Asymptot. Anal.*, 33(2):153–187.

Symes, W. W. and Qian, J. (2003). A slowness matching Eulerian method for multivalued solutions of Eikonal equations. *J. Sci. Comput.*, 19(1-3):501–526. Special issue in honor of the sixtieth birthday of Stanley Osher.

Teufel, S. (2003). *Adiabatic perturbation theory in quantum dynamics*, volume 1821 of *Lecture Notes in Mathematics*. Springer-Verlag, Berlin.

Tornberg, A.-K. and Engquist, B. (2003). Regularization techniques for numerical approximation of PDEs with singularities. *J. Sci. Comput.*, 19(1-3):527–552. Special issue in honor of the sixtieth birthday of Stanley Osher.

Tornberg, A.-K. and Engquist, B. (2004). Numerical approximations of singular source terms in differential equations. *J. Comput. Phys.*, 200(2):462–488.

Trier, J. V. and Symes, W. W. (1991). Upwind finite-difference calculation of traveltimes. *Geophysics*, 56:812–821.

Tsai, Y.-H. R., Giga, Y., and Osher, S. (2003). A level set approach for computing discontinuous solutions of Hamilton-Jacobi equations. *Math. Comp.*, 72(241):159–181 (electronic).

Whitham, G. B. (1974). *Linear and nonlinear waves*. Wiley-Interscience [John Wiley & Sons], New York. Pure and Applied Mathematics.

Wigner, E. P. (1932). On the quantum correction for thermodynamic equilibrium. *Phys. Rev.*, 40:749–759.

Wilcox, C. H. (1978). Theory of Bloch waves. *J. Analyse Math.*, 33:146–167.

Zak, J. (1968). Dynamics of electrons in solids in external fields. *Phys. Rev.*, 1368:686–695.

Zhang, P., Zheng, Y., and Mauser, N. J. (2002). The limit from the Schrödinger-Poisson to the Vlasov-Poisson equations with general data in one dimension. *Comm. Pure Appl. Math.*, 55(5):582–632.

ACKNOWLEDGEMENTS

It is my pleasure to take this opportunity to express my thanks to those who made this thesis possible.

First and foremost, I would like to express my gratitude to my advisor Dr. Hailiang Liu. His guidance, patience and support throughout my stay in Iowa made this work possible. His insights and helpful discussions often inspired me and renewed my hopes for completing my graduate education. It is difficult to overstate my gratitude to him. I would also like to thank my committee members for their efforts and contributions to this work: Dr. Lisheng Hou, Dr. Paul Sacks, Dr. Sunder Sethuraman and Dr. Moulay Tidriri.

I also want to thank my family for their support. Though my parents were far from me during my graduate education in Iowa, their support and love were always with me. I would also like to thank my wife and daughter for their love.

Last but not least, I want to thank all the colleagues, friends and staffs here in Mathematics Department of Iowa State University.